

A learning scheme by sparse grids and Picard approximations for semilinear parabolic PDEs

J.-F. Chassagneux ^{*}, J. Chen [†], N. Frikha [‡], C. Zhou [§]

February 2, 2022

Abstract

Relying on the classical connection between Backward Stochastic Differential Equations (BSDEs) and non-linear parabolic partial differential equations (PDEs), we propose a new probabilistic learning scheme for solving high-dimensional semilinear parabolic PDEs. This scheme is inspired by the approach coming from machine learning and developed using deep neural networks in Han and al. [32]. Our algorithm is based on a Picard iteration scheme in which a sequence of linear-quadratic optimisation problem is solved by means of stochastic gradient descent (SGD) algorithm. In the framework of a linear specification of the approximation space, we manage to prove a convergence result for our scheme, under some smallness condition. In practice, in order to be able to treat high-dimensional examples, we employ sparse grid approximation spaces. In the case of periodic coefficients and using pre-wavelet basis functions, we obtain an upper bound on the global complexity of our method. It shows in particular that the curse of dimensionality is tamed in the sense that in order to achieve a root mean squared error of order ε , for a prescribed precision ε , the complexity of the Picard algorithm grows polynomially in ε^{-1} up to some logarithmic factor $|\log(\varepsilon)|$ which grows linearly with respect to the PDE dimension. Various numerical results are presented to validate the performance of our method and to compare them with some recent machine learning schemes proposed in Han and al. [20] and Huré and al. [37].

1 Introduction

In the present work, we are interested in the numerical approximation in high dimension of the solution to the semilinear parabolic PDE

$$\begin{cases} \partial_t u(t, x) + \mathcal{L}u(t, x) + f(u(t, x), \sigma^\top(x) \nabla_x u(t, x)) = 0, & (t, x) \in [0, T) \times \mathbb{R}^d, \\ u(T, x) = g(x), & x \in \mathbb{R}^d \end{cases} \quad (1.1)$$

^{*}Université de Paris, Laboratoire de Probabilités, Statistiques et Modélisation, F-75013 Paris, France. Email: chassagneux@lpsm.paris.

[†]Université de Paris, Laboratoire de Probabilités, Statistiques et Modélisation, F-75013 Paris, France. Part of the work was done during a visit at NUSRI, Suzhou, China, whose hospitality is greatly appreciated. Email: juchen@lpsm.paris

[‡]Université de Paris, Laboratoire de Probabilités, Statistiques et Modélisation, F-75013 Paris, France. Email: frikha@lpsm.paris

[§]Department of Mathematics, City University of Hong Kong, Kowloon Tong, Hong Kong. On leave from Department of Mathematics, National University of Singapore. Research supported by NSFC Grant No. 11871364 as well as Singapore MOE (Ministry of Educations) AcRF Grants R-146-000-271-112 and R-146-000-284-114. Email: chaozhou@cityu.edu.hk

where $f : \mathbb{R} \times \mathbb{R}^d \rightarrow \mathbb{R}$, $g : \mathbb{R}^d \rightarrow \mathbb{R}$ are measurable functions and \mathcal{L} is the infinitesimal generator of the forward diffusion process with dynamics

$$d\mathcal{X}_t = b(\mathcal{X}_t) dt + \sigma(\mathcal{X}_t) d\mathcal{W}_t \quad (1.2)$$

and defined, for a smooth function φ , by

$$\mathcal{L}\varphi(t, x) := b(x) \cdot \nabla_x \varphi(t, x) + \frac{1}{2} \text{Tr}[(\sigma \sigma^\top)(x) \nabla_x^2 \varphi(t, x)]. \quad (1.3)$$

Here, \mathcal{W} is a d -dimensional brownian motion defined on a complete probability space $(\mathfrak{D}, \mathcal{A}, \mathbb{P})$, $b : \mathbb{R}^d \rightarrow \mathbb{R}^d$ and $\sigma : \mathbb{R}^d \rightarrow \mathcal{M}_d$ are measurable functions, \mathcal{M}_d being the set of $d \times d$ matrix. The initial condition \mathcal{X}_0 is a square integrable random variable independent from the Brownian Motion \mathcal{W} . We denote by $(\mathcal{F}_t)_{0 \leq t \leq T}$ the filtration generated by \mathcal{W} and \mathcal{X}_0 , augmented with \mathbb{P} null sets.

Developing efficient algorithms for the numerical approximation of high-dimensional non-linear PDEs is a challenging task that has attracted considerable attention from the research community in the last two decades. We can quote various approaches (limiting to the "stochastic" ones) that have proven to be efficient in a high dimensional setting: branching methods, see e.g. [35], machine learning methods (especially using deep neural networks), see e.g. [32], and full history recursive multilevel Picard method (abbreviated MLP in the literature) see e.g. [38]. This is a very active field of research, we refer to the recent survey papers [33, 4] for more references and an overview of the numerical and theoretical results available. We focus now more on one stream of research which uses the celebrated link between semilinear parabolic PDEs of the form (1.1) and BSDEs. This connection, initiated in [45], reads as follows: denoting by u a classical solution to (1.1), $(u(t, \mathcal{X}_t), \sigma^\top(\mathcal{X}_t) \nabla_x u(t, \mathcal{X}_t)) = (\mathcal{Y}_t, \mathcal{Z}_t)$ where the pair $(\mathcal{Y}, \mathcal{Z})$ is the $\mathbb{R} \times \mathbb{R}^d$ -valued and (\mathcal{F}_t) -adapted process solution to the BSDE with dynamics

$$\mathcal{Y}_t = g(\mathcal{X}_T) + \int_t^T f(\mathcal{Y}_s, \mathcal{Z}_s) ds - \int_t^T \mathcal{Z}_s \cdot d\mathcal{W}_s, \quad 0 \leq t \leq T, \quad (1.4)$$

so that, the original problem boils down to the numerical approximation of the above stochastic system. Various strategies have been used to numerically approximate the stochastic system $(\mathcal{X}_t, \mathcal{Y}_t, \mathcal{Z}_t)_{t \in [0, T]}$. The most studied one is based on a time discretization of (1.4) leading to a backward programming algorithm to approximate (Y, Z) , as exposed in e.g [10, 49] (see the references therein for early works). This involves computing a sequence of conditional expectations and various methods have been developed: Malliavin calculus based methods [10, 18, 36], optimal quantization methods [1, 2, 44], cubature methods [16, 17, 14] and (linear) regression methods, see among others [26, 28, 27]. It is acknowledged that such approaches will be feasible for problems up to dimension 10. This limitation is a manifestation of the so-called "curse of dimensionality". Recently, non-linear regression methods using deep neural networks were successfully combined with this approach and proved to be capable of tackling problems in high dimension [37]. However, other strategies have been introduced in the last five years or so to approximate (1.4) trying to adopt a "forward point of view". Relying on Wiener chaos expansion and Picard iteration, [11, 25] introduced a method that notably works in non-Markovian setting but is still impacted by the curse of dimension. A key step forward has been realized by the so called *deep BSDEs solver* introduced in [32]. Interpreting the resolution of a BSDEs as an optimisation problem, it relies on the expressivity of deep neural network and well established SGD algorithms to show great performance in practice. More precisely, in this approach, the

\mathcal{Y} -process is now interpreted as a forward SDE controlled by the \mathcal{Z} -process. Then, an Euler-Maruyama approximation scheme is derived in which the derivative of the solution u appearing in the non-linear function f (through the \mathcal{Z} -process) is approximated by a multi-layer neural network. The optimal weights are then computed by minimizing the mean-squared error between the value of the approximation scheme at time T and a good approximation of the target $g(\mathcal{X}_T)$ using stochastic gradient descent algorithms. Again, this kind of deep learning technique seems to be very efficient to numerically approximate the solution to semi-linear parabolic PDEs in practice. However a complete theory concerning its theoretical performance is still not achieved [4]. One important observation is that, due to highly non-linear specification, the optimisation problem that has to be solved in practice, has no convexity property. The numerical procedure designed can only converge to local minima, whose properties (with respect to the approximation question) are still not completely understood.

Inspired by this new forward approach, we introduce here an algorithm which is shown to converge to a global minimum. This, of course, comes with a price. First, we move from the deep neural networks approximation space to a more classical linear specification of the approximation space. However, due the non-linearity in the BSDE driver, the global optimisation problem to be solved is still non-convex. To circumvent this issue, we employ a *Picard iteration procedure*. The overall procedure becomes then a sequence of linear-quadratic optimisation problems which are solved by a SGD algorithm. Our first main result is a control of the global error between the *implemented algorithm* and the solution to the BSDE which notably shows the convergence of the method under some smallness conditions, see Theorem 2.1. In particular, contrary to [32, 34] or [37], our result takes into account the error induced by the SGD algorithm. In our numerical experiments, we rely on sparse grid approximation spaces which are known to be well-suited to deal with high-dimensional problems. Under the framework of periodic coefficients, we establish as our second main result, an upper bound on the global complexity for our *implemented algorithm*, see Theorem 3.1. We notably prove that the curse of dimensionality is tamed in the sense that the complexity is of order $\varepsilon^{-p} |\log(\varepsilon)|^{q(d)}$, where p is a constant which does not depend on the PDE dimension and $d \mapsto q(d)$ is an affine function. We also demonstrate numerically the efficiency of our methods in high dimensional setting.

The rest of the paper is organized as follows. In Section 2, we first recall the *deep BSDEs solver* of [32] but adapted to our framework. Namely, we use a linear specification of the approximation space together with SGD algorithms. For sake of clarity, we denote this method: the *direct algorithm*. Then, we introduce our new numerical method : the *Picard algorithm*. We present our main assumptions on the coefficients and state our main convergence results. In Section 3, we use sparse grid approximation with the *direct and Picard algorithms*, using two types of basis functions: pre-wavelet [9] and modified hat function [24]. We discuss their numerical performances in practice through various test examples. We also compare them with some deep learning techniques [32, 37]. We also state our main theoretical complexity result. Section 4 is devoted to the theoretical analysis required to establish our main theorems: all the proofs are contained in this section. Finally, we give a complete list of the algorithm parameters that have been used to obtain the numerical results in Appendix.

Notation: Elements of \mathbb{R}^q are seen as column vectors. For $x \in \mathbb{R}^q$, x_i is the i th component and $|x|$ corresponds to its Euclidian norm, $x \cdot y$ denotes the scalar product of x and $y \in \mathbb{R}^q$. \mathcal{M}_q is the set of $q \times q$ real matrices. We denote by \mathbf{e}^ℓ the ℓ th vector of the standard basis of \mathbb{R}^q . The vector $(1, \dots, 1)^\top$ is denoted $\mathbf{1}$, I_d is the $d \times d$ identity matrix. We use the bold face

notations $\mathbf{l} \in \mathbb{N}^d$ for multidimensional indices $\mathbf{l} := (l_1, \dots, l_d)$ with (index) norms denoted by $|\mathbf{l}|_p := (\sum_{i=1}^d l_i^p)^{1/p}$ and $|\mathbf{l}|_\infty := \max_{1 \leq i \leq d} |l_i|$. For later use, for a positive integer k , we introduce the set $\mathbf{J}_{d,k}^\infty$ of multidimensional indices $\mathbf{l} \in \mathbb{N}^d$ satisfying $|\mathbf{l}|_\infty \leq k$. For a finite set A , we denote by $|A|$ its cardinality.

For a function $f : \mathbb{R}^d \rightarrow \mathbb{R}$, we denote by $\partial_{x_l} f$ the partial derivative function with respect to x_l , ∇f denotes the gradient function of f , valued in \mathbb{R}^d . We also use $\nabla^2 f = (\partial_{x_i, x_j}^2 f)_{1 \leq i, j \leq d}$ to denote the Hessian matrix of f , valued in \mathcal{M}_d . For a sufficiently smooth real-valued function f defined in \mathbb{R}^d , we let $D^{\mathbf{l}} f = \partial_{x_1}^{l_1} \dots \partial_{x_d}^{l_d} f$ denote the differentiation operator with respect to the multi-index $\mathbf{l} \in \mathbb{N}^d$. For a fixed positive integer k and a function f defined on an open domain $\mathcal{U} \subset \mathbb{R}^d$, we define its Sobolev norm of mixed smoothness

$$\|f\|_{H_{mix}^k(\mathcal{U})} := \left(\sum_{\mathbf{l} \in \mathbf{J}_{d,k}^\infty} \|D^{\mathbf{l}} f\|_{L_2(\mathcal{U})}^2 \right)^{\frac{1}{2}} \quad (1.5)$$

where the derivative $D^{\mathbf{l}} f$ in the above formula has to be understood in the weak sense and for a map $g : \mathcal{U} \mapsto \mathbb{R}$, $\|g\|_{L_2(\mathcal{U})}^2 := \int_{\mathcal{U}} |g(x)|^2 dx$. The Sobolev space of mixed smoothness $H_{mix}^k(\mathcal{U})$ is then defined by

$$H_{mix}^k(\mathcal{U}) := \left\{ f \in L_2(\mathcal{U}) : \|f\|_{H_{mix}^k(\mathcal{U})} < \infty \right\}. \quad (1.6)$$

For a positive integer q , the set \mathcal{H}_q^2 is the set of progressively measurable processes V defined on the probability space $(\mathfrak{D}, \mathcal{A}, \mathbb{P})$ with values in \mathbb{R}^q and satisfying $\mathbb{E} \left[\int_0^T |V_t|^2 dt \right] < +\infty$. The set \mathcal{S}_q^2 is the set of adapted càdlàg processes U defined on the probability space $(\mathfrak{D}, \mathcal{A}, \mathbb{P})$ with values in \mathbb{R}^q and satisfying $\mathbb{E} \left[\sup_{t \in [0, T]} |U_t|^2 \right] < +\infty$. We also define $\mathcal{B}^2 := \mathcal{S}_1^2 \times \mathcal{H}_d^2$.

2 The *direct* and *Picard algorithms*

We describe here the numerical methods studied in this work. The first one, the *direct algorithm* is an adaptation of the *Deep BSDEs solver* introduced in [20] to the linear specification of the parametric space that we use here. The second one, the *Picard algorithm*, is new and is the main contribution of our work. We also give here the main general convergence results related to the *Picard algorithm*. The complexity analysis is postponed to the next section.

The methods we introduce below have for goal to compute an approximation of the value function u , satisfying the PDE (1.1), at the initial time on a given domain or at a specific point. This lead us to introduce the following setup for the initial value \mathcal{X}_0 :

Assumption 2.1. *One of the two following cases holds:*

- (i) *The law of \mathcal{X}_0 has compact support and is absolutely continuous with respect to the Lebesgue measure.*
- (ii) *The law of \mathcal{X}_0 is a Dirac mass at some point $x_0 \in \mathbb{R}^d$.*

Most of our numerical applications are done in the setting of Assumption 2.1(ii), see next section. Then, obviously, the approximation of the value function is known only at the point x_0 at the initial time. However, one should note that it could also be interesting to work in the setting of Assumption 2.1(i) if one seeks to obtain an approximation of the *whole* value function (on the support of \mathcal{X}_0) at the initial time.

2.1 Assumptions on the coefficients and connection with the semilinear PDE

In this subsection, we first give the assumptions on the BSDE coefficients that will be required for our approach and then recall the connection with semilinear PDEs. In particular, under these assumptions, the underlying PDE admits a unique classical solution. Under an additional regularity assumption on the coefficients, the unique solution to the PDE admits smooth derivatives of enough order which are controlled on the whole domain by known parameters. This additional regularity, together with a periodicity assumption, will be used to obtain our theoretical complexity result, see Section 3.1.2. For sake of simplicity, it is also assumed that the coefficients b , σ and f do not depend on time and that f does not depend on the space variable.

Assumption 2.2. (i) *The coefficients b , σ , f and g are bounded, Lipschitz-continuous with respect to all variables and $g \in \mathcal{C}^{2+\alpha}(\mathbb{R}^d)$, for some $\alpha \in (0, 1]$. We will denote by L the Lipschitz-modulus of the map f .*

(ii) *The coefficient $a = \sigma\sigma^\top$ is uniformly elliptic, that is, there exists $\lambda_0 \geq 1$ such that for any $(x, \zeta) \in (\mathbb{R}^d)^2$ it holds*

$$\lambda_0^{-1}|\zeta|^2 \leq a(x)\zeta \cdot \zeta \leq \lambda_0|\zeta|^2. \quad (2.1)$$

(iii) *For any $(i, j) \in \{1, \dots, d\}^2$, the coefficients b_i , $\sigma_{i,j}$, g belong to $\mathcal{C}^{2d+1}(\mathbb{R}^d, \mathbb{R})$ and f belongs to $\mathcal{C}^{2d+1}(\mathbb{R} \times \mathbb{R}^d, \mathbb{R})$. Moreover, their derivatives of any order up and equal to $2d + 1$ are bounded and Lipschitz continuous.*

(iv) *The coefficients b , σ , f and g are periodic functions.*

From now on, we will say that Assumption 2.2 holds if and only if Assumption 2.2 (i), (ii), (iii) and (iv) are satisfied.

Under Assumption 2.2 (i) and (ii), it is known (see e.g. [45]) that for any square integrable initial condition \mathcal{X}_0 there exists a unique couple $(\mathcal{Y}, \mathcal{Z}) \in \mathcal{B}^2$ satisfying equation (1.4) \mathbb{P} -a.s. Moreover, from [40] Chapter VI and [23] Chapter 7, the PDE (1.1) admits a unique solution $u \in \mathcal{C}^{1,2}([0, T] \times \mathbb{R}^d, \mathbb{R})$ satisfying: there exists a positive constant C , depending on T and the parameters appearing in Assumption 2.2 (i) and (ii), such that for all $(t, x) \in [0, T] \times \mathbb{R}^d$

$$|u(t, x)| + |\partial_t u(t, x)| + |\nabla_x u(t, x)| + |\nabla_x^2 u(t, x)| \leq C.$$

From [48, 46, 47], the semilinear PDE (1.1) and the BSDE (1.2)-(1.4) are connected, namely, for all $(t, x) \in [0, T] \times \mathbb{R}^d$, it holds

$$\mathcal{Y}_t = u(t, \mathcal{X}_t), \quad \mathcal{Z}_t = \sigma^\top(\mathcal{X}_t) \nabla_x u(t, \mathcal{X}_t).$$

Finally, under Assumption 2.2, still from [40] Chapter IV and [23] Chapter III, the unique solution u to the PDE (1.1) is smooth, namely, setting $v_i = (\sigma^\top \nabla_x u)_i$, $1 \leq i \leq d$, for any $\mathbf{l} \in \mathbf{J}_{d,2}^\infty$, $D^{\mathbf{l}}v_i(t, \cdot)$ exists and is bounded. In particular, there exists a positive constant, depending on T and the known parameters appearing in Assumption 2.2 (i), (ii) and (iii) such that for all $\mathbf{l} \in \mathbf{J}_{d,2}^\infty$ and all $(t, x) \in [0, T] \times \mathbb{R}^d$,

$$\max_{1 \leq i \leq d} |D^{\mathbf{l}}v_i(t, x)| \leq C. \quad (2.2)$$

2.2 Direct algorithm

We first consider the approximation of the forward component (1.2). Given an equidistant grid $\pi := \{t_0 = 0 < \dots < t_n < \dots < t_N = T\}$ of the time interval $[0, T]$, $t_n = nh$, $n = 0, \dots, N$, with time-step $h := T/N$, we denote by $W := (\mathcal{W}_{t_n})_{0 \leq n \leq N}$ the discrete-time version of the Brownian motion \mathcal{W} and define $\Delta W_n = W_{t_{n+1}} - W_{t_n}$, $0 \leq n \leq N-1$.

We then introduce a standard Euler-Maruyama approximation scheme of \mathcal{X} on π defined by $X_0 = \mathcal{X}_0$ and for $0 \leq n \leq N-1$,

$$X_{t_{n+1}} = X_{t_n} + b(X_{t_n})h + \sigma(X_{t_n})\Delta W_n. \quad (2.3)$$

Before discussing the approximation of the backward component, we here state an important lemma concerning the existence of two-sided Gaussian estimates for the transition density of the above Euler-Maruyama approximation scheme. These estimates will prove very useful in the sequel, when studying the theoretical complexity of the *Picard algorithm*. We denote by $p^\pi(t_i, t_j, x, \cdot)$ the transition density function of the Euler-Maruyama scheme starting from the point x at time t_i and taken at time t_j , with $0 \leq t_i < t_j \leq T$. We refer e.g. to [42] for a proof of the following result.

Lemma 2.1. *Assume that the coefficients b and σ satisfies Assumption 2.2 (i) and (ii). There exist constants $\mathfrak{c} := \mathfrak{c}(\lambda_0, b, \sigma, d) \in (0, 1]$ and $\mathfrak{C} := \mathfrak{C}(T, \lambda, b, \sigma, d) \geq 1$ such that for any $(x, x') \in (\mathbb{R}^d)^2$ and for any $0 \leq i < j \leq N$*

$$\mathfrak{C}^{-1}p(\mathfrak{c}(t_j - t_i), x - x') \leq p^\pi(t_i, t_j, x, x') \leq \mathfrak{C}p(\mathfrak{c}^{-1}(t_j - t_i), x' - x) \quad (2.4)$$

where for any $(t, x) \in (0, \infty) \times \mathbb{R}^d$, $p(t, x) := (1/(2\pi t))^{d/2} \exp(-|x|^2/(2t))$.

We now turn to the approximation of the backward component (1.4). We first introduce a linear parametrization of the process \mathcal{Z} . For each discrete date $t_n \in \pi \setminus \{T\}$, we consider a parametric functional approximation space \mathcal{V}_n^z generated by a set of basis functions $(\psi_n^k)_{1 \leq k \leq K_n^z}$, for $0 \leq n \leq N-1$ and some positive integer K_n^z . The measurable functions $\psi_n^k : \mathbb{R}^d \mapsto \mathbb{R}$ have at most polynomial growth. Note that, for $n \geq 1$, the specification of the basis function could depend on the time t_n , but in order to simplify the discussion, we let the number of basis functions be the same and set to K . Namely, $K_n^z = K$, for all $n \geq 1$. For $n = 0$, the specification will depend on the nature of \mathcal{X}_0 : if Assumption 2.1(i) holds, then we will set $K_0^z = K$; if Assumption 2.1(ii) holds, then we simply set $K_0^z = 1$ and ψ_0^1 is a function satisfying $\psi_0^1(x_0) = 1$. For latter use, we set:

$$\bar{K}^z := \sum_{n=0}^{N-1} K_n^z = K_0^z + (N-1)K. \quad (2.5)$$

Remark that there is no need to introduce an approximation space at T since the function g is explicitly known.

For $0 \leq n \leq N-1$, each component of $(\sigma^\top \nabla_x u)(t_n, \cdot)$ should be approximated in an optimal way by a function in \mathcal{V}_n^z . The process \mathcal{Z} appearing in the dynamics of the controlled process \mathcal{Y} , that has to be optimized, is parametrized using the spaces $(\mathcal{V}_n^z)_{0 \leq n \leq N-1}$. Namely, the \mathbb{R}^d -valued random variable \mathcal{Z}_{t_n} will be approximated by

$$\sum_{k=1}^{K_n^z} \psi_n^k(X_{t_n}) \mathfrak{z}^{n,k}, \quad (2.6)$$

where $\mathfrak{z}^{n,k} \in \mathbb{R}^d$ for any $1 \leq k \leq K_n^z$ and $0 \leq n \leq N-1$. Importantly, we denote, for later use, $\mathfrak{z}^\top := ((\mathfrak{z}^{n,k})^\top)_{0 \leq n \leq N-1, 1 \leq k \leq K_n^z}$ so that $\mathfrak{z} \in \mathbb{R}^{d\bar{K}^z}$.

Definition 2.1 (Class of discrete control process). *We let $\mathcal{H}^{\pi,\psi}$ be the set of discrete control process Z defined by: for $\mathfrak{z} \in \mathbb{R}^{d\bar{K}^z}$,*

$$Z_{t_n} := \sum_{k=1}^{K_n^z} \psi_n^k(X_{t_n}) \mathfrak{z}^{n,k}, \quad \text{for } 0 \leq n \leq N-1, \quad (2.7)$$

and where we set $Z_t = Z_{t_n}$, $t_n \leq t < t_{n+1}$, $0 \leq n \leq N-1$ with the convention $Z_T = 0$.

Remark 2.1. *We insist on the fact that for a given $Z \in \mathcal{H}^{\pi,\psi}$, the \mathbb{R}^d -valued random variable Z_{t_n} depends only on \mathfrak{z}^n , for any $0 \leq n \leq N-1$. The approximation space we consider is a finite dimensional vector space. This notably differs from the recent works [3, 31, 37] where a non-linear approximation using neural network is used.*

The dynamics of \mathcal{Y} given by (1.4), in turn, has to be approximated. As previously mentioned in the introduction, we first rewrite it in forward form as follows

$$\mathcal{Y}_t = \mathcal{Y}_0 - \int_0^t f(\mathcal{Y}_s, \mathcal{Z}_s) ds + \int_0^t \mathcal{Z}_s \cdot d\mathcal{W}_s, \quad t \in [0, T], \quad \text{with } \mathcal{Y}_0 = u(0, \mathcal{X}_0).$$

The main goal of the algorithm is to obtain a good estimate of $u(0, \cdot)$ on the support of \mathcal{X}_0 . In order to do so, we define the starting point of Y , standing for the approximation of \mathcal{Y} , by using a linear functional approximation space denoted \mathcal{Y}^y , namely

$$Y_0 := \sum_{k=1}^{K^y} \psi_y^k(X_0) \mathfrak{y}^k \quad \text{with } \mathfrak{y} \in \mathbb{R}^{K^y}. \quad (2.8)$$

The specification of \mathcal{Y}^y will depend also on the nature of \mathcal{X}_0 . Namely, if Assumption 2.1(i) holds, then we set $K^y = K$, while if Assumption 2.1(ii) holds, then we simply set $K^y = 1$ and ψ_y^1 is a function satisfying $\psi_y^1(x_0) = 1$.

Then, employing a standard Euler scheme on π together with the above approximation $Z \in \mathcal{H}^{\pi,\psi}$ of the control process \mathcal{Z} , we are naturally led to consider the following approximation scheme for \mathcal{Y} .

Definition 2.2. *i) Given $\mathfrak{u} = (\mathfrak{y}, \mathfrak{z}) \in \mathbb{R}^{K^y} \times \mathbb{R}^{d\bar{K}^z}$, we denote by $Z^u \in \mathcal{H}^{\pi,\psi}$ the discrete control process as given in (2.7). Then, the discrete controlled process Y^u is defined as follows.*

(a) *Initialization: Set*

$$Y_0^u = \sum_{k=1}^K \psi_y^k(X_0) \mathfrak{y}^k. \quad (2.9)$$

(b) *Discrete version: for any $0 \leq n \leq N-1$:*

$$Y_{t_{n+1}}^u = Y_{t_n}^u - hf(Y_{t_n}^u, Z_{t_n}^u) + Z_{t_n}^u \cdot \Delta W_n \quad (2.10)$$

where we recall that $\Delta W_n = W_{t_{n+1}} - W_{t_n}$.

(c) *Continuous version:* for any $0 \leq n \leq N-1$ and any $t_n \leq t < t_{n+1}$,

$$Y_t^u = Y_{t_n}^u - (t - t_n)f(Y_{t_n}^u, Z_{t_n}^u) + Z_{t_n}^u \cdot (W_t - W_{t_n}) \quad (2.11)$$

ii) Based on the previous step, we define $\mathcal{B}^{\pi, \psi} \subset \mathcal{B}^2$ as the set of processes (Y^u, Z^u) , with $Z^u \in \mathcal{H}^{\pi, \psi}$, Y^u defined as above for some $u \in \mathbb{R}^{K^y} \times \mathbb{R}^{d\bar{K}^z}$.

Remark 2.2. Let us note that the discrete process $(X_t, Y_t^u, Z_t^u)_{t \in \pi}$ depends on \mathcal{X}_0 and $(W_t)_{t \in \pi}$ but we omit these dependences in the notation.

The main idea of *approximation by learning* methods is to force the discrete controlled process Y_T^u at maturity T to match the approximated terminal condition $g(X_T)$, by minimizing a loss function. Here, we work with the quadratic loss function, so that one faces the optimization problem

$$\inf_{u=(\mathfrak{y}, \mathfrak{z}) \in \mathbb{R}^{K^y} \times \mathbb{R}^{d\bar{K}^z}} \mathfrak{g}(u) := \mathbb{E}[G(\mathcal{X}_0, W, u)] \quad \text{with } G(\mathcal{X}_0, W, u) = |g(X_T) - Y_T^u|^2. \quad (2.12)$$

However, one has to come up with a numerical procedure to compute the solution in practice.

In order to numerically compute a solution to the optimization problem (2.12) (if any exists), one generally employs a stochastic approximation scheme such as a SGD algorithm. For an overview of the theory of stochastic approximation, the reader may refer to [19], [39] and [6] and to [3, 20, 31, 37, 30] for applications to deep learning approximation of PDEs.

We now describe the SGD algorithm that we implement in order to compute a solution $(\mathfrak{y}, \mathfrak{z}) \in \mathbb{R}^{K^y} \times \mathbb{R}^{d\bar{K}^z}$ to the optimization problem (2.12).

For a prescribed positive integer M representing the number of steps in the stochastic algorithm and two deterministic non increasing sequences of positive real number $(\gamma_m^y)_{m \geq 1}$ and $(\gamma_m^z)_{m \geq 1}$ representing the learning rates, we design the following *direct algorithm*.

Definition 2.3. (*Implemented direct algorithm*)

1. Simulate M independent discrete paths of the Brownian motion $\mathfrak{W} = (W^m)_{1 \leq m \leq M}$ and M independent samples of the initial condition $(\mathcal{X}_0^m)_{1 \leq m \leq M}$.
2. Initialization: select a random vector $u_0 = (\mathfrak{y}_0, \mathfrak{z}_0)$ with values in $\mathbb{R}^{K^y} \times \mathbb{R}^{d\bar{K}^z}$, independent of \mathfrak{W} and $(\mathcal{X}_0^m)_{1 \leq m \leq M}$, and such that $\mathbb{E}[|u_0|^2] < \infty$.
3. Iteration: For $0 \leq m \leq M-1$, compute

$$\mathfrak{y}_{m+1} = \mathfrak{y}_m - \gamma_{m+1}^y \nabla_{\mathfrak{y}} G(\mathcal{X}_0^{m+1}, W^{m+1}, u_m), \quad (2.13)$$

$$\mathfrak{z}_{m+1}^n = \mathfrak{z}_m^n - \gamma_{m+1}^z \nabla_{\mathfrak{z}^n} G(\mathcal{X}_0^{m+1}, W^{m+1}, u_m), \quad (2.14)$$

for $0 \leq n \leq N-1$.

The output of the algorithm is then $u_M = (\mathfrak{y}_M, \mathfrak{z}_M)$.

Remark 2.3. In order to analyse the asymptotic properties of stochastic approximation schemes, one usually chooses the learning sequences $(\gamma_m)_{m \geq 1} = (\gamma_m^y)_{m \geq 1}$ or $(\gamma_m)_{m \geq 1} = (\gamma_m^z)_{m \geq 1}$ such that

$$\sum_{m \geq 1} \gamma_m = \infty \quad \text{and} \quad \sum_{m \geq 1} \gamma_m^2 < \infty, \quad (2.15)$$

see e.g. [19, 39, 6].

The following lemma, whose proof is postponed to Section 4.2, provides the analytic expression of the local gradient functions $\nabla_\lambda G(\mathcal{X}_0, W, \mathbf{u})$, $\lambda \in \{\mathfrak{y}, \mathfrak{z}^n, 0 \leq n \leq N-1\}$ appearing in the above SGD algorithm. It shows that $(\mathfrak{y}_{m+1}, \mathfrak{z}_{m+1})$ can be easily computed once $(Y^{\mathbf{u}_m}, Z^{\mathbf{u}_m})$ have been simulated for any $0 \leq m \leq M-1$.

Lemma 2.2. *For $\lambda \in \{\mathfrak{y}^k, 1 \leq k \leq K^y\} \cup \{\mathfrak{z}^{n,k}, 1 \leq k \leq K_n^z, 0 \leq n \leq N-1\}$ and $\mathbf{u} = (\mathfrak{y}, \mathfrak{z}) \in \mathbb{R}^{K^y} \times \mathbb{R}^{d\bar{K}^z}$, it holds*

$$\nabla_\lambda G(\mathcal{X}_0, W, \mathbf{u}) = -2(g(X_T) - Y_T^{\mathbf{u}}) \nabla_\lambda Y_T^{\mathbf{u}} \quad (2.16)$$

with

$$\nabla_{\mathfrak{y}^k} Y_T^{\mathbf{u}} = \psi_y^k(X_0) \prod_{l=0}^{N-1} (1 - h \nabla_y f(Y_{t_l}^{\mathbf{u}}, Z_{t_l}^{\mathbf{u}})), \quad 1 \leq k \leq K^y,$$

and for any $0 \leq n \leq N-1$ and any $1 \leq k \leq K_n^z$,

$$\nabla_{\mathfrak{z}^{n,k}} Y_T^{\mathbf{u}} = \psi_n^k(X_{t_n}) (\Delta W_n^\top - h \nabla_z f(Y_{t_n}^{\mathbf{u}}, Z_{t_n}^{\mathbf{u}})) \prod_{l=n+1}^{N-1} (1 - h \nabla_y f(Y_{t_l}^{\mathbf{u}}, Z_{t_l}^{\mathbf{u}}))$$

with the convention $\prod_{\emptyset} = 1$.

Under Assumption 2.1, Assumption 2.2 (i) and Assumption 2.3, the well-posedness of Algorithm 2.3, that is, the fact that it holds

$$\arg \min_{\mathbf{u} \in \mathbb{R}^{K^y} \times \mathbb{R}^{d\bar{K}^z}} \mathbf{g}(\mathbf{u}) \neq \emptyset,$$

is proved in Lemma 4.1.

Additionally, for any $\mathbf{u}^* \in \arg \min_{\mathbf{u} \in \mathbb{R}^{K^y} \times \mathbb{R}^{d\bar{K}^z}} \mathbf{g}(\mathbf{u})$, we show in Proposition 4.2 that

$$\mathbb{E} \left[|u(0, \mathcal{X}_0) - Y_0^{\mathbf{u}^*}|^2 + h \sum_{n=0}^{N-1} |\mathcal{Z}_{t_n} - Z_{t_n}^{\mathbf{u}^*}|^2 \right] \leq C (\mathcal{E}_\pi + \mathcal{E}_\psi),$$

for some positive constant C . The quantities \mathcal{E}_π and \mathcal{E}_ψ represents the discrete-time error and the error due to the approximation in the functional spaces $(\mathcal{Y}^y, \mathcal{Y}_n^z)$, respectively. They are defined by

$$\mathcal{E}_\pi := \mathbb{E} \left[\sum_{n=0}^{N-1} \int_{t_n}^{t_{n+1}} (|\mathcal{Y}_s - \mathcal{Y}_{t_n}|^2 + |\mathcal{Z}_s - \mathcal{Z}_{t_n}|^2 + |\mathcal{X}_{t_n} - X_{t_n}|^2) ds \right] \quad (2.17)$$

and

$$\mathcal{E}_\psi := \inf_{\mathbf{u} \in \mathbb{R}^{K^y} \times \mathbb{R}^{d\bar{K}^z}} \mathbb{E} \left[|u(0, \mathcal{X}_0) - Y_0^{\mathbf{u}}|^2 + \sum_{n=0}^{N-1} h |(\sigma^\top \nabla_x u)(t_n, X_{t_n}) - Z_{t_n}^{\mathbf{u}}|^2 \right]. \quad (2.18)$$

Let us mention, for later use, that, in the setting of Assumptions 2.1 and 2.2(i),

$$\mathcal{E}_\pi \leq Ch, \quad (2.19)$$

for some positive constant C , see e.g. Ma and Zhang [41] and Pagès [43].

We shall not seek to obtain theoretical convergence results for the *direct algorithm* itself. However, we illustrate its performance numerically in Section 3 when using sparse grids approximations [12].

Remark 2.4. The numerical complexity \mathcal{C} will be measured by the number of coefficients update realized to obtain the approximation. From the previous description, we obtain straightforwardly that the complexity at worst satisfies

$$\mathcal{C} = O_d(NKM) . \quad (2.20)$$

2.3 A Picard algorithm

An issue with the above algorithm comes from the fact that the optimization problem (2.12) is generally not convex. Even though $\mathbf{u} \mapsto (Y_0^{\mathbf{u}}, Z^{\mathbf{u}})$ is linear for our choice of parametrisation, in general the mapping $\mathbf{u} \mapsto Y^{\mathbf{u}}$ is non-linear since f itself is non-linear. As a consequence, in practical implementation, we have no guarantee that the algorithm converges to local or global minima. On top of practical problems, this renders the theoretical analysis of the implemented *direct algorithm* difficult, in particular if one wants to obtain rates of convergence to assess precisely the numerical complexity of the method.

In this section, we introduce a *Picard algorithm* which transforms this non-convex optimisation problem into a sequence of linear-quadratic optimization problems. This is done by using the special structure of the original problem. Indeed, it is well known that the solution of the BSDE (1.4) itself is obtained as the limit of a sequence of Picard iterations, see e.g. [21] and [5] from a numerical perspective.

2.3.1 Theoretical Picard algorithm

Our *Picard algorithm* is based on the iteration of the following operator:

$$\mathbb{R}^{K^y} \times \mathbb{R}^{d\bar{K}^z} \ni \tilde{\mathbf{u}} \mapsto \Phi(\tilde{\mathbf{u}}) := \check{\mathbf{u}} \in \mathbb{R}^{K^y} \times \mathbb{R}^{d\bar{K}^z} \quad (2.21)$$

where,

$$\check{\mathbf{u}} = \arg \min_{\mathbf{u} \in \mathbb{R}^{K^y} \times \mathbb{R}^{d\bar{K}^z}} \mathbb{E} \left[|g(X_T) - U_T^{\check{\mathbf{u}}, \mathbf{u}}|^2 \right] . \quad (2.22)$$

In the above expectation, the process X is the Euler-Maruyama approximation scheme on the time grid π with dynamics (2.3) and $U^{\tilde{\mathbf{u}}, \mathbf{u}}$ (simply denoted as U below) is given by the following decoupling approximation scheme:

1. For $\tilde{\mathbf{u}} \in \mathbb{R}^{K^y} \times \mathbb{R}^{d\bar{K}^z}$, we first consider $(Y^{\tilde{\mathbf{u}}}, Z^{\tilde{\mathbf{u}}}) \in \mathcal{B}^{\pi, \psi}$ as introduced in Definition 2.2.
2. Then, for any $\mathbf{u} \in \mathbb{R}^{K^y} \times \mathbb{R}^{d\bar{K}^z}$, consider the discrete control process $Z^{\mathbf{u}} \in \mathcal{H}^{\pi, \psi}$ as introduced in (2.7) of Definition 2.1 and define the control process $U^{\tilde{\mathbf{u}}, \mathbf{u}}$ by

$$U_0^{\tilde{\mathbf{u}}, \mathbf{u}} = Y_0^{\mathbf{u}} \quad (2.23)$$

recall (2.9) and for any $0 \leq n \leq N-1$,

$$U_{t_{n+1}}^{\tilde{\mathbf{u}}, \mathbf{u}} = U_{t_n}^{\tilde{\mathbf{u}}, \mathbf{u}} - hf(Y_{t_n}^{\tilde{\mathbf{u}}}, Z_{t_n}^{\tilde{\mathbf{u}}}) + Z_{t_n}^{\mathbf{u}} \cdot (W_{t_{n+1}} - W_{t_n}) , \quad (2.24)$$

and its continuous version, for any $t_n \leq t \leq t_{n+1}$,

$$U_t^{\tilde{\mathbf{u}}, \mathbf{u}} = U_{t_n}^{\tilde{\mathbf{u}}, \mathbf{u}} - (t - t_n)f(Y_{t_n}^{\tilde{\mathbf{u}}}, Z_{t_n}^{\tilde{\mathbf{u}}}) + Z_{t_n}^{\mathbf{u}} \cdot (\mathcal{W}_t - W_{t_n}) .$$

Note that under Assumption 2.2(i) it holds $\mathbb{E}\left[\sup_{t \in [0, T]} |U_t^{\tilde{\mathbf{u}}, \mathbf{u}}|^2\right] < +\infty$.

Definition 2.4 (Theoretical Picard algorithm). *For a prescribed positive integer P :*

1. *Initialization:* set $\mathbf{u}^0 \in \mathbb{R}^{K^y} \times \mathbb{R}^{d\bar{K}^z}$.
2. *Iteration:* for $1 \leq p \leq P$, compute: $\mathbf{u}^p = \Phi(\mathbf{u}^{p-1})$.

The output of the algorithm is then \mathbf{u}^P .

2.3.2 Well-posedness of the theoretical algorithm

The main novelty compared to the optimization problem (2.12) comes from the fact that the map $\mathbf{u} \mapsto U^{\tilde{\mathbf{u}}, \mathbf{u}}$ is now linear. This linearity is achieved by freezing the driver f in the dynamics of the control process along the process $(Y^{\tilde{\mathbf{u}}}, Z^{\tilde{\mathbf{u}}}) \in \mathcal{B}^{\pi, \psi}$. The parameter $\tilde{\mathbf{u}} \in \mathbb{R}^{K^y} \times \mathbb{R}^{d\bar{K}^z}$ is then updated through the Picard iteration procedure. This is of course the main purpose of this *Picard algorithm*, compared to the *direct algorithm* of Section 2.2. At this stage, the above algorithm is theoretical and its solution (if any exists) still needs to be numerically approximated. This will be discussed in full details in the next section.

We here discuss the well-posedness of the optimization problem (2.22). We first introduce some notations that will be useful in the sequel to study the *Picard algorithm* as iterated least-square optimization problems.

First, to clarify the linear structure, we introduce the following notations

- i) For $1 \leq k \leq K^y$, $\theta^k := \psi_y^k(X_0)$.
- ii) For $0 \leq n \leq N-1$, $1 \leq k \leq K$, the \mathbb{R}^d -valued random vectors $\omega^{n,k}$ is defined by

$$\omega^{n,k} = \Psi^{n,k} \Delta W_n \text{ with } \Psi^{n,k} = \psi_n^k(X_{t_n}), \quad (2.25)$$

and we set $\omega^\top := ((\omega^{n,k})^\top)_{0 \leq n \leq N-1, 1 \leq k \leq K^z}$ (so that ω is an $\mathbb{R}^{d\bar{K}^z}$ -valued random vector).

- iii) the random vector $\Omega = (\theta^\top, \omega^\top)^\top$ which takes values in $\mathbb{R}^{K^y} \times \mathbb{R}^{d\bar{K}^z}$.

Note that both ω and Ω depends on W and \mathcal{X}_0 , but we will omit this in the notation. Then, we rewrite

$$g(X_T) - U_T^{\tilde{\mathbf{u}}, \mathbf{u}} = \mathfrak{G}^{\tilde{\mathbf{u}}} - \mathbf{u} \cdot \Omega \quad (2.26)$$

where

$$\mathfrak{G}^{\tilde{\mathbf{u}}} = \mathfrak{G}^{\tilde{\mathbf{u}}}(\mathcal{X}_0, W) := g(X_T) + \sum_{n=0}^{N-1} hf(Y_{t_n}^{\tilde{\mathbf{u}}}, Z_{t_n}^{\tilde{\mathbf{u}}}). \quad (2.27)$$

Thus, the optimization problem (2.22) is given by

$$\tilde{\mathbf{u}} = \operatorname{argmin}_{\mathbf{u} \in \mathbb{R}^{K^y} \times \mathbb{R}^{d\bar{K}^z}} \mathfrak{H}(\tilde{\mathbf{u}}, \mathbf{u}) \quad \text{with} \quad \mathfrak{H}(\tilde{\mathbf{u}}, \mathbf{u}) := \mathbb{E}\left[|\mathfrak{G}^{\tilde{\mathbf{u}}} - \mathbf{u} \cdot \Omega|^2\right] \quad (2.28)$$

and simply reads as a Linear-Quadratic optimization problem. Classically, we introduce semi-norms on the parameter spaces.

Definition 2.5. For $\mathbf{u} = (\mathfrak{y}, \mathfrak{z}) \in \mathbb{R}^{K^y} \times \mathbb{R}^{d\bar{K}^z}$, we define

$$\|\mathfrak{y}\|_y^2 := \mathbb{E}[|\mathfrak{y} \cdot \theta|^2], \quad \|\mathfrak{z}\|_z^2 := \mathbb{E}[|\mathfrak{z} \cdot \omega|^2] \quad \text{and} \quad \|\mathbf{u}\|^2 := \mathbb{E}[|\mathbf{u} \cdot \Omega|^2].$$

Let us insist on the fact that these quantities depend on the choices of π, ψ though this is not reflected in the notation.

Remark 2.5. i) Observe that from the very definition of the random vector Ω , for any $\mathbf{u} = (\mathfrak{y}, \mathfrak{z}) \in \mathbb{R}^{K^y} \times \mathbb{R}^{d\bar{K}^z}$, it holds

$$\|\mathbf{u}\|^2 = \|\mathfrak{y}\|_y^2 + \|\mathfrak{z}\|_z^2. \quad (2.29)$$

ii) With the notations of Section 2.2, the following relations hold

$$\|\mathbf{u}\|^2 = \mathbb{E}\left[\left|Y_0^{\mathbf{u}} + \int_0^T Z_t^{\mathbf{u}} d\mathcal{W}_t\right|^2\right], \quad \|\mathfrak{y}\|_y^2 = \mathbb{E}[|Y_0^{\mathbf{u}}|^2] \quad \text{and} \quad \|\mathfrak{z}\|_z^2 = \sum_{n=0}^{N-1} h \mathbb{E}[|Z_{t_n}^{\mathbf{u}}|^2], \quad (2.30)$$

for any $\mathbf{u} = (\mathfrak{y}, \mathfrak{z}) \in \mathbb{R}^{K^y} \times \mathbb{R}^{d\bar{K}^z}$.

iii) For later use, see Section 2.3.3, we also note that $\|\cdot\|_z$ develops as

$$\|\mathfrak{z}\|_z^2 = \sum_{n=0}^{N-1} h \sum_{l=1}^d (\mathfrak{z}_l^{n,\cdot})^\top \mathbb{E}[\Psi^{n,\cdot} (\Psi^{n,\cdot})^\top] \mathfrak{z}_l^{n,\cdot} \quad (2.31)$$

by using the independence of the increments $(\Delta W_n)_l$, for $0 \leq n \leq N-1$ and $l \in \{1, \dots, d\}$ and where we used the notations $\mathfrak{z}_l^{n,\cdot} = (\mathfrak{z}_l^{n,1}, \dots, \mathfrak{z}_l^{n,K_n^z})$ and $\Psi^{n,\cdot} = (\Psi^{n,1}, \dots, \Psi^{n,K_n^z})$.

A key assumption to ensure the well-posedness of our approach is the following.

Assumption 2.3. There exist two positive constants $\kappa_K \geq 1 \geq \alpha_K$ such that for any $(\mathfrak{y}, \mathfrak{z}) \in \mathbb{R}^{K^y} \times \mathbb{R}^{d\bar{K}^z}$

$$\alpha_K |\mathfrak{y}|^2 \leq \|\mathfrak{y}\|_y^2 \leq \kappa_K |\mathfrak{y}|^2 \quad \text{and} \quad h \alpha_K |\mathfrak{z}|^2 \leq \|\mathfrak{z}\|_z^2 \leq h \kappa_K |\mathfrak{z}|^2.$$

Lemma 2.3. For all $(\tilde{\mathbf{u}}, \mathbf{u}) \in \left(\mathbb{R}^{K^y} \times \mathbb{R}^{d\bar{K}^z}\right)^2$, it holds

$$\mathbf{u}^\top \nabla_{\tilde{\mathbf{u}}}^2 \mathfrak{H}(\tilde{\mathbf{u}}, \mathbf{u}) \mathbf{u} = 2 \|\mathbf{u}\|^2, \quad (2.32)$$

where $\nabla_{\tilde{\mathbf{u}}}^2 \mathfrak{H}$ denotes the Hessian of the function $\mathbf{u} \mapsto \mathfrak{H}(\tilde{\mathbf{u}}, \mathbf{u})$.

Moreover, under Assumption 2.3, the optimization problem (2.22) admits a unique solution and for any $\tilde{\mathbf{u}} \in \mathbb{R}^{K^y} \times \mathbb{R}^{d\bar{K}^z}$ and $(\mathfrak{y}, \mathfrak{z}) \in \mathbb{R}^{K^y} \times \mathbb{R}^{d\bar{K}^z}$, it holds

$$(\mathfrak{y} - \check{\mathfrak{y}}) \cdot \nabla_{\mathfrak{y}} \mathfrak{H}(\tilde{\mathbf{u}}, \mathbf{u}) = 2 \|\mathfrak{y} - \check{\mathfrak{y}}\|_y^2 \geq 2 \alpha_K |\mathfrak{y} - \check{\mathfrak{y}}|^2 \quad (2.33)$$

$$(\mathfrak{z} - \check{\mathfrak{z}}) \cdot \nabla_{\mathfrak{z}} \mathfrak{H}(\tilde{\mathbf{u}}, \mathbf{u}) = 2 \|\mathfrak{z} - \check{\mathfrak{z}}\|_z^2 \geq 2 h \alpha_K |\mathfrak{z} - \check{\mathfrak{z}}|^2 \quad (2.34)$$

where $\check{\mathbf{u}} = (\check{\mathfrak{y}}, \check{\mathfrak{z}}) \in \mathbb{R}^{K^y} \times \mathbb{R}^{d\bar{K}^z}$ is the unique solution to (2.22).

Proof. From (2.28), we straightforwardly compute

$$\nabla_{\mathbf{u}} \mathfrak{H}(\tilde{\mathbf{u}}, \mathbf{u}) = -2\mathbb{E}[(\mathfrak{G}^{\tilde{\mathbf{u}}} - \mathbf{u} \cdot \Omega)\Omega] \quad \text{and} \quad \nabla_{\mathbf{u}}^2 \mathfrak{H}(\tilde{\mathbf{u}}, \mathbf{u}) = 2\mathbb{E}[\Omega\Omega^\top] \quad (2.35)$$

which, recalling Definition 2.5, directly yields (2.32). In particular, we have

$$\nabla_{\boldsymbol{\eta}} \mathfrak{H}(\tilde{\mathbf{u}}, \mathbf{u}) = -2\mathbb{E}[(\mathfrak{G}^{\tilde{\mathbf{u}}} - \mathbf{u} \cdot \Omega)\theta] = -2\mathbb{E}[(\mathfrak{G}^{\tilde{\mathbf{u}}} - \boldsymbol{\eta} \cdot \theta)\theta] \quad (2.36)$$

and, for any $0 \leq n \leq N-1$ and any $1 \leq l \leq d$,

$$\nabla_{\mathfrak{z}_l^{n,\cdot}} \mathfrak{H}(\tilde{\mathbf{u}}, \mathbf{u}) = -2\mathbb{E}[(\mathfrak{G}^{\tilde{\mathbf{u}}} - \Omega \cdot \mathbf{u})\omega_l^{n,\cdot}] = -2\mathbb{E}[(\mathfrak{G}^{\tilde{\mathbf{u}}} - \omega_l^{n,\cdot} \cdot \mathfrak{z}_l^{n,\cdot})\omega_l^{n,\cdot}]. \quad (2.37)$$

Under Assumption 2.3, we deduce from (2.32) that the problem is strictly convex and has a unique (global) minimum $\tilde{\mathbf{u}} = (\tilde{\boldsymbol{\eta}}, \tilde{\mathfrak{z}})$. The inequalities (2.33) and (2.34) then follow from (2.36) and (2.37) combined with the fact that $\nabla_{\tilde{\mathfrak{z}}} \mathfrak{H}(\tilde{\mathbf{u}}, \tilde{\mathbf{u}}) = 0$. \square

2.3.3 Algorithm implementation

From a practical point of view, the sequence of theoretical Linear-Quadratic optimization problem described in the previous section has to be approximated. Due to the possibly high dimension of the matrix $\mathbb{E}[\Omega\Omega^\top]$, we will rely on a SGD algorithm¹ to compute the unique solution to (2.22). Indeed, for a fixed vector $\tilde{\mathbf{u}}$ in $\mathbb{R}^{K^y} \times \mathbb{R}^{d\bar{K}^z}$, the key point is to observe that the unique minimizer $\tilde{\mathbf{u}}$ is the unique solution to the equation

$$\nabla_{\mathbf{u}} \mathfrak{H}(\tilde{\mathbf{u}}, \mathbf{u}) = 0. \quad (2.38)$$

We importantly remark, using (2.36) and (2.37) that the above relation (2.38) holds true if and only if

$$\mathbb{E}[H^y(\mathcal{X}_0, W, \tilde{\mathbf{u}}, \boldsymbol{\eta})] = 0, \quad \text{and} \quad \mathbb{E}[H^{n,l}(\mathcal{X}_0, W, \tilde{\mathbf{u}}, \mathfrak{z}_l^{n,\cdot})] = 0, \quad (2.39)$$

where H^y is a map from $\mathbb{R}^d \times (\mathbb{R}^d)^N \times (\mathbb{R}^{K^y} \times \mathbb{R}^{d\bar{K}^z}) \times \mathbb{R}^{K^y}$ to \mathbb{R}^{K^y} and defined by

$$H^y(\mathcal{X}_0, W, \tilde{\mathbf{u}}, \boldsymbol{\eta}) := -\frac{2}{\beta_K}(\mathfrak{G}^{\tilde{\mathbf{u}}} - \boldsymbol{\eta} \cdot \theta)\theta, \quad (2.40)$$

and $H^{n,l}$ are maps defined on $\mathbb{R}^d \times (\mathbb{R}^d)^N \times (\mathbb{R}^{K^y} \times \mathbb{R}^{d\bar{K}^z}) \times \mathbb{R}^{K_n^z}$ taking values in $\mathbb{R}^{K_n^z}$ and given by

$$H^{n,l}(\mathcal{X}_0, W, \tilde{\mathbf{u}}, \mathfrak{z}_l^{n,\cdot}) := -\frac{2}{\beta_K \sqrt{h}}(\mathfrak{G}^{\tilde{\mathbf{u}}} - \omega_l^{n,\cdot} \cdot \mathfrak{z}_l^{n,\cdot})\omega_l^{n,\cdot}, \quad 0 \leq n \leq N-1, \quad 1 \leq l \leq d. \quad (2.41)$$

We importantly point out that we abuse the notation in (2.40) and (2.41) since the variable (\mathcal{X}_0, W) stands for a vector of $\mathbb{R}^d \times (\mathbb{R}^d)^N$ and $(\mathcal{X}_0, W) \mapsto \mathfrak{G}^{\tilde{\mathbf{u}}} = \mathfrak{G}^{\tilde{\mathbf{u}}}(\mathcal{X}_0, W)$ is also defined by (2.27) while in (2.39) the random vector $W = (\mathcal{W}_{t_n})_{1 \leq n \leq N}$ stands for the discrete path of the Brownian motion \mathcal{W} and \mathcal{X}_0 for the starting value of X .

¹Since it is also the procedure used for the *direct algorithm*, the numerical comparison between the two will be more relevant.

In (2.40) and (2.41), the deterministic constant β_K corresponding to a normalizing factor is introduced in order to control the $L^2(\mathbb{P})$ -moment of the random vectors $(\mathfrak{G}^{\tilde{\mathbf{u}}} - \mathfrak{y} \cdot \theta)\theta$ and $(\mathfrak{G}^{\tilde{\mathbf{u}}} - \omega_l^{n,\cdot} \cdot \mathfrak{z}_l^{n,\cdot})\omega_l^{n,\cdot}$. Namely, we select β_K large enough so that

$$(\beta_K)^2 \geq (1 + \mathbb{E}[|\theta|^4]) \vee \max_{0 \leq n \leq N-1, 1 \leq l \leq d} (1 + \mathbb{E}[|\tilde{\omega}_l^{n,\cdot}|^4]) \quad (2.42)$$

with $\tilde{\omega}_l^{n,\cdot} = \frac{\omega_l^{n,\cdot}}{\sqrt{h}}$. Let us insist on the fact that the chosen β_K above should be uniform for all time grid π . It depends only on the level of approximation coming from the definition of the approximation spaces. This qualitative level of approximation is controlled by the number of basis function per time step, namely K .

For latter use, comparing (2.40) to (2.36) and (2.41) to (2.37), we remark that

$$\mathbb{E}[H^y(\mathcal{X}_0, W, \tilde{\mathbf{u}}, \mathfrak{y})] = \frac{1}{\beta_K} \nabla_{\mathfrak{y}} \mathfrak{H}(\tilde{\mathbf{u}}, \mathbf{u}) \quad \text{and} \quad \mathbb{E}[H^{n,l}(\mathcal{X}_0, W, \tilde{\mathbf{u}}, \mathfrak{z}_l^{n,\cdot})] = \frac{1}{\beta_K \sqrt{h}} \nabla_{\mathfrak{z}_l^{n,\cdot}} \mathfrak{H}(\tilde{\mathbf{u}}, \mathbf{u}), \quad (2.43)$$

for $0 \leq n \leq N-1$, $l \in \{1, \dots, d\}$ and $(\tilde{\mathbf{u}}, \mathbf{u}) \in (\mathbb{R}^{K^y} \times \mathbb{R}^{d\bar{K}^z})^2$.

The implemented *Picard algorithm* is obtained by iterating a stochastic gradient operator which is the counterpart of Φ defined by (2.21) obtained by the numerical approximation that we now introduce.

Definition 2.6. Let M be a positive integer. Let $\mathfrak{W} := (W^m)_{1 \leq m \leq M}$, be M discrete paths along the time grid π of the Brownian motion \mathcal{W} , $\mathfrak{X}_0 := (\mathcal{X}_0^m)_{1 \leq m \leq M}$, be M independent samples of the initial condition (and independent from \mathfrak{W}) and $(\gamma_m)_{m \geq 1}$ a deterministic sequence of positive real numbers satisfying:

$$\sum_{m \geq 1} \gamma_m = \infty \quad \text{and} \quad \sum_{m \geq 1} \gamma_m^2 < \infty. \quad (2.44)$$

We set, for all $m \geq 1$,

$$\gamma_m^y = \gamma_m \quad \text{and} \quad \gamma_m^z = \frac{\gamma_m}{\sqrt{h}}. \quad (2.45)$$

Let $\mathbf{u}_0 = (\mathfrak{y}_0, \mathfrak{z}_0)$ be a random vector taking values in $\mathbb{R}^{K^y} \times \mathbb{R}^{d\bar{K}^z}$, independent of $(\mathfrak{X}_0, \mathfrak{W})$ and such that $\mathbb{E}[|\mathbf{u}_0|^2] < \infty$.

The operator Φ_M , parametrized by $(\mathbf{u}_0, \mathfrak{X}_0, \mathfrak{W})$, is given by

$$\mathbb{R}^{K^y} \times \mathbb{R}^{d\bar{K}^z} \ni \tilde{\mathbf{u}} \mapsto \Phi_M(\mathbf{u}_0, \mathfrak{X}_0, \mathfrak{W}, \tilde{\mathbf{u}}) = \mathbf{u}_M \quad (2.46)$$

where \mathbf{u}_M is the output of the SGD algorithm after M steps and is obtained as follows:

1. The initial value is set to \mathbf{u}_0 .

2. Iteration: For $0 \leq m \leq M-1$, compute

$$\mathfrak{y}_{m+1} = \mathfrak{y}_m - \gamma_{m+1}^y H^y(\mathcal{X}_0^{m+1}, W^{(m+1)}, \tilde{\mathbf{u}}, \mathfrak{y}_m), \quad (2.47)$$

and

$$\mathfrak{z}_{l,m+1}^{n,\cdot} = \mathfrak{z}_{l,m}^{n,\cdot} - \gamma_{m+1}^z H^{n,l}(\mathcal{X}_0^{m+1}, W^{(m+1)}, \tilde{\mathbf{u}}, \mathfrak{z}_{l,m}^{n,\cdot}), \quad (2.48)$$

for any $0 \leq n \leq N-1$ and any $1 \leq l \leq d$.

Definition 2.7 (Implemented Picard algorithm). For a prescribed positive integer P :

1. Initialization: Select a random vector \mathbf{u}_0^0 taking values in $\mathbb{R}^{K^y} \times \mathbb{R}^{d\bar{K}^z}$ such that $\mathbb{E}[|\mathbf{u}_0^0|^2] < \infty$. Set $\mathbf{u}_M^0 := \mathbf{u}_0^0$.
2. Iteration: for $1 \leq p \leq P$, simulate independently a set of M independent discrete paths \mathfrak{W}^p of the Brownian motion \mathcal{W} , independent initial condition \mathfrak{X}_0^p and an initial starting point \mathbf{u}_0^p (independently also of \mathbf{u}_0^0 , \mathbf{u}_0^j and of the previous $(\mathfrak{X}_0^j, \mathfrak{W}^j)$, $1 \leq j \leq p-1$), and compute $\mathbf{u}_M^p := \Phi_M(\mathbf{u}_0^p, \mathfrak{X}_0^p, \mathfrak{W}^p, \mathbf{u}_M^{p-1})$ as in Definition 2.6.

The output of the algorithm is then \mathbf{u}_M^P .

Remark 2.6. i) The choice of the learning sequence γ for the SGD algorithm (2.47), (2.48) might be delicate in practice, see e.g. Section 3.1.3.

ii) The initialisation is random in the above algorithm. We do not always follow this procedure in our numerical experiments, see Section 3.

iii) The numerical complexity \mathcal{C} of the full algorithm is the sum of the local complexity of each SGD algorithm so that

$$\mathcal{C} = O_d(PNKM). \quad (2.49)$$

Using the output \mathbf{u}_M^P of the Picard algorithm, we set the approximating function at time 0 to be:

$$\mathcal{U}_M^P(x) := \sum_{k=1}^{K^y} (\mathfrak{h}_M^P)^k \psi_y^k(x), \quad (2.50)$$

recalling (2.8).

We then aim to control the following mean squared error:

$$\mathcal{E}_{\text{MSE}} := \mathbb{E} \left[|\mathcal{U}_M^P(\mathcal{X}_0) - u(0, \mathcal{X}_0)|^2 \right]. \quad (2.51)$$

We obtain an explicit upper bound on the mean-squared error when specifying the parameters of the algorithm as follows. For $\gamma > 0$, $\rho \in (\frac{1}{2}, 1)$, we set $\gamma_m := \gamma m^{-\rho}$, $m \geq 1$ and we assume that the number of steps M in the SGD algorithm satisfies, for some $\eta \geq 0$,

$$\gamma \frac{\alpha_K}{\beta_K} M^{1-\rho} \geq \frac{\sqrt{2}}{2} \quad \text{and} \quad \frac{\kappa_K}{h \wedge \alpha_K} \left(e^{-2\sqrt{2}\ln(2)\gamma \frac{\alpha_K}{\beta_K} M^{1-\rho}} + \frac{\beta_K}{\alpha_K M^\rho} \right) \leq \eta. \quad (2.52)$$

Theorem 2.1. Let Assumption 2.1, Assumption 2.2 (i), (ii), Assumption 2.3 and (2.52) hold. If LT^2 and η are small enough, then there exists $\delta < 1$ such that

$$\mathcal{E}_{\text{MSE}} \leq C_{\rho, \gamma} \left(\delta^P + \frac{\kappa_K}{h \wedge \alpha_K} \left(e^{-2\sqrt{2}\ln(2)\gamma \frac{\alpha_K}{\beta_K} M^{1-\rho}} + \frac{\beta_K}{\alpha_K M^\rho} \right) + h + \mathcal{E}_\psi \right). \quad (2.53)$$

for some positive constant $C_{\rho, \gamma}$, where we recall that \mathcal{E}_ψ is given by (2.18).

Remark 2.7. 1. As expected, the above upper bound is the sum of the error due to the Picard iteration, the error induced by the SGD algorithm, the discrete-time approximation error, recall (2.19), and the error \mathcal{E}_ψ generated by the approximation in the functional spaces $(\mathcal{V}^y, \mathcal{V}_n^z)$.

2. The smallness condition on LT^2 is precisely given in the statement of Proposition 4.4. This condition should not come as a surprise since we use Picard iteration. The smallness condition on η is not restrictive in practice as the quantity it controls should go to zero to obtain the convergence of the numerical procedure.

To deduce a rate of convergence from (2.53), one has to chose the approximation basis functions $(\psi_y^k)_{1 \leq k \leq K^y}$ and $(\psi_n^k)_{0 \leq n \leq N-1, 1 \leq k \leq K_n^z}$ and to set optimally the algorithm's parameters. The choice of the basis function has a dramatic impact on the complexity of the algorithm. In the next section, we work with sparse grid approximation and we are able to show that the complexity is controlled both theoretically and in practice under Assumption 2.2.

3 Convergence results for sparse grid approximation

Both the implemented *direct algorithm*, see Definition 2.3, and the implemented *Picard algorithm*, see Definition 2.7, rely on the choice of the approximation spaces \mathcal{V}^y and \mathcal{V}_n^z , $0 \leq n \leq N-1$ and the choice of the related basis functions $(\psi_y^k)_{1 \leq k \leq K^y}$ and $(\psi_n^k)_{0 \leq n \leq N-1, 1 \leq k \leq K_n^z}$. The impact is both theoretical, in terms of convergence rate and numerical complexity, and practical in terms of computational time. We choose here to use sparse grid approximations. This will allow us to obtain interesting numerical complexity results in the setting of Assumption 2.2, see Theorem 3.1. We carefully investigate the convergence of the implemented *Picard Algorithm*. It is not the first time that sparse grid approximations are investigated in the context of linear regression. We will use the framework introduced in [9]. Note however that some restriction in the choice of sparse grid approximations are introduced by Assumption 2.3.

The basis functions are built using elementary bricks that have a compact support included in the bounded domain

$$\mathcal{O}_n = \prod_{l=1}^d [\mathbf{a}_l^n, \mathbf{b}_l^n] \quad \text{where} \quad \mathbf{a}_l^n < \mathbf{b}_l^n \quad \text{for } l \in \{1, \dots, d\}. \quad (3.1)$$

The domain specification strongly depends on the applications under study. We will consider two main cases in this work.

1. For all $1 \leq n \leq N-1$,

$$\mathcal{O}_n = \prod_{l=1}^d [\mathbf{a}_l, \mathbf{b}_l] =: \mathcal{O}. \quad (3.2)$$

Namely, the coefficients \mathbf{a} and \mathbf{b} do not depend on n . This will be the case in Section 3.1.2 where we consider coefficient functions that are \mathcal{O} -periodic.

2. Alternatively, the coefficient \mathbf{a} and \mathbf{b} are functions of the time-step but also of the diffusion coefficients (b, σ) , recall (1.2), and the PDE dimension d . Namely

$$\mathbf{a}^n := \mathbf{a}(t_n, b, \sigma, d) \quad \text{and} \quad \mathbf{b}^n := \mathbf{b}(t_n, b, \sigma, d). \quad (3.3)$$

However, In both cases the basis functions are obtained by a transformation of the domain $[0, 1]^d$ on which we define the primary basis using *sparse grids*. The transformation is defined as follows:

$$\tau_n : \mathbb{R}^d \ni x \mapsto \tau_n(x) = \left(\frac{x_1 - \mathbf{a}_1^n}{\mathbf{b}_1^n - \mathbf{a}_1^n}, \dots, \frac{x_d - \mathbf{a}_d^n}{\mathbf{b}_d^n - \mathbf{a}_d^n} \right)^\top \in \mathbb{R}^d. \quad (3.4)$$

We will introduce two types of basis functions: the first one, based on pre-wavelet basis, follows from [9] and the second one, based on hat functions modified at the boundary of the domain, follows from [24].

3.1 Convergence results for the pre-wavelet basis

3.1.1 Definition of the pre-wavelet basis

We describe here the elementary bricks that are used to build the basis functions of the approximation spaces.

For a level $l \in \mathbb{N}$ and an index $i \in \{0, \dots, 2^l\}$, we first consider the family of hat functions given by

$$\phi^{l,i}(x) = \phi(2^l x - i) \text{ with } \phi(x) = \begin{cases} 1 - |x| & \text{if } -1 < x < 1 \\ 0 & \text{otherwise.} \end{cases} \quad (3.5)$$

The univariate pre-wavelet basis functions $\chi^{l,i} : \mathbb{R} \rightarrow \mathbb{R}$ are defined by

$$\chi^{0,0} = 1_{[0,1]}, \chi^{0,1} = \phi^{0,1}, \chi^{1,1} = 2\phi^{1,1} - 1 \quad (3.6)$$

and for $l \geq 2$, $i \in I_l \setminus \{1, 2^l - 1\}$ with $I_l := \{1 \leq i \leq 2^l - 1 \mid i \text{ odd}\}$

$$\chi^{l,i} = 2^{\frac{l}{2}} \left(\frac{1}{10} \phi^{l,i-2} - \frac{6}{10} \phi^{l,i-1} + \phi^{l,i} - \frac{6}{10} \phi^{l,i+1} + \frac{1}{10} \phi^{l,i+2} \right). \quad (3.7)$$

For the boundary points $i \in \{1, 2^l - 1\}$, we set

$$\chi^{l,1} = 2^{\frac{l}{2}} \left(-\frac{6}{5} \phi^{l,0} + \frac{11}{10} \phi^{l,1} - \frac{3}{5} \phi^{l,2} + \frac{1}{10} \phi^{l,3} \right) \text{ and } \chi^{l,2^l-1}(x) = \chi^{l,1}(1-x), \quad x \in \mathbb{R}. \quad (3.8)$$

The multivariate pre-wavelet function on \mathbb{R}^d are obtained by a classical tensor-product approach. For a multi-index level $\mathbf{l} = (l_1, \dots, l_d)$ and a multi-index position $\mathbf{i} = (i_1, \dots, i_d)$,

$$\chi^{\mathbf{l},\mathbf{i}}(x) = \prod_{j=1}^d \chi^{l_j, i_j}(x^j). \quad (3.9)$$

In this multivariate case, the index sets are given by

$$\mathbf{I}_{\mathbf{l}} = \left\{ \mathbf{i} \in \mathbb{N}^d \mid \begin{array}{ll} 0 \leq i_j \leq 1 & \text{if } l_j = 0, \\ i_j \in I_{l_j} & \text{if } l_j > 0, \end{array} \text{ for all } 1 \leq j \leq d \right\}. \quad (3.10)$$

The hierarchical increment spaces are then defined for $\mathbf{l} \in \mathbb{N}^d$ by

$$\mathcal{W}_{\mathbf{l}} := \text{span}\{\chi^{\mathbf{l},\mathbf{i}} \mid \mathbf{i} \in \mathbf{I}_{\mathbf{l}}\}.$$

The sparse grid space approximation at level ℓ is given by

$$\mathcal{S}_\ell := \bigoplus_{\mathbf{l} \in \mathcal{L}_\ell} \mathcal{W}_{\mathbf{l}}, \quad \mathcal{L}_\ell := \{\mathbf{l} \in \mathbb{N}^d, \zeta_d(\mathbf{l}) \leq \ell\} \quad (3.11)$$

with $\zeta_d(\mathbf{0}) := 0$ and for $\mathbf{l} \neq \mathbf{0}$

$$\zeta_d(\mathbf{l}) = |\mathbf{l}|_1 - d + |\{j | l_j = 0\}| + 1,$$

where for a multi-index $\mathbf{l} \in \mathbb{N}^d$ we recall that $|\mathbf{l}|_1 = \sum_{\ell=1}^d l_\ell$ and that $|A|$ is the cardinality of A . The key point here is that the dimension of \mathcal{S}_ℓ satisfies

$$\dim(\mathcal{S}_\ell) = O(2^\ell \ell^{d-1}), \quad (3.12)$$

so that the curse of dimensionality only appears with respect to the level ℓ , see [22] (and also in the constant related to the notation $O(\cdot)$). The key point now is that the approximation error when using the sparse space is also controlled if the function to be approximated is smooth enough. To this end, for the fixed open domain $(0, 1)^d$, we consider the space of function with mixed derivatives $H_{mix}^2((0, 1)^d)$ (see the section Notation for a precise definition). Then, for any $v \in H_{mix}^2((0, 1)^d)$, it holds

$$\inf_{\xi \in \mathcal{S}_\ell} \|\xi - v\|_{L^2((0,1)^d)}^2 \leq C 2^{-4\ell} \ell^{d-1} \|v\|_{H_{mix}^2((0,1)^d)}^2 \quad (3.13)$$

for some positive constant $C := C(d)$. We refer e.g. Theorem 3.25 in [8] for a proof of this result. Again, we importantly emphasize that in the above control of the error the curse of dimensionality only appears with respect to the level ℓ .

Remark 3.1. *The number of basis functions is thus $K = \dim(\mathcal{S}_\ell)$. We denote by $k : \mathcal{C} \mapsto \{1, \dots, K\}$ any bijection enumerating \mathcal{C} . We will often slightly abuse the notation and write directly $(\psi_n^k)_{1 \leq k \leq K}$ instead of $(\psi_n^{(\mathbf{l}, \mathbf{i})})_{(\mathbf{l}, \mathbf{i}) \in \mathcal{C}}$ to be consistent with the notation introduced in the previous section.*

3.1.2 The Picard Algorithm in the case of periodic coefficients

In this section, we work under the setting of Assumption 2.2 (iv). To alleviate the notation – but without loss of generality – we assume that the coefficients are 1-*periodic* in the following sense: for $\lambda = b, \sigma$ or g

$$\lambda(x + q) = \lambda(x), \text{ for all } (x, q) \in \mathbb{R}^d \times \mathbb{Z}^d, \quad (3.14)$$

which implies the same property for the value function u and its derivatives.

We thus consider here that $\mathcal{O} = [0, 1]^d$, recall (3.2) and $\tau = I_d$, recall (3.4). Here, we are looking for an approximation $\mathcal{U}_M^P(\cdot)$ of $u(0, \cdot)$ on the whole domain \mathcal{O} , recall (2.50). We thus set \mathcal{X}_0 to be uniformly distributed on $(0, 1)^d$, which means that Assumption 2.1(i) holds true.

For sake of clarity, we summarize the current setting in the following assumption:

Assumption 3.1. *Let Assumption 2.1(i) and Assumption 2.2 hold true. Moreover, set $\mathcal{O} = [0, 1]^d$ and $\mathcal{X}_0 \sim \mathcal{U}((0, 1)^d)$.*

To take into account the periodic setting in our approximation, let us first define the 1-periodisation of a compactly supported function φ by

$$\check{\varphi}(x) := \sum_{q \in \mathbb{Z}^d} \varphi(x + q), \text{ for all } x \in \mathbb{R}^d. \quad (3.15)$$

The basis functions ψ are then given by $\psi = \check{\chi}$. Namely, for any $0 \leq n \leq N - 1$, for an approximation date t_n , we introduce the set of functions

$$\mathcal{V}_n^z := \{\xi : \mathbb{R}^d \mapsto \mathbb{R} \mid \xi(x) = \check{v}(x), \text{ for some } v \in \mathcal{S}_\ell\}. \quad (3.16)$$

Moreover, at the initial time, the approximation of $u(0, \cdot)$ will also be computed in

$$\mathcal{V}^y := \{\xi : \mathbb{R}^d \mapsto \mathbb{R} \mid \xi(x) = \check{v}(x), \text{ for some } v \in \mathcal{S}_\ell\}. \quad (3.17)$$

Remark 3.2. *We could have set an approximation level different for each time step, however we shall not use this possibility in our theoretical or numerical convergence results. We thus simply consider a fixed positive level ℓ of approximation, that, obviously, will be chosen later in an optimal way.*

Let also introduce the function

$$\mathbb{R}^d \ni x \mapsto \hat{x} \in [0, 1)^d \quad (3.18)$$

such that \hat{x} and x belong to the same equivalence class in $\mathbb{R}^d/\mathbb{Z}^d$. Denoting by $\mathbb{P}_{X_{t_n}}$ the probability measure on \mathbb{R}^d associated to the random vector X_{t_n} given by the Euler-Maruyama scheme (2.3) taken at time t_n and starting from \mathcal{X}_0 at time 0 and using Lemma 2.1, we remark that the boundary of the domain \mathcal{O} has null $\mathbb{P}_{X_{t_n}}$ -measure. We thus deduce

$$\check{\psi}(X_{t_n}) = \psi(\hat{X}_{t_n}) \quad \mathbb{P} - a.s., \quad (3.19)$$

and in practice we should work with the latter quantity. Namely, we construct our approximation scheme using:

$$Y_0^u := \sum_{k=1}^{K^y} \psi_y^k(\hat{X}_0) \mathfrak{y}^k \quad \text{and} \quad Z_{t_n}^u := \sum_{k=1}^{K_n^z} \psi_n^k(\hat{X}_{t_n}) \mathfrak{z}^{n,k}, \text{ for } 0 \leq n \leq N - 1, \quad (3.20)$$

with $\mathbf{u} = (\mathfrak{y}, \mathfrak{z}) \in \mathbb{R}^{K^y} \times \mathbb{R}^{dK^z}$.

Under the current setting of periodic coefficients and sparse grid approximation, we take benefit of the convergence results given in Theorem 2.1 to obtain our main theoretical result on the complexity of the *Picard algorithm*. Indeed, the next theorem shows that the curse of dimensionality is tamed by using the sparse grid approximation.

Theorem 3.1. *Let Assumption 3.1 hold and assume that LT^2 is small enough. For a prescribed $\varepsilon > 0$, the complexity \mathcal{C}_ε , defined in Remark 2.6, of the full Picard algorithm in order to achieve a global error \mathcal{E}_{MSE} of order ε^2 , recall (2.51), satisfies*

$$\mathcal{C}_\varepsilon = O_d(\varepsilon^{-\frac{5}{2}(1+2\iota)} |\log_2(\varepsilon)|^{1+\frac{45+50\iota}{36}(d-1)})$$

for any $1 < \iota < \frac{9}{5}$.

The proof of this theorem is given in Section 4.4 where the algorithm's parameters are optimally set with respect to ε .

Periodic example We consider here 1-periodic coefficients on \mathbb{R}^d . The coefficients of the forward SDE (1.2) are given by, for $x \in \mathbb{R}^d$,

$$b_i(x) = 0.2 \sin(2\pi x_i), \quad \sigma_{i,j}(x) = \frac{1}{\sqrt{d\pi}} (0.25 + 0.1 \cos(2\pi x_i)) \mathbf{1}_{\{i=j\}}, \quad 1 \leq i, j \leq d.$$

The coefficients of the BSDE reads

$$g(x) = \frac{1}{\pi} \left(\sin \left(2\pi \sum_{i=1}^d x_i \right) + \cos \left(2\pi \sum_{i=1}^d x_i \right) \right), \quad x \in \mathbb{R}^d,$$

$$f(t, x, y, z) = 2\pi^2 y \sum_{i=1}^d (\sigma_{i,i}(x))^2 - \sum_{i=1}^d b_i(x) \frac{z_i}{\sigma_{i,i}(x)} + h(t, x), \quad t \in [0, T], x \in \mathbb{R}^d, y \in \mathbb{R}, z \in \mathbb{R}^d,$$

where $h(t, x) = 2 \left(\cos(2\pi \sum_{i=1}^d x_i + 2\pi(T-t)) - \sin(2\pi \sum_{i=1}^d x_i + 2\pi(T-t)) \right)$. The explicit solution is given by

$$u(t, x) = \frac{1}{\pi} \left(\sin \left(2\pi \sum_{i=1}^d x_i + 2\pi(T-t) \right) + \cos \left(2\pi \sum_{i=1}^d x_i + 2\pi(T-t) \right) \right), \quad x \in \mathbb{R}^d.$$

We perform the test for $d = 3$ and $M = 100000, N = 10, T = 0.3, level = 3$ by *Picard Algorithm* with $P = 5$, then there are $K^y = K_n^z = K = 225$ basis functions. We obtain a mean square error $\mathcal{E}_{\text{MSE}} = 0.0201$ at the 5-th Picard iteration: See Figure 1 displaying the learning performance. The parameters of the test are shown in Table 6 in the appendix.

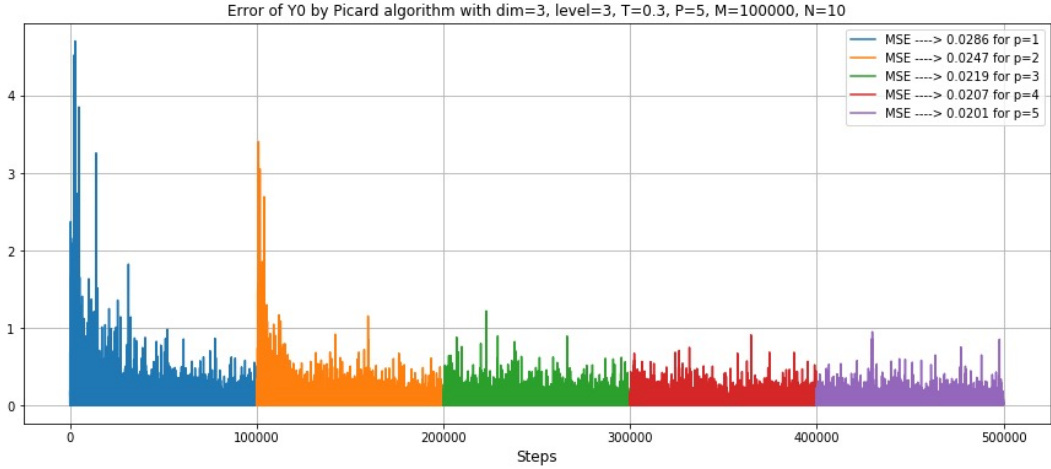


Figure 1: $m \mapsto |\hat{Y}_0^m - u(0, \mathcal{X}_0^m)|^2$ for the *Picard algorithm*, $d = 3$. The MSE is computed by the mean of the last 10000 steps of each Picard iteration.

3.1.3 Numerical convergence of the *Picard* and *direct Algorithm*

We will now investigate numerically the behavior of the *Picard algorithm* and *direct algorithm* on “test” examples that have been already considered in the literature. In particular, this will allow us also to compare our methods to existing methods as the ones investigated in [20, 37].

For this section, we work in the setting of Assumption 2.1(ii). This means that at the initial time, the output (\hat{y}_0, \hat{z}_0) of the algorithms: $(\hat{y}_0, \hat{z}_0) = (\mathfrak{y}_M, \mathfrak{z}_M^0)$, for the *direct algorithm*, recall Definition 2.3, or $(\hat{y}_0, \hat{z}_0) = (\mathfrak{y}_M^P, (\mathfrak{z}_M^P)^0)$, for the *Picard algorithm*², recall Definition 2.7, are approximating $(u(0, x_0), \sigma^\top \nabla_x u(0, x_0)) \in \mathbb{R} \times \mathbb{R}^d$. Since, these are one point values, there is no need to introduce basis functions at the initial time and the approximating spaces are just $\mathcal{V}^y = \mathbb{R}$ and $\mathcal{V}_0^z = \mathbb{R}^d$. Then, for any $1 \leq n \leq N - 1$, for the discrete time t_n , we set the approximating space as follows:

$$\mathcal{V}_n^z := \{\xi : \mathbb{R}^d \mapsto \mathbb{R} \mid \xi(x) = v(\tau_n(x)), \text{ for some } v \in \mathcal{S}_\ell\}, \quad (3.21)$$

recall (3.4). In particular, the basis functions are given by $\psi_n^k(x) = \chi^k(\tau_n(x))$, recall (3.9) and Remark 3.1.

We now report more specifically the various algorithms parameters that have been used in practice. The first thing to note is that we are able to obtain good results with a low level of approximation. Indeed, in all our numerical tests, we set the level $\ell = 3$. The Table 1 below indicates the number of basis functions that have theoretically to be considered when including boundary function.

| dimensions \ levels | $\ell \leq 3$ | $\ell \leq 4$ | $\ell \leq 5$ |
|---------------------|---------------|---------------|---------------|
| d=2 | 49 | 113 | 257 |
| d=3 | 225 | 593 | 1505 |
| d=4 | 945 | 2769 | 7681 |
| d=5 | 3753 | 12033 | 36033 |

Table 1: The number of functions in the sparse grid approximation with boundary for different dimensions and levels.

Next, we need to define the domain $\mathcal{O}_n, 1 \leq n \leq N - 1$, where the approximation will be computed, which depends on the underlying process, recall (3.1)-(3.3). We will consider two cases in our simulations, each component of the forward SDE is given by a Brownian motion with drift μ and volatility σ : $t \mapsto x_0 + \mu t + \sigma W_t$ or a geometric Brownian motion: $t \mapsto x_0 \exp((\mu - \sigma^2/2)t + \sigma W_t)$.

1. For the Brownian motion with drift, we set

$$\mathcal{O}_n = x_0 + [\mu t_n - r\sigma\sqrt{t_n}, \mu t_n + r\sigma\sqrt{t_n}]^d, \quad \text{for some } r \in \mathbb{R}^+. \quad (3.22)$$

2. For the geometric Brownian motion, we set

$$\mathcal{O}_n = [x_0 e^{R-r\sigma\sqrt{t_n}}, x_0 e^{R+r\sigma\sqrt{t_n}}], \quad R = (\mu - \frac{1}{2}\sigma^2)t_n, \quad \text{for some } r \in \mathbb{R}^+. \quad (3.23)$$

Finally, a delicate parameter to chose is the the learning rate. Empirically, it was set to:

²Deviating slightly from Definition 2.7, we will use for the initialization of the current SGD step, the last value computed at the previous step instead of a random value.

$$\gamma_m(\lambda, t_n, \alpha, \beta_0, \beta_1, m_0) = \frac{\beta_1(\lambda)n + \beta_0(\lambda)}{1 + (m + m_0(\lambda))^{\alpha(\lambda)}}, \quad 1 \leq m \leq M, \lambda \in \{\mathfrak{y}, \mathfrak{z}^{0,\cdot}\}_{n=0} \cup \{\mathfrak{z}^{n,\cdot}\}_{1 \leq n \leq N-1}, \quad (3.24)$$

where $\beta_0, \beta_1 \in \mathbb{R}^+, m_0 \in \mathbb{N}^+, \alpha \in (\frac{1}{2}, 1]$.

Remark 3.3. *i) m_0 is a suitable positive number to decrease the learning rates for avoiding a big jump of the estimated λ in the beginning steps of the algorithm.*

ii) The parameter $r \in \mathbb{R}^+$ is a suitable number to balance the running time and the errors of the algorithms.

iii) Both β_0 and α can be used to adjust the converge speed and the variance of the estimated λ . Suitable parameters make the algorithm more stable, converge faster and reduce the variance of the estimated λ .

iv) Usually, we increase the value of α or decrease the value of (β_0, β_1) gradually to decrease the convergence rate with the increase of step $p, 1 \leq p \leq P$ for Picard algorithm.

Concerning the number of steps in the SGD algorithm, we make the following remark.

Remark 3.4. *We used two techniques to control M in order to reduce the computational cost:*

i) We use $\alpha \in (0, \frac{1}{2}]$ which still works well as the SGD algorithm can converge faster.

ii) If $\beta_1(\lambda) \equiv 0$, for M large enough, the algorithm eventually converge, but $\{\mathfrak{z}^{n,k}\}_{1 \leq n \leq N-1}^{1 \leq k \leq K}$ convergence becomes slower and slower with the increase of n (the time step). We thus choose $\beta_1(\lambda) > 0$ in practice to make all $\{\mathfrak{z}^{n,k}\}_{1 \leq n \leq N-1}^{1 \leq k \leq K}$ converge altogether with a smaller M (thanks to the learning rates increase with n).

The remaining parameters are precised in the examples below. We refer also Section to the Appendix for the collection of all algorithm parameters values used in the numerical simulation.

Quadratic model First, we consider the quadratic example, whose driver is set to

$$f(y, z) = a|z|^2 = a(z_1^2 + z_2^2 + \cdots + z_d^2), \quad y \in \mathbb{R}, z \in \mathbb{R}^d, \quad (3.25)$$

where $a \in \mathbb{R}$ is a constant, and the terminal condition to

$$g(x) = \log \left(\frac{1 + |x|^2}{2} \right), \quad x \in \mathbb{R}^d. \quad (3.26)$$

The explicit solution can be obtained through the Cole-Hopf transformation(see e.g. [15, 20]):

$$y_t = u(t, x) = \begin{cases} \frac{1}{a} \log \mathbb{E}[e^{a \cdot g(x + \mathcal{W}_{T-t})}] , & a \neq 0 \\ \mathbb{E}[g(x + \mathcal{W}_{T-t})] , & a = 0 \end{cases}$$

and

$$z_t^i = \partial_{x_i} u(t, x) = \frac{\mathbb{E}[\partial_{x_i} g(x + \mathcal{W}_{T-t}) e^{a \cdot g(x + \mathcal{W}_{T-t})}]}{\mathbb{E}[e^{a \cdot g(x + \mathcal{W}_{T-t})}]}, \quad i = 1, 2, \dots, d.$$

Thus, to obtain a numerical reference solution and 95% confidence interval for y_0 and $z_0^i, i = 1, 2, \dots, d$, we use classical Monte Carlo estimation of the expectations.

The underlying diffusion \mathcal{X} is given by the Brownian motion \mathcal{W} , and the parameters are selected as follows: $a = 1, M = 2000, N = 10, T = 1$. We compute a reference solution $\bar{y}_0 = 1.0976$ with 95% confidence interval $(1.0943, 1.1009)$ when $d = 5$ by Monte Carlo method using 10^5 simulation paths. Figure 2 shows the numerical approximation of y_0 and its 95% confidence interval by the same color line of the 5-dimensional quadratic model by *direct algorithm* and the *deep learning algorithm* introduced in [20]. The difference of \hat{y}_0 between our SGD algorithm and Monte Carlo simulation is less than 10^{-2} . It turns out that for this “low” dimensional example and with this set of parameter, it is more precise than the *deep BSDEs solver*.

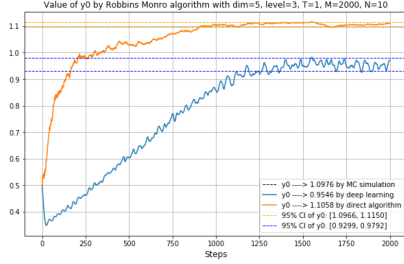


Figure 2: \hat{y}_0 for the quadratic model with $d=5$ and $T=1$ by *direct algorithm* and *deep learning algorithm*.

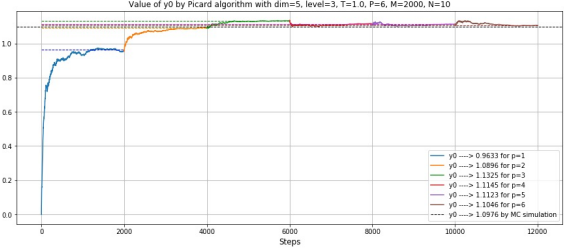


Figure 3: The value of \hat{y}_0 by *Picard algorithm* with $d=5$, level=3, $T=1$, $P=6$, $M=2000$.

For $d = 5, M = 2000, N = 10, P = 6, T = 1, a = 1$, Figure 3 shows that \hat{y}_0 converges for each Picard iteration, and overall $\hat{y}_0 \rightarrow 1.1046$. We can observe that \hat{y}_0 is very close to the reference solution \bar{y}_0 when the number of iteration p is greater or equal to 4.

A financial model We now report our numerical results for a model with a financial flavour. The underlying process \mathcal{X} follows a d -dimensional geometric Brownian motion, for $\mu \in \mathbb{R}, \sigma > 0$, namely

$$d\mathcal{X}_t^i = \mathcal{X}_t^i(\mu dt + \sigma dW_t^i), \quad i = 1, 2, \dots, d, \quad \mathcal{X}_0 = x_0 \in (\mathbb{R}_+)^d.$$

The driver of the BSDE is given by, for $(y, z) \in \mathbb{R} \times \mathbb{R}^d$,

$$f(y, z) = -R^l y - \frac{\mu - R^l}{\sigma} \sum_{i=1}^d z_i + (R^b - R^l) \max \left\{ 0, \frac{\sum_{i=1}^d z_i}{\sigma} - y \right\},$$

and the terminal condition

$$g(x) = \max \left\{ \left[\max_{1 \leq i \leq d} x_i \right] - K_1, 0 \right\} - 2 \max \left\{ \left[\max_{1 \leq i \leq d} x_i \right] - K_2, 0 \right\}.$$

Hence, for all $t \in [0, T), x \in \mathbb{R}^d$, it holds that $u(T, x) = g(x)$ and

$$\frac{\partial u}{\partial t} + \frac{\sigma^2}{2} \sum_{i=1}^d x_i^2 \frac{\partial^2 u}{\partial x_i^2} - \min \left\{ R^b \left(u - \sum_{i=1}^d x_i \frac{\partial u}{\partial x_i} \right), R^l \left(u - \sum_{i=1}^d x_i \frac{\partial u}{\partial x_i} \right) \right\} = 0. \quad (3.27)$$

This is a typical example of “non-linear market” specification, where there are two different interest rates for borrowing and lending money, see Bergman [7] and e.g. [20, 26, 11, 16, 5], where this example has been used as a test example for numerical methods for BSDEs.

In our numerical test below, we set the parameters as follows: $N = 10, M = 6000, \mu = 0.06, \sigma = 0.2, R^l = 0.04, R^b = 0.06, K_1 = 110, K_2 = 130, T = 0.5$ and $x_0 = (100, \dots, 100)$.

Table 2 compares the results of the *direct algorithm* and the *deep learning algorithm* [20] when $d = 2, 4$. The approximated value of y_0 obtained by the two methods are very close. Figure 4 and Figure 5 show the performance of the *Picard algorithm* with parameters $d = 4, P = 9$, and \hat{y}_0 converges to 7.1695 at the last step.

| dimensions | SGD algo with Sparse grids | | Deep learning scheme [20] | |
|------------|----------------------------|------------------|---------------------------|------------------|
| | y_0 | 95% CI of y_0 | y_0 | 95% CI of y_0 |
| d=2 | 4.3332 | [4.2921, 4.3743] | 4.3516 | [4.3420, 4.3612] |
| d=4 | 7.0960 | [7.0432, 7.1487] | 7.1130 | [7.0649, 7.1611] |

Table 2: Comparison of the *direct algorithm* and the *deep learning algorithm* for the financial model.

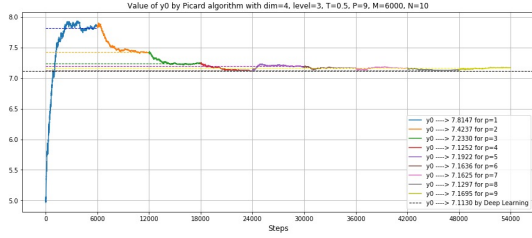


Figure 4: Approximation \hat{y}_0 by *Picard algorithm* when $d=4$ and $T=0.5$.

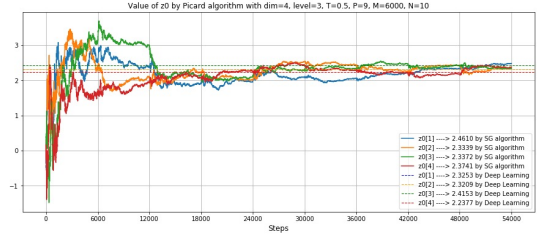


Figure 5: Approximation \hat{z}_0 by *Picard algorithm* when $d=4$ and $T=0.5$.

3.1.4 Limits of the *Picard Algorithm*

We now illustrate on a numerical example that the smallness assumption may be necessary to obtain the convergence of the *Picard Algorithm*. To this end, we consider the following model. For a given $a \in \mathbb{R}$, the BSDE driver is given by

$$f(y, z) := \arctan(ay) + \sum_{j=1}^d z_j, \quad (y, z) \in \mathbb{R} \times \mathbb{R}^d,$$

and the terminal condition

$$g(x) := \frac{e^{1+1 \cdot x}}{1 + e^{1+1 \cdot x}}, \quad x \in \mathbb{R}^d.$$

The underlying process \mathcal{X} is simply equal to the Brownian motion \mathcal{W} , namely $b = 0, \sigma = I_d$. We set the terminal time $T = 1$ and the dimension $d = 2$.

We study numerically the above model for different value of a , which controls the Lipschitz constant of f , in the case of the *Picard Algorithm*. The value obtained are compared to the ones obtained by two other methods: a multistep scheme in [13] and the *deep BSDEs solver* of [20]. The values obtained by these two methods are considered to be close to the true solution.

When $a = -0.4$, Figure 6 shows that \hat{y}_0 converges. However, this is not the case anymore when $a = -1.5$, see Figure 7, as \hat{y}_0 oscillates between two values. Actually, we see on Figure 8 that a bifurcation occurs for the *Picard Algorithm* around $a = -0.8$.

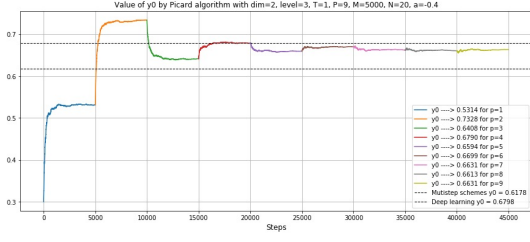


Figure 6: The value of \hat{y}_0 by *Picard algorithm* with $d=2$, level=3, $T=1$, $P=9$, $M=5000$, $a=-0.4$.

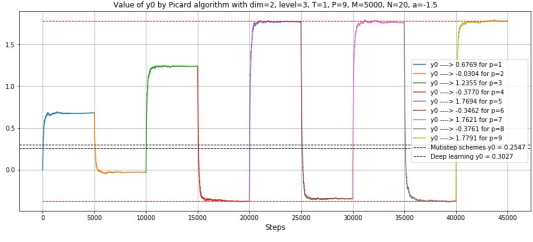


Figure 7: The value of \hat{y}_0 by *Picard algorithm* with $d=2$, level=3, $T=1$, $P=9$, $M=5000$, $a=-1.5$.

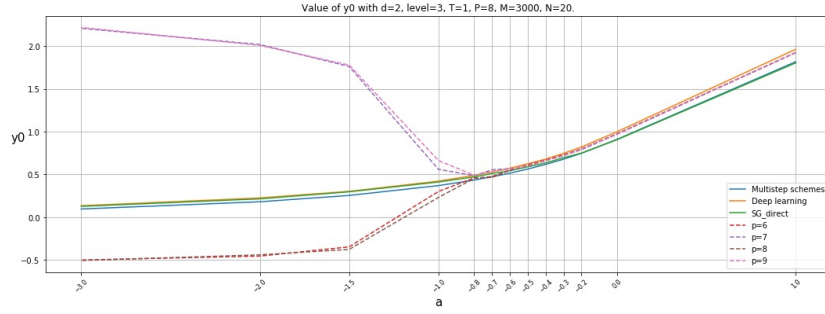


Figure 8: The value of \hat{y}_0 by *Picard algorithm*, *direct algorithm* and deep learning method with $d=2$, level=3, $T=1$, $P=9$, $M=5000$. The last four steps are shown for the *Picard Algorithm* illustrating the bifurcation phenomenon. Note that the *direct algorithm* does not exhibit such behaviour.

3.2 Numerical results with the modified hat functions basis

In the previous section, using the pre-wavelet basis, we were able to establish a theoretical upper-bound on the global complexity for the *Picard algorithm* and to show that both the *Picard algorithm* and *direct algorithm* converge in practice too. However, the number of basis functions, even though we use a sparse approximation, is still quite important which prevents us from dealing effectively with high-dimensional PDE. In particular, the number of basis functions used to capture what happens on the boundary of the domain is large. In this section, we use, the so-called “modified hat functions” that allows to get rid of the boundary basis.

3.2.1 Definition of the basis functions

The modified hat functions are defined by the following method (which corresponds to equation (2.16) in [24]),

$$\tilde{\phi}^{l,i}(x) := \begin{cases} \begin{cases} 1 & \text{if } x \in [0, 2h_l] \\ 1 - 2^{l-1} \cdot x & \text{otherwise} \end{cases} & \text{if } l = 1 \wedge i = 1 \\ \begin{cases} 0 & \text{if } x \in [0, 2h_l] \\ 2^{l-1} \cdot x + (1-i)/2 & \text{otherwise} \end{cases} & \text{if } l > 1 \wedge i = 1 \\ \begin{cases} 2^{l-1} \cdot x + (1-i)/2 & \text{if } x \in [1 - 2h_l, 1] \\ 0 & \text{otherwise} \end{cases} & \text{if } l > 1 \wedge i = 2^l - 1 \\ \phi^{l,i}(x) & \text{otherwise,} \end{cases} \quad (3.28)$$

The multivariate hat function on \mathbb{R}^d are obtained by a classical tensor-product approach. For these basis functions, we can remove the points on the boundary of the space so that all the components $l_j, j = 1, \dots, d$, are positive for a multi-index level $\mathbf{l} = (l_1, \dots, l_d)$ and a multi-index position $\mathbf{i} = (i_1, \dots, i_d)$,

$$\tilde{\phi}^{\mathbf{l}, \mathbf{i}}(x) = \prod_{j=1}^d \tilde{\phi}^{l_j, i_j}(x^j). \quad (3.29)$$

In this multivariate case, the index set are given by

$$\mathbf{I}_{\mathbf{l}} = \left\{ i \in \mathbb{N}^d \mid i_j \in I_{l_j} \text{ for all } 1 \leq j \leq d \right\}. \quad (3.30)$$

Table 3 shows the number of points in the sparse grids without boundary. In particular, we observe that it is much less than sparse grids with boundary for the same dimensions and levels, recall Table 1.

| dimensions \ levels | $l \leq 3$ | $l \leq 4$ | $l \leq 5$ |
|---------------------|------------|------------|------------|
| d=2 | 17 | 49 | 129 |
| d=4 | 49 | 209 | 769 |
| d=5 | 71 | 351 | 1471 |
| d=10 | 241 | 2001 | 13441 |
| d=20 | 881 | 13201 | 154881 |
| d=25 | 1351 | 24751 | 352351 |
| d=50 | 5201 | 182001 | 4867201 |
| d=100 | 20401 | 1394001 | \searrow |

Table 3: The number of points in the sparse grid approximation without boundary functions for different dimensions and levels.

The quadratic model We come back to the quadratic model introduced in (3.25)-(3.26). In this setting, we can test the 100-dimensional version of this model. Let $M = 2000, N = 10, T = 1, a = 1$, the convergence of \hat{y}_0 and \hat{z}_0 , when using the *direct algorithm*, is shown in Figure 9 and Figure 10: 3819 seconds were spent on this test. The error for \hat{y}_0 appears to be less than 0.01. For Z , the true solution is $\tilde{z}_0^i = \frac{2\mathcal{W}_0^i}{\mathbb{E}[1+|\mathcal{W}_T|^2]} = 0, \forall i = 1, \dots, d$. The gain in computational time is important in comparison with the pre-wavelet specification of the last section. Not only less basis functions are used, but one should also note that the computational cost of a hat function is less than a pre-wavelet function up to a factor 5. We do also test the *Picard algorithm* in 25-dimensional setting. We set $M = 1500, N = 10, T = 1, a = 1, P = 3$ and get $\hat{y}_0 \approx 2.5481$ quite quickly, see Figure 11 (all the initial value of $\mathbf{z}^{n,k}, 1 \leq n \leq N-1, 1 \leq k \leq K_n^z$ are set to 0 in this test).

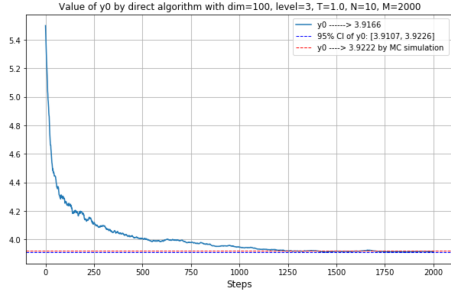


Figure 9: \hat{y}_0 for the quadratic model with $d=100$ and $T=1$

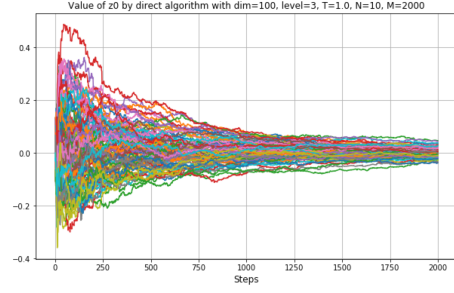


Figure 10: \hat{z}_0^i for the quadratic model with $d=100$ and $T=1$

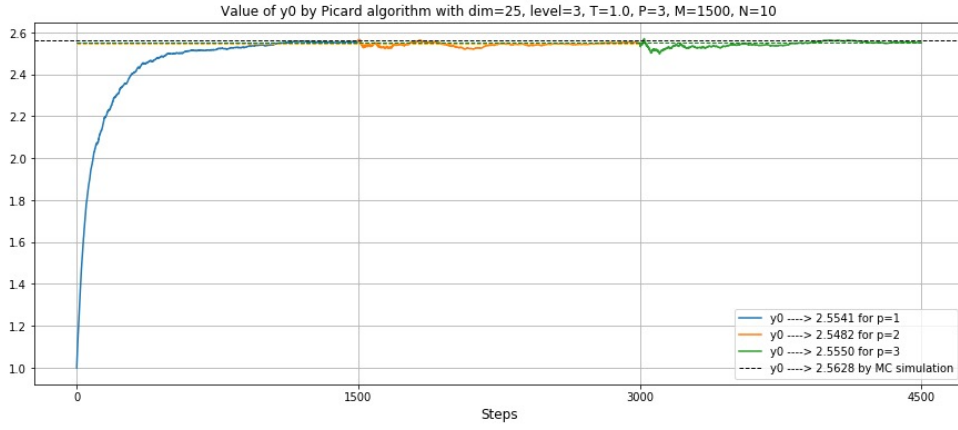


Figure 11: \hat{y}_0 for the quadratic model by *Picard algorithm* with $d=25$, $T=1$, $P=3$, $N=10$, $M=1500$

The financial model of (3.27) For the *direct algorithm* in this example, we set the parameters $N = 10$, $M = 5000$, $\mu = 0.06$, $\sigma = 0.2$, $R^l = 0.04$, $R^b = 0.06$, $K_1 = 110$, $K_2 = 130$, $T = 0.5$. Table 4 compares the results for the *direct algorithm* and *deep BSDEs solver*: the approximated value for y_0 obtained by the two methods are very close. The running time for the *deep BSDEs solver* shows almost no increase up to $d \leq 25$. For the *direct algorithm*, it does increase with the dimensions but it stays reasonable. Actually, it is even competitive when $d \leq 25$ ³. Figure 12 shows the performance of the *direct algorithm* when $d = 20$. Finally in Figure 13, the *Picard algorithm* is tested on this model with parameter $d = 20$, $P = 4$, and $\hat{y}_0 \approx 12.1386$ at the last iteration.

³The numerical experiments were realised by C++ 17 on a MacBook Pro 6-core Intel Core i7, using only one core and compiling with optimisation flag ‘-O3’ in gcc. The *deep BSDEs solver* [20], using *Tensorflow*, spends most of the time to build the graph for the NN and initialize the variables when the dimension is small then the learning phase is quick. On the contrary, our algorithm builds the approximation grid space quite efficiently (less than 1 second when $d \leq 100$, $level \leq 3$) and then the runtime is spent on the the SG algorithm.

| dimensions | direct SGD algo with Sparse grids | | | Deep BSDEs solver[20] | | |
|------------|-----------------------------------|--------------------|-------|-----------------------|--------------------|-------|
| | y_0 | 95% CI of y_0 | time | y_0 | 95% CI of y_0 | time |
| d=5 | 8.0966 | [8.0226, 8.1705] | 3 s | 8.1010 | [8.0747, 8.1273] | 115 s |
| d=10 | 10.9865 | [10.9224, 11.0506] | 12 s | 10.9216 | [10.8944, 10.9489] | 120 s |
| d=15 | 11.848 | [11.7853, 11.9107] | 33 s | 11.8226 | [11.7750, 11.8702] | 122 s |
| d=20 | 11.8674 | [11.7962, 11.9387] | 61 s | 11.9508 | [11.8965, 12.0051] | 127 s |
| d=25 | 11.7801 | [11.6467, 11.9135] | 130 s | 11.6416 | [11.5316, 11.7517] | 132 s |

Table 4: Comparison of the *direct algorithm* and the *deep learning algorithm*.

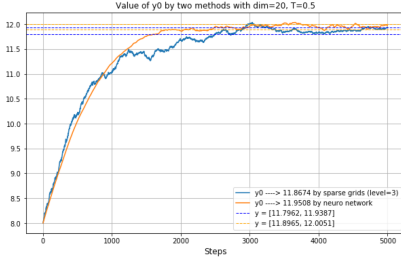


Figure 12: \hat{y}_0 by *direct algorithm* for d=20 and T=0.5.

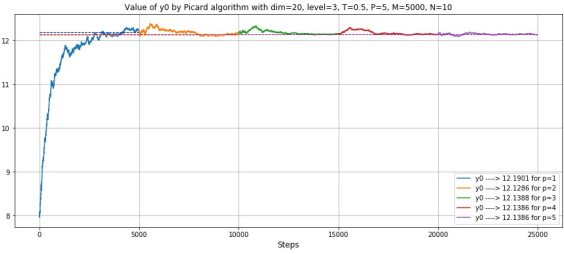


Figure 13: \hat{y}_0 by *Picard algorithm* for d=20, T=0.5, P=4, M=5000, N=10.

A challenging example We now consider a model with an unbounded and complex structure solution, which has been analyzed in [37]. The value function in this case is given by:

$$u(t, x) = \frac{T-t}{d} \sum_{i=1}^d (\sin(x_i) \mathbb{1}_{\{x_i < 0\}} + x_i \mathbb{1}_{\{x_i \geq 0\}}) + \cos \left(\sum_{i=1}^d i x_i \right), \quad x \in \mathbb{R}^d. \quad (3.31)$$

It corresponds to a BSDE, with underlying process given by $\mathcal{X}_t = x + \frac{1}{\sqrt{d}} \mathbf{I}_d \mathcal{W}_t$, and $x_0 = 0.5 \mathbf{1}_d$ and driver and terminal condition given respectively by

$$\begin{aligned} f(t, x, y, z) &= \left(1 + (T-t) \left(\frac{1}{2d} - C \right) \right) A(x) + (1 - (T-t)C) B(x) + C y, \\ &= \left(1 + \frac{T-t}{2d} \right) A(x) + B(x) + C \cos \left(\sum_{i=1}^d i x_i \right), \quad x \in \mathbb{R}^d, y \in \mathbb{R}, z \in \mathbb{R}^d, \\ g(x) &= u(T, x) = \cos \left(\sum_{i=1}^d i x_i \right), \quad x \in \mathbb{R}^d, \end{aligned}$$

where

$$A(x) = \frac{1}{d} \sum_{i=1}^d \sin(x_i) \mathbb{1}_{\{x_i < 0\}}, B(x) = \frac{1}{d} \sum_{i=1}^d x_i \mathbb{1}_{\{x_i \geq 0\}}, C = \frac{(d+1)(2d+1)}{12}.$$

In Table 5, we compare the approximation of y_0 by using five different algorithms to the theoretical solution. When the dimension $d \leq 2$, all the algorithms perform well. However, as already mentioned in [37] the *deep learning algorithm* [31] fails when $d \geq 3$ (no matter the

chosen initial learning rate and the activation function for the hidden layers, among the tanh, ELU, ReLu and sigmoid ones; besides, taking 3 or 4 hidden layers does not improve the results.) The two deep learning schemes of [37] and our algorithms with sparse grids still works well when $d \leq 8$. Figure 14 shows the performance of the *direct algorithm*, \hat{y}_0 converges to 1.1745 when $d = 8$, it is close to the theoretical solution 1.1603, and the 95% confidence interval of \hat{y}_0 is [1.1611, 1.1881]. When the dimension $d = 10$, all the algorithms failed at providing correct estimates of the solution as shown in the table, but the errors of our algorithms appear to be smaller than the errors of deep learning methods. Figure 15 and Figure 16 show the performance of the *direct algorithm*, *Picard algorithm* respectively.

| dimensions | Theoretical solution | SGD algo with L^2 sparse grids and hat functions | | DL scheme of HPW [37] | | DL scheme of HJE [31] |
|------------|----------------------|--|--------------------|-----------------------|---------|-----------------------|
| | | <i>direct algo</i> | <i>Picard algo</i> | DBDP1 | DBDP2 | |
| d=1 | 1.3776 | 1.3790 | 1.3825 | 1.3720 | 1.3736 | 1.3724 |
| d=2 | 0.5707 | 0.5795 | 0.5794 | 0.5715 | 0.5708 | 0.5715 |
| d=5 | 0.8466 | 0.8734 | 0.8606 | 0.8666 | 0.8365 | NC |
| d=8 | 1.1603 | 1.1745 | 1.1801 | 1.1694 | 1.0758 | NC |
| d=10 | -0.2149 | -0.2439 | -0.2594 | -0.3105 | -0.3961 | NC |

Table 5: The approach value of \hat{y}_0 of different methods when $T = 1$.

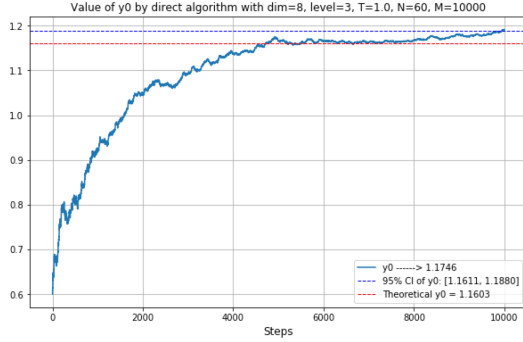


Figure 14: $\hat{y}_0 \rightarrow 1.1745$ by direct SGD algorithm when $d=8$, $N=60$, $M=10000$.

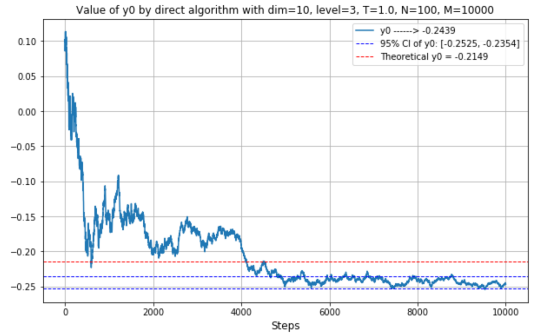


Figure 15: $\hat{y}_0 \rightarrow -0.2439$ by direct algorithm when $d=10$, $N=100$, $M=10000$.

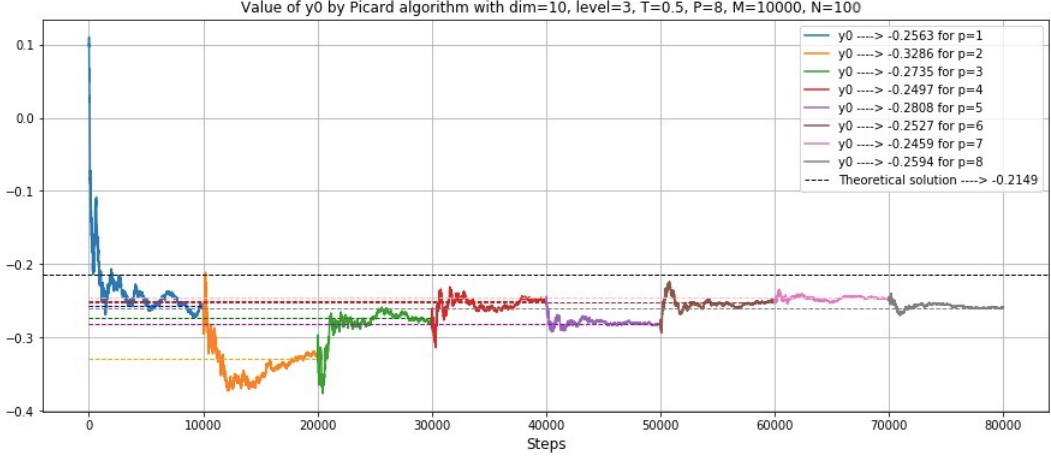


Figure 16: $\hat{y}_0 \rightarrow -0.2594$ by picard SGD algorithm when $d=10$, $P=8$, $N=100$, $M=10000$.

4 Study of the discrete optimization problems

In this section, we study theoretically the *direct algorithm* and the *Picard algorithm* in order to prove the results stated in Section 2 and 3.1.2. We first obtain forward and backward estimates on perturbed BSDEs. This allows in particular to derive the wellposedness of the *direct algorithm*. However, most of the work concentrates on the *Picard algorithm* in Section 4.3. A careful study of the iterated SGD algorithms allows to prove the convergence announced in Theorem 2.1. Finally, we prove Theorem 3.1 concerning the complexity of the method in the case of periodic coefficients and using pre-wavelet basis.

4.1 Preliminary estimates

In this subsection, we prove general technical estimates for the backward component of a BSDE that will be used in the proof of the convergence of the numerical methods under study. We will essentially compare two processes with dynamics given by (2.11) but taken at two different starting points and controlled processes.

The first process, denoted by V , is a scheme built with a random driver F satisfying:

Assumption 4.1. 1. For all $(y, z) \in \mathbb{R} \times \mathbb{R}^d$, $F(\cdot, y, z)$ is progressively measurable.

2. There exists some deterministic constant $C \geq 0$ such that for any $t \in [0, T]$ and any $(y, y', z, z') \in \mathbb{R}^2 \times \mathbb{R}^{2d}$

$$|F(t, y, z) - F(t, y', z')| \leq C (|y - y'| + |z - z'|).$$

For $Z \in \mathcal{S}_d^2$ and $\zeta \in \mathcal{L}^2(\mathcal{F}_0)$, we thus define

$$V_t^{\zeta, Z} = \zeta - \int_0^t F(\bar{s}, V_{\bar{s}}^{\zeta, Z}, Z_{\bar{s}}) d\bar{s} + \int_0^t Z_{\bar{s}} dW_{\bar{s}}, \quad (4.1)$$

where we introduced the notation $\bar{s} := t_n$ for $t_n \leq s < t_{n+1}$. The second one, denoted \tilde{V} , corresponds to the true solution to the BSDE

$$\tilde{V}_t^{\zeta, Z} = \zeta - \int_0^t \tilde{F}(s, \tilde{V}_s^{\zeta, Z}, Z_s) ds + \int_0^t Z_s dW_s, \quad (4.2)$$

where \tilde{F} satisfies the same assumptions as F above.

Proposition 4.1. *Let Assumption 4.1 hold for F and \tilde{F} . For $(\zeta, \zeta') \in \mathcal{L}^2(\mathcal{F}_0) \times \mathcal{L}^2(\mathcal{F}_0)$ and $(Z, Z') \in \mathcal{S}_d^2 \times \mathcal{S}_d^2$, we consider $V^{\zeta, Z}$ and $\tilde{V}^{\zeta', Z'}$ as defined in (4.1)-(4.2) and we set $\delta F := \tilde{F}(\cdot, V^{\zeta, Z}, Z) - F(\cdot, V^{\zeta, Z}, Z)$, $\eta_s^f = \tilde{F}(s, \tilde{V}_s^{\zeta', Z'}, Z'_s) - \tilde{F}(s, \tilde{V}_s^{\zeta', Z'}, Z'_s)$ and $\eta_s^z = Z'_s - Z_s$. Then, under the above assumptions on F and \tilde{F} , it holds*

1. *Forward estimate:*

$$\mathbb{E} \left[\sup_{t \in [0, T]} |\tilde{V}_t^{\zeta', Z'} - V_t^{\zeta, Z}|^2 \right] \leq C \left(\mathbb{E} \left[|\zeta - \zeta'|^2 + h \sum_{i=0}^{N-1} |Z_{t_n} - Z'_{t_n}|^2 \right] + \mathbb{E} \left[\int_0^T (|\delta F_{\bar{s}}|^2 + |\eta_s^f|^2 + |\eta_s^z|^2) ds \right] \right).$$

2. *Backward estimate:*

$$\mathbb{E} \left[\sup_{t \in [0, T]} |\tilde{V}_t^{\zeta', Z'} - V_t^{\zeta, Z}|^2 + h \sum_{i=0}^{N-1} |Z_{t_n} - Z'_{t_n}|^2 \right] \leq C \mathbb{E} \left[|\tilde{V}_T^{\zeta', Z'} - V_T^{\zeta, Z}|^2 + \int_0^T (|\delta F_{\bar{s}}|^2 + |\eta_s^f|^2 + |\eta_s^z|^2) ds \right].$$

Proof.

1. Denote $\Delta V := \tilde{V}^{\zeta', Z'} - V^{\zeta, Z}$, $\Delta Z = Z' - Z$, $\Delta F = \tilde{F}(\cdot, \tilde{V}^{\zeta', Z'}, Z') - \tilde{F}(\cdot, V^{\zeta, Z}, Z)$ and $\Delta \Gamma_s = \Delta Z_{\bar{s}} + \eta_s^z$. Applying Itô's formula, we compute

$$|\Delta V_t|^2 = |\Delta V_0|^2 + \int_0^t \{-2\Delta V_s(\Delta F_{\bar{s}} + \delta F_{\bar{s}} + \eta_s^f) + |\Delta \Gamma_s|^2\} ds + 2 \int_0^t \Delta V_s \Delta \Gamma_s dW_s. \quad (4.3)$$

Since \tilde{F} is Lipschitz-continuous, we have

$$2|\Delta V_s(\Delta F_{\bar{s}} + \delta F_{\bar{s}} + \eta_s^f)| \leq (4 + L) \sup_{0 \leq r \leq s} |\Delta V_r|^2 + L|\Delta Z_{\bar{s}}|^2 + |\delta F_{\bar{s}}|^2 + |\eta_s^f|^2$$

which combined with (4.3) leads to

$$\begin{aligned} \mathbb{E} \left[\sup_{0 \leq s \leq t} |\Delta V_s|^2 \right] &\leq \mathbb{E} \left[|\Delta V_0|^2 + C \int_0^t \left\{ \sup_{0 \leq r \leq s} |\Delta V_r|^2 + |\Delta Z_{\bar{s}}|^2 + |\delta F_{\bar{s}}|^2 + |\eta_s^f|^2 + |\eta_s^z|^2 \right\} ds \right] \\ &\quad + 2 \mathbb{E} \left[\sup_{0 \leq r \leq t} \left| \int_0^r \Delta V_s (\Delta Z_{\bar{s}} + \eta_s^z) dW_s \right| \right]. \end{aligned} \quad (4.4)$$

Applying the Burkholder-Davis-Gundy inequality, we obtain

$$\begin{aligned} \mathbb{E} \left[\sup_{r \in [0, t]} \left| \int_0^r \Delta V_s (\Delta Z_{\bar{s}} + \eta_s^z) dW_s \right| \right] &\leq C \mathbb{E} \left[\left| \int_0^t |\Delta V_s (\Delta Z_{\bar{s}} + \eta_s^z)|^2 ds \right|^{\frac{1}{2}} \right] \\ &\leq C \left(\mathbb{E} \left[\sup_{0 \leq s \leq t} |\Delta V_s|^2 + \int_0^t (|\Delta Z_{\bar{s}}|^2 + |\eta_s^z|^2) ds \right] \right) \end{aligned}$$

where we used Young's inequality for the last inequality. Inserting the previous inequality into (4.4), we get

$$\mathbb{E} \left[\sup_{0 \leq r \leq t} |\Delta V_t|^2 \right] \leq |\Delta V_0|^2 + C \int_0^t \mathbb{E} \left[\sup_{0 \leq r \leq s} |\Delta V_r|^2 + |\Delta Z_{\bar{s}}|^2 + |\eta_s^f|^2 + |\delta F_{\bar{s}}|^2 + |\eta_s^z|^2 \right] ds.$$

The proof for this step is concluded by applying Grönwall's Lemma.

2. From (4.3), we compute

$$\mathbb{E} \left[|\Delta V_t|^2 + \int_t^T |\Delta \Gamma_s|^2 ds \right] \leq \mathbb{E} \left[|\Delta V_T|^2 + 2 \int_t^T \Delta V_s (\Delta F_{\bar{s}} + \delta F_{\bar{s}} + \eta_s^f) ds \right].$$

We observe that, since \tilde{F} is Lipschitz continuous,

$$\Delta V_s \Delta F_{\bar{s}} \leq C(|\Delta V_s|^2 + |\Delta V_{\bar{s}}|^2 + |\Delta V_s \Delta Z_{\bar{s}}|).$$

For $\alpha > 0$, to be fixed later on, we get using Young's inequality,

$$\begin{aligned} \Delta V_s \Delta F_{\bar{s}} &\leq C \left(\left(1 + \frac{1}{\alpha}\right) |\Delta V_s|^2 + |\Delta V_{\bar{s}}|^2 + \alpha |\Delta Z_{\bar{s}}|^2 \right), \\ &\leq C \left(\left(1 + \frac{1}{\alpha}\right) |\Delta V_s|^2 + |\Delta V_{\bar{s}}|^2 + \alpha |\Delta \Gamma_s|^2 + |\eta_s^z|^2 \right). \end{aligned}$$

For α small enough, we thus obtain

$$\mathbb{E} \left[|\Delta V_t|^2 + \frac{1}{2} \int_t^T |\Delta \Gamma_s|^2 ds \right] \leq \mathbb{E} \left[|\Delta V_T|^2 + C \int_t^T \left(|\Delta V_s|^2 + |\Delta V_{\bar{s}}|^2 + |\delta F_{\bar{s}}|^2 + |\eta_s^f|^2 + |\eta_s^z|^2 \right) ds \right]. \quad (4.5)$$

Applying Grönwall's Lemma leads to, for all $t \leq T$,

$$\mathbb{E}[|\Delta V_t|^2] \leq C \mathbb{E} \left[\mathcal{B}_T + \int_t^T |\Delta V_{\bar{s}}|^2 ds \right] \text{ with } \mathcal{B}_T := |\Delta V_T|^2 + \int_0^T (|\eta_s^f|^2 + |\eta_s^z|^2 + |\delta F_{\bar{s}}|^2) ds. \quad (4.6)$$

In particular, for $n \leq N$ and $t_n \in \pi$, we have

$$\mathbb{E}[|\Delta V_{t_n}|^2] \leq C \mathbb{E} \left[\mathcal{B}_T + h \sum_{j=n}^{N-1} |\Delta V_{t_j}|^2 \right]$$

which in turn, using the discrete-time Grönwall Lemma, leads to $\max_{n \leq N} \mathbb{E}[|\Delta V_{t_n}|^2] \leq C \mathbb{E}[\mathcal{B}_T]$. Combining this inequality with (4.5) and (4.6), we obtain

$$\mathbb{E} \left[|\Delta V_t|^2 + \frac{1}{2} \int_t^T |\Delta \Gamma_s|^2 ds \right] \leq C \mathbb{E}[\mathcal{B}_T], \quad t \leq T.$$

To conclude the proof one applies the Burkholder-Davis-Gundy inequality as in step 1. \square

4.2 Application to the *direct algorithm*

We here prove the results announced in Section 2.2. We start by proving the analytic expression of the main quantities appearing in the *direct algorithm*, recall Definition 2.3.

Proof of Lemma 2.2 By standard computations, recall (2.6), for any $0 \leq n \leq N-1$,

$$\nabla_{\mathfrak{y}^k} Z_{t_n}^u = 0, \quad \text{and} \quad \nabla_{\mathfrak{z}^{n,k}} (Z_t^u)^l = \psi_n^k(X_{t_n}) \mathbf{1}_{\{t=t_n\}} \mathbf{e}^l.$$

This leads to, for $0 \leq q \leq N-1$,

$$\nabla_{\mathfrak{z}^{n,k}} (Z_{t_q}^u \cdot \Delta W_q) = \psi_n^k(X_{t_n}) \Delta W_n \mathbf{1}_{\{q=n\}} \quad (4.7)$$

and

$$\nabla_{\mathfrak{z}^{n,k}} f(Y_{t_q}^u, Z_{t_q}^u) = \nabla_y f(Y_{t_q}^u, Z_{t_q}^u) \nabla_{\mathfrak{z}^{n,k}} Y_{t_q}^u + \psi_n^k(X_{t_n}) \nabla_z f(Y_{t_q}^u, Z_{t_q}^u) \mathbf{1}_{\{q=n\}}. \quad (4.8)$$

Now, differentiating both side of (2.10) with respect to the variable \mathfrak{y}^k , $1 \leq k \leq K^y$ yields

$$\nabla_{\mathfrak{y}^k} Y_{t_n}^u = \psi_y^k(X_0) \prod_{j=0}^{n-1} \left(1 - h \nabla_y f(Y_{t_j}^u, Z_{t_j}^u) \right) \text{ for } n \geq 0.$$

From (2.10), by differentiation, we obtain $\nabla_{\mathfrak{z}^{n,k}} Y_0^u = 0$ and using (4.7) and (4.8), for $q \geq 1$,

$$\nabla_{\mathfrak{z}^{n,k}} Y_{t_q}^u = \nabla_{\mathfrak{z}^{n,k}} Y_{t_{q-1}}^u \left(1 - h \nabla_y f(Y_{t_{q-1}}^u, Z_{t_{q-1}}^u) \right) + \psi_n^k(X_{t_n}) \mathbf{1}_{\{n=q-1\}} \left(\Delta W_{q-1}^\top - h \nabla_z f(Y_{t_{q-1}}^u, Z_{t_{q-1}}^u) \right),$$

which in turn yields

$$\nabla_{\mathfrak{z}^{n,k}} Y_{t_q}^u = 0 \text{ for } q \leq n, \quad \nabla_{\mathfrak{z}^{n,k}} Y_{t_{n+1}}^u = \psi_n^k(X_{t_n}) (\Delta W_n^\top - h \nabla_z f(Y_{t_n}^u, Z_{t_n}^u))$$

and for $q \geq n+2$,

$$\nabla_{\mathfrak{z}^{n,k}} Y_{t_q}^u = \psi_n^k(X_{t_n}) (\Delta W_n - h \nabla_z f(Y_{t_n}^u, Z_{t_n}^u)) \prod_{j=n+1}^{q-1} \left(1 - h \nabla_y f(Y_{t_j}^u, Z_{t_j}^u) \right).$$

This concludes the proof. \square

Recall that, the time discretization error that will appear in our estimates is classically given by

$$\mathcal{E}_\pi = \mathbb{E} \left[\sum_{n=0}^{N-1} \int_{t_n}^{t_{n+1}} (|\mathcal{Y}_s - \mathcal{Y}_{t_n}|^2 + |\mathcal{Z}_s - \mathcal{Z}_{t_n}|^2 + |\mathcal{X}_{t_n} - X_{t_n}|^2) ds \right]. \quad (4.9)$$

The approximation error due to the restriction to the functional space, expressed in (2.18), is also given by

$$\mathcal{E}_\psi = \mathbb{E} \left[|u(0, \mathcal{X}_0) - \bar{u}_0(\mathcal{X}_0)|^2 + \sum_{n=1}^{N-1} h |(\sigma^\top \nabla_x u)(t_n, X_{t_n}) - \bar{v}_n(X_{t_n})|^2 \right], \quad (4.10)$$

where, \bar{v}_n is the $L^2(\mathbb{R}^d, \mathbb{P}_{X_{t_n}})$ -projection of the map $(\sigma^\top \nabla_x u)(t_n, \cdot)$ onto \mathcal{V}_n^z , $0 \leq n \leq N-1$ and \bar{u}_0 is the $L^2(\mathbb{R}^d, \mathbb{P}_{\mathcal{X}_0})$ -projection of the map $u(0, \cdot)$ onto \mathcal{V}^y . We denote $\bar{\mathfrak{y}}$ the coefficient associated to the decomposition of \bar{u} , namely

$$\mathbb{R}^d \ni x \mapsto \bar{u}_0(x) = \sum_{k=1}^{K^y} \bar{\mathfrak{y}}^k \psi_0^k(x) \in \mathbb{R}, \quad (4.11)$$

and also $\bar{\mathfrak{z}}^n$ the coefficient associated to the decomposition of \bar{v}_n , namely

$$\mathbb{R}^d \ni x \mapsto \bar{v}_n(x) = \sum_{k=1}^{K_n^z} \bar{\mathfrak{z}}^{n,k} \psi_n^k(x) \in \mathbb{R}^d, \quad 0 \leq n \leq N-1. \quad (4.12)$$

For later use, we introduce a *reference solution*

$$\bar{\mathbf{u}} = (\bar{\mathfrak{y}}, \bar{\mathfrak{z}}) \in \mathbb{R}^{K^y} \times \mathbb{R}^{d\bar{K}^z}. \quad (4.13)$$

We first discuss the well-posedness of the optimization problem (2.12).

Lemma 4.1. *Under Assumption 2.1, Assumption 2.2 (i) and Assumption 2.3, it holds*

$$\arg \min_{\mathbf{u} \in \mathbb{R}^{K^y} \times \mathbb{R}^{d\bar{K}^z}} \mathfrak{g}(\mathbf{u}) \neq \emptyset.$$

Proof. Let $\mathbf{u} = (\mathfrak{y}, \mathfrak{z}) \in \mathbb{R}^{K^y} \times \mathbb{R}^{d\bar{K}^z}$. Using the backward estimate of Proposition 4.1 with $V^{\zeta, Z} := Y^u$ and $\tilde{V}^{\zeta', Z'} := Y^0$ ($\zeta' = 0$, $Z' \equiv 0$) yields

$$\|\mathbf{u}\|^2 = \mathbb{E} \left[|Y_0^u|^2 + \sum_{n=0}^{N-1} h |Z_{t_n}^u|^2 \right] \leq C \mathbb{E}[|Y_T^u - Y_T^0|^2] \leq C(1 + \mathbb{E}[|g(X_T) - Y_T^u|^2]).$$

Under Assumption 2.3, we thus deduce that the continuous function $\mathbb{R}^{K^y} \times \mathbb{R}^{d\bar{K}^z} \ni \mathbf{u} \mapsto \mathfrak{g}(\mathbf{u})$ is coercive. As a consequence, it admits a global minimizer so that the optimization problem (2.12) is well-posed. \square

The following proposition can be seen as a version of the results in [34] (see Theorem 1 & 2) adapted to our context. Let us note that our setting is simpler as we do not deal with fully coupled Forward Backward SDEs.

Proposition 4.2. *Under Assumption 2.1, Assumption 2.2 (i), (ii) and Assumption 2.3, there exists a positive constant C such that for any*

$$\mathbf{u}^* := (\mathfrak{y}^*, \mathfrak{z}^*) \in \arg \min_{\mathbf{u} \in \mathbb{R}^{K^y} \times \mathbb{R}^{d\bar{K}^z}} \mathfrak{g}(\mathbf{u}),$$

it holds

$$\mathbb{E} \left[|u(0, \mathcal{X}_0) - Y_0^{u^*}|^2 + h \sum_{n=0}^{N-1} |Z_{t_n} - Z_{t_n}^{u^*}|^2 \right] \leq C(\mathcal{E}_\pi + \mathcal{E}_\psi) \quad (4.14)$$

and

$$\mathfrak{g}(\mathbf{u}^*) \leq \mathfrak{g}(\bar{\mathbf{u}}) \leq C(\mathcal{E}_\pi + \mathcal{E}_\psi). \quad (4.15)$$

Proof. We use the backward estimate of Proposition 4.1 with $V^{\zeta, Z} := Y^{u^*}$ and $\tilde{V}^{\zeta', Z} := Y^{\bar{u}}$ where \bar{u} is given in (4.13), to obtain

$$\begin{aligned} \mathbb{E} \left[\sup_{t \in [0, T]} |Y_t^{u^*} - Y_t^{\bar{u}}|^2 + h \sum_{n=0}^{N-1} \mathbb{E} \left[|Z_{t_n}^{\bar{u}} - Z_{t_n}^{u^*}|^2 \right] \right] &\leq C \mathbb{E} \left[|Y_T^{u^*} - Y_T^{\bar{u}}|^2 \right] \\ &\leq C \mathbb{E} \left[|Y_T^{u^*} - g(X_T^x)|^2 + |g(X_T^x) - Y_T^{\bar{u}}|^2 \right]. \end{aligned}$$

By optimality of u^* , we get

$$\mathbb{E} \left[\sup_{t \in [0, T]} |Y_t^{u^*} - Y_t^{\bar{u}}|^2 + h \sum_{n=0}^{N-1} \mathbb{E} \left[|Z_{t_n}^{\bar{u}} - Z_{t_n}^{u^*}|^2 \right] \right] \leq C \mathbb{E} \left[|g(X_T^x) - Y_T^{\bar{u}}|^2 \right]. \quad (4.16)$$

We now use the forward estimate of Proposition 4.1 with $V^{\zeta, Z} := Y^{\bar{u}}$ and $\tilde{V}^{\zeta', Z} := \mathcal{Y}$. We obtain

$$\mathfrak{g}(\bar{u}) = \mathbb{E} \left[|g(X_T^x) - Y_T^{\bar{u}}|^2 \right] \leq C \mathbb{E} \left[|\mathcal{Y}_0 - Y_0^{\bar{u}}|^2 + \int_0^T (|\mathcal{Y}_s - \mathcal{Y}_{\bar{s}}|^2 + |\mathcal{Z}_s - \mathcal{Z}_{\bar{s}}|^2) \, ds + \sum_{n=0}^{N-1} h |\mathcal{Z}_{t_n} - Z_{t_n}^{\bar{u}}|^2 \right]. \quad (4.17)$$

Observe now that in our current smooth coefficients framework $\mathcal{Z}_{t_n} = (\sigma^\top \nabla_x u)(t_n, \mathcal{X}_{t_n})$ so that one has

$$\begin{aligned} \mathbb{E} \left[|\mathcal{Z}_{t_n} - Z_{t_n}^{\bar{u}}|^2 \right] &= \mathbb{E} \left[|(\sigma^\top \nabla_x u)(t_n, \mathcal{X}_{t_n}) - Z_{t_n}^{\bar{u}}|^2 \right] \\ &\leq 2 \left(\mathbb{E} \left[|(\sigma^\top \nabla_x u)(t_n, \mathcal{X}_{t_n}) - (\sigma^\top \nabla_x u)(t_n, X_{t_n})|^2 \right] + \mathbb{E} \left[|(\sigma^\top \nabla_x u)(t_n, X_{t_n}) - Z_{t_n}^{\bar{u}}|^2 \right] \right) \\ &\leq C \left(\mathbb{E} \left[|\mathcal{X}_{t_n} - X_{t_n}|^2 \right] + \mathbb{E} \left[|(\sigma^\top \nabla_x u)(t_n, X_{t_n}^{x_0}) - Z_{t_n}^{\bar{u}}|^2 \right] \right) \end{aligned} \quad (4.18)$$

where we used the Lipschitz regularity of $x \mapsto (\sigma^\top \nabla_x u)(t_n, x)$ uniformly with respect to the variable t_n . Combining (4.17) and (4.18) leads to

$$\mathfrak{g}(\bar{u}) \leq C (\mathcal{E}_\pi + \mathcal{E}_\psi)$$

which, since $\mathfrak{g}(u^*) \leq \mathfrak{g}(\bar{u})$, proves (4.15).

The above estimate together with (4.16) leads to

$$\mathbb{E} \left[\sup_{t \in [0, T]} |Y_t^{u^*} - Y_t^{\bar{u}}|^2 + h \sum_{n=0}^{N-1} \mathbb{E} \left[|Z_{t_n}^{\bar{u}} - Z_{t_n}^{u^*}|^2 \right] \right] \leq C (\mathcal{E}_\pi + \mathcal{E}_\psi).$$

Then, using the inequalities $|\mathcal{Z}_{t_n} - Z_{t_n}^{u^*}|^2 \leq 2|Z_{t_n}^{u^*} - Z_{t_n}^{\bar{u}}|^2 + 2|\mathcal{Z}_{t_n} - Z_{t_n}^{\bar{u}}|^2$, $0 \leq n \leq N-1$, and $|Y_t^{u^*} - \mathcal{Y}_t|^2 \leq 2|Y_t^{u^*} - Y_t^{\bar{u}}|^2 + 2|\mathcal{Y}_t - Y_t^{\bar{u}}|^2$ yields (4.14) and concludes the proof. \square

4.3 Study of the *Picard algorithm*

We introduce the following mean squared error:

$$\mathcal{E}_p := \mathbb{E} \left[\|\mathbf{u}_M^p - \bar{\mathbf{u}}\|^2 \right], \quad 0 \leq p \leq P, \quad (4.19)$$

where the sequence $(\mathbf{u}_M^p)_{0 \leq p \leq P}$ is given by Definition 2.7, $\|\cdot\|$ is given by Definition 2.5 and $\bar{\mathbf{u}}$ is the reference solution introduced in (4.13). In this subsection, our aim is to establish an upper bound for the quantity \mathcal{E}_P that will allow us to prove Theorem 2.1.

4.3.1 Preliminary estimates

Proposition 4.3. *Suppose that Assumption 2.1, Assumption 2.2 (i), (ii) and Assumption 2.3 hold. If $T(1 + 2L^2(1 + h)) < 1$ and $\delta_h := \frac{8L^2T}{1-T(1+2L^2(1+h))} < 1$, then for any $\varepsilon > 0$ such that $\delta_{h,\varepsilon} := \delta_h(1 + \varepsilon) < 1$ there exists a positive constant C_ε such that for any positive integer P*

$$\mathcal{E}_P \leq \delta_{h,\varepsilon}^P \mathcal{E}_0 + C_\varepsilon (\mathcal{E}_{\text{RM}} + \mathcal{E}_\psi + \mathcal{E}_\pi) \quad (4.20)$$

with the notation

$$\mathcal{E}_{\text{RM}} := \max_{1 \leq p \leq P} \mathbb{E} \left[\left\| \mathbf{u}_M^p - \Phi(\mathbf{u}_M^{p-1}) \right\|^2 \right]. \quad (4.21)$$

Proof. From the decomposition,

$$\mathbf{u}_M^p - \bar{\mathbf{u}} = \Phi_M(\mathbf{u}_M^{p-1}) - \Phi(\mathbf{u}_M^{p-1}) + \Phi(\mathbf{u}_M^{p-1}) - \bar{\mathbf{u}}$$

we obtain, for any $\varepsilon > 0$,

$$\mathcal{E}_p \leq \left(1 + \frac{1}{\varepsilon}\right) \mathcal{E}_{\text{RM}} + (1 + \varepsilon) \mathbb{E} \left[\left\| \Phi(\mathbf{u}_M^{p-1}) - \bar{\mathbf{u}} \right\|^2 \right].$$

Then, using Lemma 4.2 below, we get

$$\mathcal{E}_p \leq \delta_{h,\varepsilon} \mathcal{E}_{p-1} + C_\varepsilon (\mathcal{E}_\psi + \mathcal{E}_\pi + \mathcal{E}_{\text{RM}})$$

up to a modification of ε . By an induction argument, we derive

$$\mathcal{E}_P \leq \delta_{h,\varepsilon}^P \mathcal{E}_0 + C_\varepsilon (\mathcal{E}_{\text{RM}} + \mathcal{E}_\psi + \mathcal{E}_\pi)$$

which concludes the proof. \square

Lemma 4.2. *Suppose that Assumption 2.1, Assumption 2.2 (i), (ii) and Assumption 2.3 hold. If $T(1 + 2L^2(1 + h)) < 1$ and $\delta_h := \frac{8L^2T}{1-T(1+2L^2(1+h))} < 1$, then, for any $\varepsilon > 0$ there exists a positive constant C_ε ($\varepsilon \mapsto C_\varepsilon$ being non-increasing) such that for any $\tilde{\mathbf{u}} \in \mathbb{R}^{K^y} \times \mathbb{R}^{d\bar{K}^z}$ it holds*

$$\left\| \Phi(\tilde{\mathbf{u}}) - \bar{\mathbf{u}} \right\|^2 \leq \delta_h(1 + \varepsilon) \left\| \tilde{\mathbf{u}} - \bar{\mathbf{u}} \right\|^2 + C_\varepsilon (\mathcal{E}_\psi + \mathcal{E}_\pi).$$

Proof.

Step 1: We denote $\check{\mathbf{u}} = \Phi(\tilde{\mathbf{u}})$ where $\check{\mathbf{u}} = (\check{\mathbf{y}}, \check{\mathbf{z}})$ and $\tilde{\mathbf{u}} = (\tilde{\mathbf{y}}, \tilde{\mathbf{z}})$ belongs to $\mathbb{R}^{K^y} \times \mathbb{R}^{d\bar{K}^z}$. We first observe that, recalling (2.21), (2.30) and (2.23),

$$\begin{aligned} \left\| \Phi(\tilde{\mathbf{u}}) - \bar{\mathbf{u}} \right\|^2 &= \mathbb{E} \left[|Y_0^{\check{\mathbf{u}}} - Y_0^{\bar{\mathbf{u}}}|^2 + \int_0^T |Z_t^{\check{\mathbf{u}}} - Z_t^{\bar{\mathbf{u}}}|^2 dt \right] \\ &= \mathbb{E} \left[|U_T^{\check{\mathbf{u}}, \check{\mathbf{u}}} - U_T^{\bar{\mathbf{u}}, \bar{\mathbf{u}}}|^2 \right]. \end{aligned}$$

Moreover, by optimality of $\check{\mathbf{u}}$

$$\begin{aligned} \mathbb{E} \left[|U_T^{\check{\mathbf{u}}, \check{\mathbf{u}}} - U_T^{\bar{\mathbf{u}}, \bar{\mathbf{u}}}|^2 \right] &\leq 2 \left(\mathbb{E} \left[|U_T^{\check{\mathbf{u}}, \check{\mathbf{u}}} - g(X_T)|^2 \right] + \mathbb{E} \left[|g(X_T) - U_T^{\bar{\mathbf{u}}, \bar{\mathbf{u}}}|^2 \right] \right) \\ &\leq 4 \mathbb{E} \left[|g(X_T) - U_T^{\bar{\mathbf{u}}, \bar{\mathbf{u}}}|^2 \right]. \end{aligned}$$

We now compute, for any $\varepsilon > 0$,

$$\mathbb{E}[|g(X_T) - U_T^{\tilde{u}, \bar{u}}|^2] \leq (1 + \frac{1}{\varepsilon})\mathbb{E}[|g(X_T) - U_T^{\bar{u}, \bar{u}}|^2] + (1 + \varepsilon)\mathbb{E}[|U_T^{\bar{u}, \bar{u}} - U_T^{\tilde{u}, \bar{u}}|^2],$$

which, combined with the previous inequality, yields

$$\|\Phi(\tilde{u}) - \bar{u}\|^2 \leq 4(1 + \frac{1}{\varepsilon})\mathbb{E}[|g(X_T) - U_T^{\bar{u}, \bar{u}}|^2] + 4(1 + \varepsilon)\mathbb{E}[|U_T^{\bar{u}, \bar{u}} - U_T^{\tilde{u}, \bar{u}}|^2]. \quad (4.22)$$

Since $U^{\bar{u}, \bar{u}} = Y^{\bar{u}}$, we can give an upper bound for the first term appearing on the right-hand side of the above inequality by using (4.15),

$$\mathbb{E}[|g(X_T) - U_T^{\bar{u}, \bar{u}}|^2] = \mathbf{g}(\bar{u}) \leq C(\mathcal{E}_\psi + \mathcal{E}_\pi). \quad (4.23)$$

Step 2: We now turn to the study of the second term appearing on the right hand side of (4.22). Recalling the dynamics (2.24), denoting $\delta U := U^{\tilde{u}, \bar{u}} - Y^{\bar{u}}$, $\delta Z = Z^{\tilde{u}} - Z^{\bar{u}}$, $\delta Y = Y^{\tilde{u}} - Y^{\bar{u}}$ and $\delta f_{t_n} = f(Y_{t_n}^{\tilde{u}}, Z_{t_n}^{\tilde{u}}) - f(Y_{t_n}^{\bar{u}}, Z_{t_n}^{\bar{u}})$, $0 \leq n \leq N-1$, using the Cauchy-Schwarz inequality and the Lipschitz-regularity of the map f , we get

$$\mathbb{E}[|\delta U_T|^2] \leq T \int_0^T \mathbb{E}[|\delta f_s|^2] ds \leq 2L^2 T \sum_{n=0}^{N-1} h \mathbb{E}[|\delta Y_{t_n}|^2 + |\delta Z_{t_n}|^2] ds. \quad (4.24)$$

For all $0 \leq n \leq N-1$, one has

$$\delta Y_{t_{n+1}} = \delta Y_{t_n} - h \delta f_{t_n} + \delta Z_{t_n} \Delta W_n$$

which in turn, setting $\Delta M_n := 2(\delta Y_{t_n} - h \delta f_{t_n}) \delta Z_{t_n} \Delta W_n$, yields

$$|\delta Y_{t_{n+1}}|^2 = |\delta Y_{t_n}|^2 - 2h \delta Y_{t_n} \delta f_{t_n} + h^2 |\delta f_{t_n}|^2 + |\delta Z_{t_n} \Delta W_n|^2 + \Delta M_n.$$

Using the fact that $\mathbb{E}[\Delta M_n] = 0$ and the Lipschitz regularity of the map f , we deduce

$$\begin{aligned} \mathbb{E}[|\delta Y_{t_{n+1}}|^2] &\leq \mathbb{E}[|\delta Y_{t_n}|^2 + h |\delta Y_{t_n}|^2 + (h + h^2) |\delta f_{t_n}|^2 + h |\delta Z_{t_n}|^2] \\ &\leq \mathbb{E}[|\delta Y_{t_n}|^2 + (h + 2L^2(h + h^2)) (|\delta Y_{t_n}|^2 + |\delta Z_{t_n}|^2)]. \end{aligned}$$

Summing the previous inequality, we obtain

$$\mathbb{E}[|\delta Y_{t_n}|^2] \leq |\delta Y_0|^2 + \mathbb{E}\left[\sum_{j=0}^{N-1} (h + 2L^2(h + h^2)) (|\delta Y_{t_j}|^2 + |\delta Z_{t_j}|^2)\right]$$

so that, multiplying both side of the previous inequality by h and summing again, we get

$$\begin{aligned} \sum_{n=0}^{N-1} h \mathbb{E}[|\delta Y_{t_n}|^2] &\leq T |\delta Y_0|^2 + T(1 + 2L^2(1 + h)) \left(\mathbb{E}\left[\sum_{j=0}^{N-1} h |\delta Y_{t_j}|^2\right] + \mathbb{E}\left[\sum_{j=0}^{N-1} h |\delta Z_{t_j}|^2\right] \right) \\ &\leq \frac{T}{1 - T(1 + 2L^2(1 + h))} \left(|\delta Y_0|^2 + (1 + 2L^2(1 + h)) \mathbb{E}\left[\sum_{j=0}^{N-1} h |\delta Z_{t_j}|^2\right] \right) \end{aligned}$$

where, for the last inequality, we used the fact that $T(1 + 2L^2(1 + h)) < 1$. Combining the previous inequality with (4.24), we obtain

$$\mathbb{E}[|\delta U_T|^2] \leq \frac{2L^2 T}{1 - T(1 + 2L^2(1 + h))} \left(T |\delta Y_0|^2 + \sum_{n=0}^{N-1} h \mathbb{E}[|\delta Z_{t_n}|^2] \right). \quad (4.25)$$

We finally complete the proof by combining (4.22), (4.23) and (4.25). \square

4.3.2 Study of the approximation error of the stochastic gradient descent algorithm

In this subsection, our aim is to study the approximation error of Φ by Φ_M where Φ_M has been introduced in Definition 2.6.

Lemma 4.3. *Suppose that Assumption 2.1, Assumption 2.2 (i) and Assumption 2.3 hold. Let $\tilde{\mathbf{u}}$ be a fixed $\mathbb{R}^{K^y} \times \mathbb{R}^{dK^z}$ -valued random vector and set $\tilde{\mathbf{u}} = (\tilde{\mathbf{y}}, \tilde{\mathbf{z}}) := \Phi(\tilde{\mathbf{u}})$ and $\mathbf{u}_M = (\mathbf{y}_M, \mathbf{z}_M) := \Phi_M(\mathbf{u}_0, \mathbf{x}_0, \mathbf{W}, \tilde{\mathbf{u}})$, M being a positive integer and where $(\mathbf{u}_0, \mathbf{x}_0, \mathbf{W})$ (recall Definition 2.6) is independent of $\tilde{\mathbf{u}}$. We denote by $\mathbb{E}_{\tilde{\mathbf{u}}}[\cdot]$, the conditional expectation with respect to the sigma-field $\sigma(\tilde{\mathbf{u}})$ generated by $\tilde{\mathbf{u}}$. Then, for any positive integer M , the random vector $(\mathbf{y}_M, \mathbf{z}_M)$ satisfies:*

$$\mathbb{E}_{\tilde{\mathbf{u}}} \left[|\mathbf{y}_M - \tilde{\mathbf{y}}|^2 \right] \leq L_{K,M} (1 + |\tilde{\mathbf{y}}|^2) \quad \text{and} \quad \mathbb{E}_{\tilde{\mathbf{u}}} \left[|\mathbf{z}_{M,l}^{n,\cdot} - \tilde{\mathbf{z}}_l^{n,\cdot}|^2 \right] \leq L_{K,M} \left(\frac{1}{h} + |\tilde{\mathbf{z}}_l^{n,\cdot}|^2 \right) \quad (4.26)$$

for any $l \in \{1, \dots, d\}$, with

$$L_{K,M} := \varrho_0 \varrho_1 \left(1 + \mathbb{E} \left[|\mathbf{u}_0|^2 \right] \right) \sum_{m=1}^M \exp \left(-4 \frac{\alpha_K}{\beta_K} (\Gamma_M - \Gamma_m) \right) \gamma_m^2 \quad (4.27)$$

$$\Gamma_m := \sum_{k=1}^m \gamma_k, \quad m \geq 1, \quad (4.28)$$

where the constants ϱ_0, ϱ_1 are defined respectively in equation (4.31) and (4.35) below. Moreover, it holds

$$\mathbb{E}_{\tilde{\mathbf{u}}} \left[\|\Phi_M(\tilde{\mathbf{u}}) - \Phi(\tilde{\mathbf{u}})\|^2 \right] \leq \kappa_K L_{K,M} (1 + dN) + \frac{\kappa_K}{\alpha_K} L_{K,M} \|\Phi(\tilde{\mathbf{u}})\|^2. \quad (4.29)$$

Proof.

Step 1: We prove the estimate for the difference $\mathbf{z}_{M,l}^{n,\cdot} - \tilde{\mathbf{z}}_l^{n,\cdot}$. The proof for $\mathbf{y}_M - \tilde{\mathbf{y}}$ follows from similar arguments and we omit some technical details. From (2.41), one gets

$$|H^{n,l}(\mathcal{X}_0, W, \tilde{\mathbf{u}}, \mathbf{z}_l^{n,\cdot})|^2 = \frac{4}{(\beta_K \sqrt{h})^2} |\mathfrak{G}^{\tilde{\mathbf{u}}} - \omega_l^{n,\cdot} \cdot \mathbf{z}_l^{n,\cdot}|^2 |\omega_l^{n,\cdot}|^2 \leq \frac{8}{\beta_K^2} (|\mathfrak{G}^{\tilde{\mathbf{u}}}|^2 + h |\tilde{\omega}_l^{n,\cdot}|^2 |\mathbf{z}_l^{n,\cdot}|^2) |\omega_l^{n,\cdot}|^2.$$

Under the boundedness Assumption 2.2 (i), recalling (2.27), we obtain

$$|\mathfrak{G}^{\tilde{\mathbf{u}}}|^2 \leq 2 (|g|_\infty^2 + T^2 |f|_\infty^2) \quad (4.30)$$

so that setting

$$\varrho_0 := 8 \max\{(|g|_\infty + T|f|_\infty)^2, 2\} \quad (4.31)$$

and from the lower bound (2.42), we obtain

$$\mathbb{E}_{\tilde{\mathbf{u}}} \left[|H^{n,l}(\mathcal{X}_0, W, \tilde{\mathbf{u}}, \mathbf{z}_l^{n,\cdot})|^2 \right] \leq \varrho_0 (1 + h |\mathbf{z}_l^{n,\cdot} - \tilde{\mathbf{z}}_l^{n,\cdot}|^2 + h |\tilde{\mathbf{z}}_l^{n,\cdot}|^2). \quad (4.32)$$

Step 2: We now introduce the natural filtration of the algorithm namely $\mathcal{F} = (\mathcal{F}_m)_{0 \leq m \leq M}$, defined by $\mathcal{F}_m = \sigma(\mathbf{u}_0, \mathcal{X}_0^{(k)}, W^{(k)}, 1 \leq k \leq m)$, $m \geq 1$, and $\mathcal{F}_0 = \sigma(\mathbf{u}_0)$. From the dynamics (2.48), we directly get

$$\begin{aligned} |\mathbf{z}_{l,m+1}^{n,\cdot} - \tilde{\mathbf{z}}_l^{n,\cdot}|^2 &= |\mathbf{z}_{l,m}^{n,\cdot} - \tilde{\mathbf{z}}_l^{n,\cdot}|^2 - 2\gamma_{m+1}^z H^{n,l}(\mathcal{X}_0^{(m+1)}, W^{(m+1)}, \tilde{\mathbf{u}}, \mathbf{z}_{l,m}^{n,\cdot}) \cdot (\mathbf{z}_{l,m}^{n,\cdot} - \tilde{\mathbf{z}}_l^{n,\cdot}) \\ &\quad + (\gamma_{m+1}^z)^2 |H^{n,l}(\mathcal{X}_0^{(m+1)}, W^{(m+1)}, \tilde{\mathbf{u}}, \mathbf{z}_{l,m}^{n,\cdot})|^2 \end{aligned}$$

so that introducing the sequence of \mathcal{F} -martingale increments,

$$\Delta M_{m+1} := \left(\frac{1}{\beta_K \sqrt{h}} \nabla_{\mathfrak{z}_l^{n,\cdot}} \mathfrak{H}^{n,l}(\tilde{\mathbf{u}}, \mathbf{u}_m) - H^{n,l}(\mathcal{X}_0^{(m+1)}, W^{(m+1)}, \tilde{\mathbf{u}}, \mathfrak{z}_{l,m}^{n,\cdot}) \right) \cdot (\mathfrak{z}_{l,m+1}^{n,\cdot} - \check{\mathfrak{z}}_l^{n,\cdot}), \quad m \geq 0,$$

we have

$$\begin{aligned} |\mathfrak{z}_{l,m+1}^{n,\cdot} - \check{\mathfrak{z}}_l^{n,\cdot}|^2 &= |\mathfrak{z}_{l,m}^{n,\cdot} - \check{\mathfrak{z}}_l^{n,\cdot}|^2 - \frac{2}{\beta_K \sqrt{h}} \gamma_{m+1}^z \nabla_{\mathfrak{z}_l^{n,\cdot}} \mathfrak{H}^{n,l}(\tilde{\mathbf{u}}, \mathbf{u}_m) \cdot (\mathfrak{z}_{l,m}^{n,\cdot} - \check{\mathfrak{z}}_l^{n,\cdot}) \\ &\quad + 2\gamma_{m+1}^z \Delta M_{m+1} + (\gamma_{m+1}^z)^2 |H^{n,l}(\mathcal{X}_0^{(m+1)}, W^{(m+1)}, \tilde{\mathbf{u}}, \mathfrak{z}_{l,m}^{n,\cdot})|^2. \end{aligned}$$

Now, from the previous equality, (2.34) and the fact that $\mathbb{E}_{\tilde{\mathbf{u}}}[\Delta M_{m+1} | \mathcal{F}_m] = 0$, recall (2.43), we obtain

$$\begin{aligned} \mathbb{E}_{\tilde{\mathbf{u}}} \left[|\mathfrak{z}_{l,m+1}^{n,\cdot} - \check{\mathfrak{z}}_l^{n,\cdot}|^2 \right] &\leq \mathbb{E}_{\tilde{\mathbf{u}}} \left[|\mathfrak{z}_{l,m}^{n,\cdot} - \check{\mathfrak{z}}_l^{n,\cdot}|^2 \right] \left(1 - 4 \frac{h\alpha_K}{\beta_K \sqrt{h}} \gamma_{m+1}^z \right) + (\gamma_{m+1}^z)^2 \mathbb{E}_{\tilde{\mathbf{u}}} \left[|H^{n,l}(\mathcal{X}_0^{(m+1)}, W^{(m+1)}, \tilde{\mathbf{u}}, \mathfrak{z}_{l,m}^{n,\cdot})|^2 \right] \\ &\leq \mathbb{E}_{\tilde{\mathbf{u}}} \left[|\mathfrak{z}_{l,m}^{n,\cdot} - \check{\mathfrak{z}}_l^{n,\cdot}|^2 \right] \left(1 - 4 \frac{h\alpha_K}{\beta_K \sqrt{h}} \gamma_{m+1}^z + \varrho_0 h (\gamma_{m+1}^z)^2 \right) + \varrho_0 (\gamma_{m+1}^z)^2 (1 + h |\check{\mathfrak{z}}_l^{n,\cdot}|^2) \end{aligned} \quad (4.33)$$

where, for the last inequality, we used (4.32) together with the fact that, since $(\mathcal{X}_0^{(m+1)}, W^{(m+1)})$ is independent of \mathcal{F}_m and \mathfrak{z}_m is \mathcal{F}_m -measurable, one has

$$\mathbb{E}_{\tilde{\mathbf{u}}} \left[|H^{n,l}(\mathcal{X}_0^{(m+1)}, W^{(m+1)}, \tilde{\mathbf{u}}, \mathfrak{z}_{l,m}^{n,\cdot})|^2 | \mathcal{F}_m \right] = \mathbb{E}_{\tilde{\mathbf{u}}} \left[|H^{n,l}(\mathcal{X}_0, W, \tilde{\mathbf{u}}, \mathfrak{z}_l^{n,\cdot})|^2 \right]_{|\mathfrak{z}_l^{n,\cdot} = \mathfrak{z}_{l,m}^{n,\cdot}}.$$

Observe now that by the very definition (2.45) of the sequence $(\gamma_m^z)_{m \geq 1}$ and using the fact that $\alpha_K/\beta_K \leq 1$ and $\varrho_0 \geq 16$, one gets $1 - 4 \frac{h\alpha_K}{\beta_K \sqrt{h}} \gamma_{m+1}^z + \varrho_0 h (\gamma_{m+1}^z)^2 = 1 - (4 \frac{\alpha_K}{\beta_K} \gamma_{m+1} - \varrho_0 \gamma_{m+1}^2) \geq 1 - (\sqrt{\varrho_0} \gamma_{m+1} - \varrho_0 \gamma_{m+1}^2) \geq 1 - 1/4 = 3/4$. As a consequence, $\Pi_m := \prod_{k=1}^m (1 - 4 \frac{h\alpha_K}{\beta_K \sqrt{h}} \gamma_k^z + \varrho_0 h (\gamma_k^z)^2) = \prod_{k=1}^m (1 - 4 \frac{\alpha_K}{\beta_K} \gamma_k + \varrho_0 \gamma_k^2)$ is a product of positive terms. From (4.33), we thus deduce

$$\begin{aligned} \mathbb{E}_{\tilde{\mathbf{u}}} \left[|\mathfrak{z}_{l,m+1}^{n,\cdot} - \check{\mathfrak{z}}_l^{n,\cdot}|^2 \right] &\leq \Pi_{m+1} \mathbb{E}_{\tilde{\mathbf{u}}} \left[|\mathfrak{z}_{l,0}^{n,\cdot} - \check{\mathfrak{z}}_l^{n,\cdot}|^2 \right] + \varrho_0 \left(\frac{1}{h} + |\check{\mathfrak{z}}_l^{n,\cdot}|^2 \right) \sum_{q=1}^{m+1} \frac{\Pi_{m+1}}{\Pi_q} \gamma_q^2 \\ &\leq 2\varrho_1 \exp \left(-4 \frac{\alpha_K}{\beta_K} \Gamma_{m+1} \right) \left(\mathbb{E}_{\tilde{\mathbf{u}}} \left[|\mathfrak{z}_{l,0}^{n,\cdot}|^2 \right] + |\check{\mathfrak{z}}_l^{n,\cdot}|^2 \right) \\ &\quad + \varrho_1 \varrho_0 \left(\frac{1}{h} + |\check{\mathfrak{z}}_l^{n,\cdot}|^2 \right) \sum_{q=1}^{m+1} \exp \left(-4 \frac{\alpha_K}{\beta_K} (\Gamma_{m+1} - \Gamma_q) \right) \gamma_q^2 \\ &\leq \varrho_0 \varrho_1 \left(1 + \mathbb{E}_{\tilde{\mathbf{u}}} \left[|\mathfrak{z}_{l,0}^{n,\cdot}|^2 \right] \right) \left(\frac{1}{h} + |\check{\mathfrak{z}}_l^{n,\cdot}|^2 \right) \sum_{q=1}^{m+1} \exp \left(-4 \frac{\alpha_K}{\beta_K} (\Gamma_{m+1} - \Gamma_q) \right) \gamma_q^2 \end{aligned} \quad (4.34)$$

where we used the standard inequality $1 + x \leq e^x$, the fact that $\rho_0 \geq 2$ and introduced the quantity

$$\varrho_1 := \exp(\varrho_0 \sum_{m \geq 1} \gamma_m^2). \quad (4.35)$$

This concludes the proof for (4.26).

Step 3: Recalling Definition 2.5 and using (2.29) as well as Assumption 2.3, we directly deduce

$$\mathbb{E}_{\tilde{\mathbf{u}}}\left[\|\Phi_M(\tilde{\mathbf{u}}) - \Phi(\tilde{\mathbf{u}})\|^2\right] \leq \mathbb{E}_{\tilde{\mathbf{u}}}\left[\kappa_K |\mathfrak{y}_M - \mathfrak{y}|^2 + h\kappa_K \sum_{n=1}^{N-1} \sum_{l=1}^d |\hat{\mathbf{z}}_{l,M}^{n,\cdot} - \check{\mathbf{z}}_l^{n,\cdot}|^2\right]$$

so that, using (4.26)

$$\begin{aligned} \mathbb{E}_{\tilde{\mathbf{u}}}\left[\|\Phi_M(\tilde{\mathbf{u}}) - \Phi(\tilde{\mathbf{u}})\|^2\right] &\leq \kappa_K L_{K,M}(1 + |\mathfrak{y}|^2) + h\kappa_K L_{K,M} \sum_{n=1}^{N-1} \sum_{l=1}^d \left(\frac{1}{h} + |\check{\mathbf{z}}_l^{n,\cdot}|^2\right), \\ &\leq \kappa_K L_{K,M} + \frac{\kappa_K}{\alpha_K} L_{K,M} \|\mathfrak{y}\|_y^2 + h\kappa_K L_{K,M} Nd \frac{1}{h} + \frac{\kappa_K}{\alpha_K} L_{K,M} \|\check{\mathbf{z}}\|_z^2, \\ &\leq \kappa_K L_{K,M} (1 + dN) + \frac{\kappa_K}{\alpha_K} L_{K,M} \|\check{\mathbf{u}}\|^2, \end{aligned}$$

which concludes the proof. \square

The following result provides an upper-bound for the quantity $L_{K,M}$ for a given specification of the learning step that is useful to study the complexity of the global algorithm.

Lemma 4.4. *Let Assumption 2.3 hold. For $\gamma > 0$, $\rho \in (\frac{1}{2}, 1)$, set $\gamma_m := \gamma m^{-\rho}$, $m \geq 1$. If the number of steps M in the stochastic gradient descent algorithm satisfies*

$$\gamma \frac{\alpha_K}{\beta_K} M^{1-\rho} \geq \frac{\sqrt{2}}{2}, \quad (4.36)$$

then, there exists some positive constant $C := C(\rho, \gamma)$ such that

$$L_{K,M} \leq C \left(e^{-2\sqrt{2}\ln(2)\gamma \frac{\alpha_K}{\beta_K} M^{1-\rho}} + \frac{\beta_K}{\alpha_K M^\rho} \right). \quad (4.37)$$

Remark 4.1. 1. In practice, $L_{K,M}$ should go to zero with respect to the optimal parameters.

Thus, we must have that $\frac{\beta_K}{\alpha_K M^\rho}$ goes to zero and $\frac{\alpha_K}{\beta_K} M^{1-\rho}$ goes to infinity at the same time as M goes to infinity. This will be carefully discussed in Section 4.4.3. With these constraints, we will naturally have that (4.36) is satisfied.

2. A careful analysis of the proof below shows that $\lim_{\rho \rightarrow 0.5+} C(\rho, \gamma) = +\infty$, which comes from the dependence of $C(\rho, \gamma)$ with respect to $\sum_1^{+\infty} \frac{1}{m^{2\rho}}$. However, one must bear in mind that ρ is a fixed (but optimised) parameter.

Proof of Lemma 4.4. We have, since $\Gamma_m = \gamma \sum_{q=1}^m \frac{1}{q^\rho}$, for $m \geq 1$,

$$\frac{\gamma}{1-\rho} (m^{1-\rho} - 1) \leq \Gamma_m \leq \frac{\gamma}{1-\rho} (m^{1-\rho} - 1) + \gamma \quad (4.38)$$

by standard computations based on comparison between series and integral, leading to

$$\Gamma_m - \Gamma_M \leq \frac{\gamma}{1-\rho} (m^{1-\rho} - M^{1-\rho}) + \gamma. \quad (4.39)$$

Recalling (4.27), we employ the following decomposition

$$L_{K,M} = \varrho_0 \varrho_1 \left(1 + \mathbb{E}[|\mathbf{u}_0|^2]\right) \sum_{m=1}^M \exp\left(-4 \frac{\alpha_K}{\beta_K} (\Gamma_M - \Gamma_m)\right) \gamma_m^2 \quad (4.40)$$

$$\leq \varrho_0 \varrho_1 \left(1 + \mathbb{E}[|\mathbf{u}_0|^2]\right) \exp\left(4 \gamma \frac{\alpha_K}{\beta_K}\right) (A_M + B_M + \gamma_M^2) \quad (4.41)$$

with

$$A_M := \sum_{m=1}^{\lfloor M/2 \rfloor} \exp\left(4 \frac{\alpha_K}{\beta_K} \frac{\gamma}{1-\rho} \{m^{1-\rho} - M^{1-\rho}\}\right) \frac{\gamma^2}{m^{2\rho}},$$

$$B_M := \sum_{m=\lfloor M/2 \rfloor + 1}^{M-1} \exp\left(4 \frac{\alpha_K}{\beta_K} \frac{\gamma}{1-\rho} \{m^{1-\rho} - M^{1-\rho}\}\right) \frac{\gamma^2}{m^{2\rho}}.$$

For the first term A_M , we observe that, for $m \leq \lfloor M/2 \rfloor \leq M/2$ and $\frac{1}{2} < \rho < 1$,

$$m^{1-\rho} - M^{1-\rho} \leq -\frac{\sqrt{2}}{2} \ln(2)(1-\rho)M^{1-\rho}. \quad (4.42)$$

We then compute

$$A_M \leq \exp\left(-2\sqrt{2} \ln(2) \gamma \frac{\alpha_K}{\beta_K} M^{1-\rho}\right) \sum_{m=1}^{\lfloor M/2 \rfloor} \frac{\gamma^2}{m^{2\rho}}$$

$$\leq C_{\rho, \gamma} \exp\left(-2\sqrt{2} \ln(2) \gamma \frac{\alpha_K}{\beta_K} M^{1-\rho}\right). \quad (4.43)$$

We now study the term B_M which reads

$$B_M = \gamma^2 \exp\left(-4 \frac{\alpha_K}{\beta_K} \frac{\gamma}{1-\rho} M^{1-\rho}\right) \sum_{m=\lfloor M/2 \rfloor + 1}^{M-1} \lambda(m)$$

where, the map λ is defined for $x \geq 1$ by

$$\lambda(x) := \exp\left(4 \frac{\alpha_K}{\beta_K} \frac{\gamma}{1-\rho} x^{1-\rho}\right) \frac{1}{x^{2\rho}}. \quad (4.44)$$

We observe that λ is increasing on $[\lfloor M/2 \rfloor + 1, +\infty)$ when (4.36) holds. This leads to

$$\begin{aligned} \sum_{m=\lfloor M/2 \rfloor + 1}^{M-1} \lambda(m) &\leq \int_{M/2}^M \lambda(x) dx \\ &\leq \frac{2^\rho}{M^\rho} \int_{M/2}^M \exp\left(4 \frac{\alpha_K}{\beta_K} \frac{\gamma}{1-\rho} x^{1-\rho}\right) \frac{1}{x^\rho} dx \\ &\leq \frac{2^{\rho-2} \beta_K}{\gamma M^\rho \alpha_K} \exp\left(4 \frac{\alpha_K}{\beta_K} \frac{\gamma}{1-\rho} M^{1-\rho}\right) \end{aligned}$$

which in turn yields $B_M \leq \frac{\gamma \beta_K}{M^\rho \alpha_K}$.

Inserting the previous inequality and estimate (4.43) into (4.41) concludes the proof, since $\mathbb{E}[|\mathbf{u}_0|^2] < \infty$, recall Definition 2.7, step 1. and $\frac{\alpha_K}{\beta_K} \leq 1$ recall Assumption 2.3 and (2.42). \square

Remark 4.2. Let us importantly point out that if one choses $\gamma_m = \gamma/m$, with $\gamma > 0$, then from standard comparison between series and integral $\Gamma_m - \Gamma_M \leq \gamma(\ln(m/M) + 1)$ so that repeating the computations of the proof of Lemma 4.4, one has to consider the two disjoint cases $\gamma < \frac{\beta_K}{4\alpha_K}$ and $\gamma > \frac{\beta_K}{4\alpha_K}$ in order to provide an upper bound for the quantity of interest $L_{K,M}$. Only the latter allows to obtain the best convergence rate of order $1/M$. However, in practice, the user does not know the exact value of $\frac{\beta_K}{4\alpha_K}$ so that one will often consider higher values of γ than requested which will have the undesirable effect to deteriorate the upper-bound as suggested by the value of ϱ_1 in (4.35). Moreover, as shown in Section 4.4, the value $\frac{\beta_K}{4\alpha_K}$ actually goes to infinity when the prescribed approximation error ε goes to zero so that the latter condition becomes more and more stringent.

We now give an upper bound for the error \mathcal{E}_P defined by (4.19), with respect to all the algorithm's parameters. These parameters will be chosen in the next section taking into account the precise specification of the functional approximation space.

Proposition 4.4. Suppose that Assumption 2.1, Assumption 2.2 (i), (ii) and Assumption 2.3 hold. Assume that there exists a positive constant η (independent of N , M and the basis functions (ψ)) such that

$$\frac{\kappa_K}{h \wedge \alpha_K} L_{K,M} \leq \eta. \quad (4.45)$$

If $T(1 + 2L^2(1 + h)) < 1$ and $\delta_{h,\eta} := \frac{16L^2T(1+\eta)}{1-T(1+2L^2(1+h))} < 1$, then for any $\varepsilon > 0$ there exists a positive constant C_ε such that

$$\mathcal{E}_{RM} \leq C_\varepsilon \frac{\kappa_K}{h \wedge \alpha_K} L_{K,M}$$

so that, with the notations of Proposition 4.3, it holds

$$\mathcal{E}_P \leq \delta_{h,\varepsilon}^P \mathcal{E}_0 + C_\varepsilon \left(\frac{\kappa_K}{h \wedge \alpha_K} L_{K,M} + \mathcal{E}_\psi + \mathcal{E}_\pi \right). \quad (4.46)$$

Remark 4.3. In practice, η will be fixed to be a small constant as the term in the left hand side of (4.45) should be asymptotically zero.

Proof of Proposition 4.4.

Step 1: From Proposition 4.3, we see that to obtain (4.46), it remains to control

$$\mathcal{E}_{RM} = \max_{1 \leq p \leq P} \mathbb{E} \left[\left\| \Phi_M(\mathbf{u}_M^{p-1}) - \Phi(\mathbf{u}_M^{p-1}) \right\|^2 \right].$$

Using Lemma 4.3, we have

$$\mathbb{E} \left[\left\| \Phi_M(\mathbf{u}_M^{p-1}) - \Phi(\mathbf{u}_M^{p-1}) \right\|^2 \right] \leq \kappa_K L_{K,M} (1 + dN) + \frac{\kappa_K}{\alpha_K} L_{K,M} \mathbb{E} \left[\left\| \Phi(\mathbf{u}_M^{p-1}) \right\|^2 \right]. \quad (4.47)$$

To conclude the proof, we will in the next step, provide an upper bound for the term $\mathbb{E} \left[\left\| \Phi(\mathbf{u}_M^{p-1}) \right\|^2 \right]$, uniformly with respect to p .

Step 2: We denote by C_ε a constant that may change from line to line along with ε . From Young's inequality and Lemma 4.2, we obtain

$$\begin{aligned}\mathbb{E}[\|\Phi(\mathbf{u}_M^p)\|^2] &\leq (1 + \varepsilon)\mathbb{E}[\|\Phi(\mathbf{u}_M^p) - \bar{\mathbf{u}}\|^2] + (1 + \frac{1}{\varepsilon})\|\bar{\mathbf{u}}\|^2 \\ &\leq \delta_h(1 + \varepsilon)\mathbb{E}[\|\mathbf{u}_M^p - \bar{\mathbf{u}}\|^2] + C_\varepsilon(\mathcal{E}_\pi + \mathcal{E}_\psi + \|\bar{\mathbf{u}}\|^2) \\ &\leq \delta_h(1 + \varepsilon)\mathbb{E}[\|\mathbf{u}_M^p\|^2] + C_\varepsilon(\mathcal{E}_\pi + \mathcal{E}_\psi + \|\bar{\mathbf{u}}\|^2)\end{aligned}$$

up to a modification of ε . From the previous inequality, we readily obtain $\mathbb{E}[\|\Phi(\mathbf{u}_M^0)\|^2] \leq C_\varepsilon$. Now, if p is a positive integer, noting again that

$$\mathbb{E}[\|\mathbf{u}_M^p\|^2] \leq 2\mathbb{E}[\|\Phi_M(\mathbf{u}_M^{p-1}) - \Phi(\mathbf{u}_M^{p-1})\|^2] + 2\mathbb{E}[\|\Phi(\mathbf{u}_M^{p-1})\|^2]$$

we obtain

$$\begin{aligned}\mathbb{E}[\|\Phi(\mathbf{u}_M^p)\|^2] &\leq 2\delta_h(1 + \varepsilon)\mathbb{E}[\|\Phi(\mathbf{u}_M^{p-1})\|^2] + 2\delta_h(1 + \varepsilon)\mathbb{E}[\|\Phi_M(\mathbf{u}_M^{p-1}) - \Phi(\mathbf{u}_M^{p-1})\|^2] \\ &\quad + C_\varepsilon(\mathcal{E}_\pi + \mathcal{E}_\psi + \|\bar{\mathbf{u}}\|^2)\end{aligned}$$

so that using (4.47), we get

$$\begin{aligned}\mathbb{E}[\|\Phi(\mathbf{u}_M^p)\|^2] &\leq 2\delta_h(1 + \varepsilon) \left(1 + \frac{\kappa_K}{\alpha_K} L_{K,M}\right) \mathbb{E}[\|\Phi(\mathbf{u}_M^{p-1})\|^2] \\ &\quad + 2\delta_h(1 + \varepsilon)\kappa_K L_{K,M} (1 + dN) + C_\varepsilon(\mathcal{E}_\pi + \mathcal{E}_\psi + \|\bar{\mathbf{u}}\|^2).\end{aligned}$$

From (4.45) and the fact that $\delta_{h,\eta}$, we can set ε such that $2\delta_h(1 + \varepsilon)(1 + \frac{\kappa_K}{\alpha_K} L_{K,M}) \leq \delta_{h,\eta}(1 + \varepsilon) < 1$ so that from the above inequality, by induction, for any positive integer p , we get

$$\mathbb{E}[\|\Phi(\mathbf{u}_M^p)\|^2] \leq (\delta_{h,\eta}(1 + \varepsilon))^p \mathbb{E}[\|\Phi(\mathbf{u}_M^0)\|^2] + C_\varepsilon(\mathcal{E}_\pi + \mathcal{E}_\psi + \|\bar{\mathbf{u}}\|^2 + \delta_h) \leq C_\varepsilon,$$

which concludes the proof. \square

We now have all the ingredients to give the proof of the main result announced in Section 2.3 on the upper bound for the global convergence error at the initial time.

Proof of Theorem 2.1 From the very definition (2.51) of the global error, we deduce

$$\mathcal{E}_{\text{MSE}} \leq 2\mathbb{E}[|u(0, \mathcal{X}_0) - \bar{u}(\mathcal{X}_0)|^2 + |Y_0^{\bar{\mathbf{u}}} - Y_0^{\mathbf{u}_M^P}|^2] \quad (4.48)$$

where we used the notations introduced in (2.9), (4.11) and (4.13). A fortiori, we have

$$\mathbb{E}[|u(0, \mathcal{X}_0) - \bar{u}_0(\mathcal{X}_0)|^2] \leq \mathcal{E}_\psi \quad \text{and} \quad \mathbb{E}[|Y_0^{\bar{\mathbf{u}}} - Y_0^{\mathbf{u}_M^P}|^2] \leq \mathcal{E}_P \quad (4.49)$$

recalling (4.10), (2.30) and (4.19). Combining (4.49) and (4.48) yields

$$\mathcal{E}_{\text{MSE}} \leq 2(\mathcal{E}_\psi + \mathcal{E}_P). \quad (4.50)$$

We eventually conclude the proof by invoking Proposition 4.4 together with Lemma 4.4. \square

4.4 Convergence and complexity analysis for sparse grid approximations

For this part, we work in the setting of Section 3.1.2. Our goal is to prove the theoretical upper-bound on the algorithm's complexity stated in Theorem 3.1.

We first state the following useful estimate.

Lemma 4.5. *Suppose that Assumption 3.1 is satisfied. Let $\phi : \mathbb{R}^d \rightarrow \mathbb{R}$ be a non-negative measurable function whose support is included in \mathcal{O} and $\check{\phi}$ be its 1-periodisation defined by (3.15). Then, it holds*

$$\mathfrak{C}^{-1} \mathbb{E}[\phi(U)] \leq \mathbb{E}[\check{\phi}(X_{t_n})] = \mathbb{E}[\phi(\hat{X}_{t_n})] \leq \mathfrak{C} \mathbb{E}[\phi(U)]$$

where U has law $\mathcal{U}((0, 1)^d)$ and \mathfrak{C} is given in Lemma 2.1.

Proof. We denote by $x' \mapsto p_X(t_n, x')$ the density function of X_{t_n} given by the Euler-Maruyama scheme taken at time t_n and starting from \mathcal{X}_0 with law $\mathcal{U}((0, 1)^d)$ at time 0. Note that we have $p_X(t_n, x') = \int p^\pi(0, t_n, x, x') \mathbf{1}_{(0,1)^d}(x) dx$ and using (2.4),

$$\mathfrak{C}^{-1} \int p(\mathfrak{C}t_n, x - x') \mathbf{1}_{(0,1)^d}(x) dx \leq p_X(t_n, x') \leq \mathfrak{C} \int p(\mathfrak{C}^{-1}t_n, x' - x) \mathbf{1}_{(0,1)^d}(x) dx.$$

Then,

$$\mathbb{E}[\phi(\hat{X}_{t_n})] = \mathbb{E}[\check{\phi}(X_{t_n})] \geq \mathfrak{C}^{-1} \int \check{\phi}(x') \int p(\mathfrak{C}t_n, x - x') \mathbf{1}_{(0,1)^d}(x) dx dx'$$

so that introducing the notation $\Xi = \xi + W_{\mathfrak{C}t_n}$,

$$\int \check{\phi}(x') \int p(\mathfrak{C}t_n, x - x') \mathbf{1}_{(0,1)^d}(x) dx dx' = \mathbb{E}[\check{\phi}(\Xi)] = \mathbb{E}[\phi(\hat{\Xi})] \quad (4.51)$$

The proof is then concluded by observing that $\mathcal{L}(\hat{\Xi}) = \mathcal{L}(U)$. The proof of the upper-bound follows from similar arguments. \square

4.4.1 Sparse grid approximation error

We now provide some upper-bound estimates for the sparse grid approximation error.

Theorem 4.1. *Under Assumption 3.1, there exists a positive constant $C := C(T, b, \sigma, d, \lambda_0)$ such that*

$$\mathcal{E}_\psi \leq C 2^{-4\ell} \ell^{d-1}. \quad (4.52)$$

To obtain an error of order ε^2 for the quantity \mathcal{E}_ψ , one may thus set $\ell_\varepsilon = \log_2(\varepsilon^{-\frac{1}{2}} |\log_2(\varepsilon)|^{\frac{d-1}{4}})$ so that, for each $n = 1, \dots, N-1$, the number of basis functions required satisfies

$$K_\varepsilon = \varepsilon^{-\frac{1}{2}} |\log_2(\varepsilon)|^{\frac{5(d-1)}{4}}.$$

Proof. For $1 \leq i \leq d$, $n = 0, \dots, N-1$, setting $v_i(t_n, x) = (\sigma^\top \nabla_x u)_i(t_n, x) \mathbf{1}_{\{x \in \mathcal{O}\}}$, $x \in \mathbb{R}^d$, from (2.2) we have

$$\|u\|_{H_{mix}^k(\mathcal{O})} + \max_{1 \leq i \leq d} \|v_i\|_{H_{mix}^k(\mathcal{O})} \leq C. \quad (4.53)$$

Moreover, from (3.19), we obtain

$$(\sigma^\top \nabla_x u)_i(t_n, X_{t_n}) = v_i(t_n, \hat{X}_{t_n}),$$

thus

$$\begin{aligned} \mathbb{E}[|(\sigma^\top \nabla_x u)(t_n, X_{t_n}) - Z_{t_n}^u|^2] &= \sum_{i=1}^d \mathbb{E} \left[\left| v_i(t_n, \hat{X}_{t_n}) - \sum_{k=1}^K \mathfrak{z}_i^{n,k} \psi_n^k(\hat{X}_{t_n}) \right|^2 \right] \\ &\leq \mathfrak{C} \sum_{i=1}^d \mathbb{E} \left[\left| v_i(t_n, U) - \sum_{k=1}^K \mathfrak{z}_i^{n,k} \psi_n^k(U) \right|^2 \right] \end{aligned}$$

with $U \sim \mathcal{U}((0, 1)^d)$ and where we use the upper-estimate given in Lemma 4.5 to obtain the last inequality. We also recall that

$$\mathbb{E}[|u(0, \mathcal{X}_0) - Y_0^u|^2] = \mathbb{E} \left[\left| u(0, U) - \sum_{k=1}^K \mathfrak{y}^k \psi_y^k(U) \right|^2 \right]. \quad (4.54)$$

From (2.18) and the previous estimates, we thus deduce

$$\begin{aligned} \mathcal{E}_\psi &\leq C \left(\inf_{\xi \in \mathcal{Y}_y} \|\xi - u(0, \cdot)\|_{L^2(\mathcal{O})}^2 + \max_{0 \leq n \leq N-1} \sum_{i=1}^d \inf_{\xi \in \mathcal{Y}_n^z} \|\xi - v_i(t_n, \cdot)\|_{L^2(\mathcal{O})}^2 \right), \\ &\leq C 2^{-4\ell} \ell^{d-1}, \end{aligned} \quad (4.55)$$

where for the last inequality we used (3.13) and (4.53).

Finally, setting $\ell_\varepsilon = \log_2(\varepsilon^{-\frac{1}{2}} |\log_2(\varepsilon)|^{\frac{d-1}{4}})$ yields $\mathcal{E}_\psi = O(\varepsilon^2)$ as $\varepsilon \downarrow 0$ and from (3.12) (see also Remark 3.1) we deduce that in this case $K_\varepsilon = \varepsilon^{-\frac{1}{2}} |\log_2(\varepsilon)|^{\frac{5(d-1)}{4}}$. \square

4.4.2 Norm equivalence constants

We now provide some estimates for the value of α_K and κ_K appearing in Assumption 2.3.

Proposition 4.5. *Suppose that Assumption 3.1 holds. In the setting of Section 3.1.2, there exists a constant $\mathfrak{k} \leq 1$ such that*

$$\mathfrak{k} = \alpha_K = \frac{1}{\kappa_K}.$$

Proof. For any $\mathbf{u} = (\mathfrak{y}, \mathfrak{z}) \in \mathbb{R}^{K_y} \times \mathbb{R}^{d\bar{K}_z}$, any $0 \leq n \leq N-1$ and any $l \in \{1, \dots, d\}$, from (2.6) we have

$$\mathbb{E}[|(Z_{t_n}^u)^l|^2] = \mathbb{E} \left[\left| \sum_{k=1}^K \mathfrak{z}_l^{n,k} \psi_n^k(\hat{X}_{t_n}) \right|^2 \right],$$

Using Lemma 4.5, we obtain

$$\mathfrak{C}^{-1} \mathbb{E} \left[\left| \sum_{k=1}^K \mathfrak{z}_l^{n,k} \psi_n^k(U) \right|^2 \right] \leq \mathbb{E} \left[|(Z_{t_n}^u)^l|^2 \right] \leq \mathfrak{C} \mathbb{E} \left[\left| \sum_{k=1}^K \mathfrak{z}_l^{n,k} \psi_n^k(U) \right|^2 \right]. \quad (4.56)$$

Note that in our setting, $\psi_n^k = \chi^k$, so it holds

$$\int_{\mathcal{O}} \left| \sum_{k=1}^K \mathfrak{z}_l^{n,k} \psi_n^k(z) \right|^2 dz = \int_{\mathcal{O}} \left| \sum_{k=1}^K \mathfrak{z}_l^{n,k} \chi^k(x) \right|^2 dx. \quad (4.57)$$

Since the basis functions $(\chi^k)_{1 \leq k \leq K}$ forms a Riesz basis [29], there exists a constant $\underline{c} \geq 1$ such that it holds

$$\underline{c}^{-1} \sum_{k=1}^K |\mathfrak{z}_l^{n,k}|^2 \leq \int_{[0,1]^d} \left| \sum_{k=1}^K \mathfrak{z}_l^{n,k} \chi^k(x) \right|^2 dx \leq \underline{c} \sum_{k=1}^K |\mathfrak{z}_l^{n,k}|^2 \quad (4.58)$$

Combining (4.56)-(4.57)-(4.58) and taking into account all the component of $Z_{t_n}^u$, we compute

$$\underline{c}^{-1} \mathfrak{C}^{-1} d \sum_{k=1}^K |\mathfrak{z}_l^{n,k}|^2 \leq \mathbb{E} \left[|(Z_{t_n}^u)|^2 \right] \leq \underline{c} \mathfrak{C} d \sum_{k=1}^K |\mathfrak{z}_l^{n,k}|^2. \quad (4.59)$$

We also observe that

$$\mathbb{E} [|Y_0^u|^2] = \mathbb{E} \left[\left| \sum_{k=1}^K \mathfrak{y}^k \chi^k(\mathcal{X}_0) \right|^2 \right]. \quad (4.60)$$

Since $\mathcal{X}_0 \sim \mathcal{U}((0,1)^d)$, we similarly deduce that

$$\underline{c}^{-1} \sum_{k=1}^K |\mathfrak{y}_l^{n,k}|^2 \leq \mathbb{E} [|Y_0^u|^2] \leq \underline{c} \sum_{k=1}^K |\mathfrak{y}_l^{n,k}|^2. \quad (4.61)$$

The proof is concluded by combining (4.59) and (4.61) with (2.30) and setting $\mathfrak{k} = \underline{c}^{-1} \mathfrak{C}^{-1} d^{-1}$. \square

4.4.3 Complexity analysis

Lemma 4.6. *Under Assumption 3.1, one can set*

$$\beta_K = C_d (1 + 2^\ell \ell^{d-1}) \quad (4.62)$$

for some positive constant C_d which depends on the PDE dimension d .

Proof.

Step 1: For any $n \in \{0, \dots, N-1\}$, any $\ell \in \{1, \dots, d\}$, one has

$$\mathbb{E} [|\tilde{\omega}_\ell^{n,\cdot}|^4] = \mathbb{E} \left[\left(\sum_{k=1}^K |\tilde{\omega}_\ell^{n,k}|^2 \right)^2 \right]. \quad (4.63)$$

Using Jensen's inequality, we obtain

$$\mathbb{E}[|\tilde{\omega}_\ell^{n,\cdot}|^4] \leq K \mathbb{E}\left[\sum_{k=1}^K |\tilde{\omega}_\ell^{n,k}|^4\right] \leq 3d^2 K \sum_{k=1}^K \mathbb{E}\left[|\psi_n^k(\hat{X}_{t_n})|^4\right]. \quad (4.64)$$

From now on, we use the indexation related to the sparse grid description introduced in Remark 3.1, namely, we write

$$\sum_{k=1}^K \mathbb{E}\left[|\psi_n^k(\hat{X}_{t_n})|^4\right] = \sum_{(\mathbf{l}, \mathbf{i}) \in \mathcal{C}} \mathbb{E}\left[|\psi_n^{(\mathbf{l}, \mathbf{i})}(\hat{X}_{t_n})|^4\right] \quad (4.65)$$

$$= \sum_{(\mathbf{l}, \mathbf{i}) \in \mathcal{C}} \mathbb{E}\left[|\chi^{(\mathbf{l}, \mathbf{i})}(\hat{X}_{t_n})|^4\right] \quad (4.66)$$

in our setting.

Step 2: Using Lemma 4.5, we observe

$$\mathbb{E}\left[|\chi^{(\mathbf{l}, \mathbf{i})}(\hat{X}_{t_n})|^4\right] \leq \mathfrak{C} \mathbb{E}\left[|\chi^{(\mathbf{l}, \mathbf{i})}(U)|^4\right]. \quad (4.67)$$

Moreover, we compute

$$\int |\phi^{(l, i)}(x)|^4 dx = \int |\phi(2^l x - i)|^4 dx \leq C 2^{-l}$$

and from the definition of $\chi^{(l_j, i_j)}$, we deduce

$$\int |\chi^{(l_j, i_j)}(x)|^4 dx \leq C 2^l.$$

Combining the previous inequality with (4.67) leads to

$$\mathbb{E}\left[|\chi^{(\mathbf{l}, \mathbf{i})}(\hat{X}_{t_n})|^4\right] \leq C 2^{|\mathbf{l}|_1}$$

and inserting the previous estimate in (4.65) yields

$$\sum_{k=1}^K \mathbb{E}\left[|\psi_n^k(\hat{X}_{t_n})|^4\right] \leq C \sum_{(\mathbf{l}, \mathbf{i}) \in \mathcal{C}} 2^{|\mathbf{l}|_1}. \quad (4.68)$$

Step 3: We now quantify the term appearing in the right-hand side of (4.68), namely

$$Q := \sum_{(\mathbf{l}, \mathbf{i}) \in \mathcal{C}} 2^{|\mathbf{l}|_1} = 1 + \sum_{k=1}^{\ell} \sum_{\mathbf{l} \in \mathbb{N}^d} 2^{|\mathbf{l}|_1} \mathbf{1}_{\{\zeta_d(\mathbf{l})=k\}}. \quad (4.69)$$

We denote by $\|\mathbf{l}\|_0 = |\{j | l_j = 0\}|$. For $\mathbf{l} \neq \mathbf{0}$, recall that $\zeta_d(\mathbf{l}) = |\mathbf{l}|_1 + \|\mathbf{l}\|_0 - (d-1)$ (from the definition of ζ_d). Thus,

$$\begin{aligned} Q &= 1 + \sum_{k=1}^{\ell} \sum_{q=0}^{d-1} \sum_{\mathbf{l} \in (\mathbb{N}_{>0})^{d-q}} 2^{|\mathbf{l}|_1} \mathbf{1}_{\{|\mathbf{l}|_1=k+d-1-q \text{ and } \|\mathbf{l}\|_0=q\}} \\ &= 1 + \sum_{k=1}^{\ell} \sum_{q=0}^{d-1} 2^{k+d-1-q} C_{k+d-q-2}^{d-q-1} C_d^q \end{aligned}$$

recall that $|\{\mathbf{l} \in (\mathbb{N}_{>0})^{d-q} \mid |\mathbf{l}|_1 = k + d - 1 - q\}| = C_{k+d-q-2}^{d-q-1}$. Introducing $\theta = d - 1 - q$, we get

$$Q = 1 + \sum_{k=1}^{\ell} d2^k + \sum_{\theta=1}^{d-1} 2^{1+\theta} C_d^{d-1-\theta} \sum_{k=1}^{\ell} 2^{k-1} C_{k-1+\theta}^{\theta} \quad (4.70)$$

From Lemma 3.6 in [12], we know that $\sum_{k=1}^{\ell} 2^{k-1} C_{k-1+\theta}^{\theta} = 2^{\ell} \left(\frac{\ell^{\theta}}{\theta!} + O_d(\ell^{\theta-1}) \right)$. We thus obtain

$$Q = 2^{\ell} \left(\frac{2^d}{(d-1)!} \ell^{d-1} + O_d(\ell^{d-2}) \right)$$

which combined with (4.68) yields

$$\sum_{k=1}^K \mathbb{E} \left[|\psi_n^k(\hat{X}_{t_n})|^4 \right] \leq C_d 2^{\ell} \ell^{d-1}. \quad (4.71)$$

Combining the previous inequality with (4.64), we obtain

$$\mathbb{E} [|\tilde{\omega}_{\ell}^{n, \cdot}|^4] \leq C_d 2^{2\ell} \ell^{2d-2}. \quad (4.72)$$

Using similar arguments, as the basis function are chosen to be the same in our setting, we also have

$$\mathbb{E} [|\theta|^4] \leq C_d 2^{2\ell} \ell^{2d-2}.$$

The proof is then concluded recalling the definition of β_K in (2.42). \square

We now turn to the analysis of the convergence and complexity of the full Picard algorithm. The following corollary is a preparatory result and expresses the main convergence results in terms of the parameters P , M , ℓ and h .

Corollary 4.1. *Suppose that Assumption 3.1 as well as (4.36) and (4.45) hold. Set $\gamma_m = \gamma/m^{\rho}$, for some $\rho \in (1/2, 1)$ and $\gamma > 0$. If $T(1 + 2L^2(1 + h)) < 1$ and $\delta_{h,\eta} = \frac{16L^2T(1+2\eta)}{1-T(1+2L^2(1+h))} < 1$, then, with the notations of Proposition 4.3, for any $\varepsilon > 0$ such that $\delta_{h,\varepsilon} := \delta_{h,\eta}(1 + \varepsilon) < 1$ there exist constants $C_{\varepsilon} := C(\varepsilon, T, b, \sigma, d, \gamma, \rho) \geq 1$, $c := c(T, b, \sigma, d, \gamma) > 0$ such that it holds*

$$\mathcal{E}_P \leq \delta_{h,\varepsilon}^P \mathcal{E}_0 + C_{\varepsilon} \left(N e^{-c \frac{M^{1-\rho}}{1+2^{\ell} \ell^{d-1}}} + \frac{1 + 2^{\ell} \ell^{d-1}}{h M^{\rho}} + 2^{-4\ell} \ell^{d-1} + h \right). \quad (4.73)$$

Proof. Combining Proposition 4.4 with Theorem 4.1 and (2.19), we obtain

$$\mathcal{E}_P \leq \delta_{h,\varepsilon}^P \mathcal{E}_0 + C_{\varepsilon} \left(\frac{\kappa_K}{h \wedge \alpha_K} L_{K,M} + 2^{-4\ell} \ell^{d-1} + h \right). \quad (4.74)$$

From Proposition 4.5, we have that $\frac{\kappa_K}{h \wedge \alpha_K} \leq \frac{C}{h}$, which combined with Lemma 4.4 gives

$$\frac{\kappa_K}{h \wedge \alpha_K} L_{K,M} \leq \frac{C_{\rho,\gamma}}{h} \left(e^{-\gamma 2\sqrt{2} \ln(2) \frac{\ell}{\beta_K} M^{1-\rho}} + \frac{\beta_K}{\ell M^{\rho}} \right) \quad (4.75)$$

$$\leq \frac{C_{\rho,\gamma}}{h} \left(e^{-c \frac{M^{1-\rho}}{1+2^{\ell} \ell^{d-1}}} + \frac{1 + 2^{\ell} \ell^{d-1}}{M^{\rho}} \right) \quad (4.76)$$

for some positive constant c , where we used Lemma 4.6 for the last inequality. \square

We are now ready to establish the complexity of the full Picard algorithm.

Proof of Theorem 3.1 *Step 1: Setting the parameters P , N , M , ℓ and ρ .*

We will chose the parameters P , N , M , ℓ and ρ in order to achieve a global error \mathcal{E}_P of order ε^2 , as this error controls \mathcal{E}_{MSE} . We first set $P = 2|\log_2(\varepsilon)|$ and $N_\varepsilon = \lceil T\varepsilon^{-2} \rceil$ so that $h_\varepsilon = T/N_\varepsilon \leq \varepsilon^2$. From Theorem 4.1, we also know that setting $\ell_\varepsilon = \log_2(\varepsilon^{-\frac{1}{2}}|\log_2(\varepsilon)|^{\frac{d-1}{4}})$, we obtain $\mathcal{E}_\psi = O_d(\varepsilon^2)$ and $K_\varepsilon = O_d(\varepsilon^{-\frac{1}{2}}|\log_2(\varepsilon)|^{\frac{5(d-1)}{4}})$.

We now set M such that the term $\frac{K_\varepsilon}{M^\rho h_\varepsilon}$ is of order ε^2 , which leads to

$$M_\varepsilon = O_d(\varepsilon^{-\frac{9}{2\rho}}|\log_2(\varepsilon)|^{\frac{5(d-1)}{4\rho}}).$$

For $\iota > 1$, we set $\bar{\rho} = \frac{9}{10\iota}$ with the constraint $\bar{\rho} > \frac{1}{2}$ and we verify that

$$\frac{M_\varepsilon^{1-\bar{\rho}}}{K_\varepsilon} \geq c\varepsilon^{5(1-\iota)}|\log_2(\varepsilon)|^{\frac{5}{4}(d-1)(\frac{1}{\bar{\rho}}-2)}$$

for some constant $c > 0$. This leads to

$$e^{-c\frac{M_\varepsilon^{1-\bar{\rho}}}{1+2^\ell\varepsilon\ell_\varepsilon^{d-1}}} = o(\varepsilon^4)$$

and we also have that (4.36) is satisfied.

Step 2: Computing the complexity \mathcal{C}_ε . Recalling Remark 2.4, we see that the overall complexity \mathcal{C}_ε to reach the prescribed approximation accuracy ε^2 satisfies

$$\begin{aligned} \mathcal{C}_\varepsilon &= P_\varepsilon N_\varepsilon K_\varepsilon M_\varepsilon \\ &= O_d\left(|\log_2(\varepsilon)|\varepsilon^{-2}\varepsilon^{-\frac{1}{2}}|\log_2(\varepsilon)|^{\frac{5(d-1)}{4}}\varepsilon^{-5\iota}|\log_2(\varepsilon)|^{\frac{25(d-1)\iota}{18}}\right) \\ &= O_d(\varepsilon^{-\frac{5}{2}(1+2\iota)}|\log_2(\varepsilon)|^{1+\frac{45+50\iota}{36}(d-1)}), \end{aligned}$$

which concludes the proof. □

5 Appendix

We gather below all the parameters values used in the various algorithms, examples and basis functions settings. In particular, we recall that the domain specification is given in (3.22) and (3.23). The learning rates are given by (3.24). Denoting

$$\Gamma(\lambda) := (\alpha(\lambda), \beta_1(\lambda), \beta_0(\lambda), m_0(\lambda)) \in \mathbb{R}^4,$$

we set the parameters in all the approximating space \mathcal{V}_n^z , $1 \leq n \leq N-1$ to be the same: namely $\Gamma(\mathfrak{z}^{n,\cdot}) = \Gamma(\mathfrak{z}^{1,\cdot})$ for all $n \geq 2$. Thus, in the table below, the parameters of the learning rates are simply denoted by:

$$\Gamma := \{\Gamma(\mathfrak{y}), \Gamma(\mathfrak{z}^{0,\cdot}), \Gamma(\mathfrak{z}^{1,\cdot})\} \in \mathbb{R}^{3 \times 4}.$$

| Algorithms | Basis functions | dim | N | M | T | Initial $\mathbf{z}^{n,k}$ | p | Γ | \mathcal{E}_{MSE} |
|-------------------------|-----------------|-----|----|--------|-----|----------------------------|---|--|----------------------------|
| <i>Picard Algorithm</i> | Pre-wavelets | 3 | 10 | 100000 | 0.3 | 0 | 1 | (0.6, 0, 3, 15000), (0.6, 0, 20, 10000) | 0.0286 |
| | | | | | | | 2 | (0.6, 0, 2, 8000), (0.6, 0, 10, 8000) | 0.0247 |
| | | | | | | | 3 | (0.6, 0, 1, 8000), (0.6, 0, 5, 8000) | 0.0219 |
| | | | | | | | 4 | (0.6, 0, 0.5, 8000), (0.6, 0, 3, 8000) | 0.0207 |
| | | | | | | | 5 | (0.6, 0, 0.5, 8000), (0.6, 0, 3, 8000) | 0.0201 |

Table 6: Parameters for the periodic example

| Examples | a | dim | M | N | Initial y_0 | Learning rate |
|-------------------------------|------|-----|------|----|---------------|---------------|
| Quadratic | 1 | 5 | 2000 | 10 | 0.5 | 0.01 |
| Limits to Picard algorithm | -0.4 | 2 | 5000 | 20 | 0.3 | 0.002 |
| | -1.5 | 2 | 5000 | 20 | 0 | 0.001 |
| Financial example | N.A. | 2 | 6000 | 20 | 2 | 0.005 |
| | | 4 | 6000 | 20 | 5 | 0.005 |
| | | 5 | 5000 | 20 | 5 | 0.005 |
| | | 10 | 5000 | 20 | 8 | 0.005 |
| | | 15 | 5000 | 20 | 8 | 0.005 |
| | | 20 | 5000 | 20 | 8 | 0.005 |
| | | 25 | 5000 | 20 | 8 | 0.005 |

Table 7: Parameters by model for the *deep learning method* with $\text{layers} = 4, \text{batchsize} = 64$

References

- [1] BALLY, V., AND PAGÈS, G. Error analysis of the optimal quantization algorithm for obstacle problems. *Stochastic Processes and their Applications* 106, 1 (2003), 1 – 40.
- [2] BALLY, V., AND PAGÈS, G. A quantization algorithm for solving multidimensional discrete-time optimal stopping problems. *Bernoulli* 9, 6 (2003), 1003–1049.
- [3] BECK, C., E, W., AND JENTZEN, A. Machine learning approximation algorithms for high-dimensional fully nonlinear partial differential equations and second-order backward stochastic differential equations. *Journal of Nonlinear Science* (2017), 1–57.
- [4] BECK, C., HUTZENTHALER, M., JENTZEN, A., AND KUCKUCK, B. An overview on deep learning-based approximation methods for partial differential equations. *arXiv preprint arXiv:2012.12348* (2020).

| Examples | Basis functions | dim | N | r | Initial value | | | Γ |
|-------------------------|-----------------|-----|-----|-----|---------------|------------------------|--------------------|--|
| | | | | | η | $\mathbf{z}^{0,\cdot}$ | $\mathbf{z}^{n,k}$ | |
| Quadratic model | Pre-wavelets | 5 | 10 | 2 | 0.5 | -0.2 | 0 | (1, 0, 1, 100), (0.8, 0, 1, 100), (0.86, 0.02, 0.05, 100) |
| | Hat | 100 | 10 | 3.2 | 5.5 | 0 | 0 | (0.9, 0, 1, 100), (0.7, 0, 1, 100), (1, 0.003, 0.01, 1000) |
| Financial example | Pre-wavelets | 2 | 10 | 2 | 2 | 0 | 0 | (1, 0, 1.5, 1000), (1, 0, 20, 1000), (1, 0.003, 0.01, 1000) |
| | | 4 | 10 | 2 | 5 | 0 | 0 | (1, 0, 1, 1000), (1, 0, 20, 1000), (1, 0.001, 0.01, 1000) |
| | Hat | 5 | 10 | 2 | 5 | 0 | 0 | (0.95, 0, 0.3, 100), (1, 0, 5, 100), (1, 0.001, 0.01, 100) |
| | | 10 | 10 | 2.5 | 8 | 0 | 0 | (0.9, 0, 0.35, 300), (1, 0, 5, 300), (1, 0.001, 0.01, 300) |
| | | 15 | 10 | 2.5 | 8 | 0 | 0 | (0.85, 0, 0.3, 500), (1, 0, 5, 500), (1, 0.001, 0.01, 500) |
| | | 20 | 10 | 2.5 | 8 | 0 | 0 | (0.8, 0, 0.2, 1000), (1, 0, 5, 1000), (1, 0.001, 0.01, 1000) |
| | | 25 | 10 | 2.8 | 8 | 0 | 0 | (0.7, 0, 0.2, 1500), (1, 0, 5, 1500), (1, 0.001, 0.01, 1500) |
| | | | | | | | | |
| The challenging example | Hat | 1 | 10 | 2 | 0.5 | 0 | 0 | (1, 0, 0.5, 100), (1, 0, 3, 100), (1, 0.1, 0.1, 100) |
| | | 2 | 20 | 2 | 0.1 | 0 | 0 | (1, 0, 0.5, 100), (1, 0, 5, 100), (1, 0.2, 0.5, 100) |
| | | 5 | 40 | 2 | 0.4 | -1 | 0 | (1, 0, 0.5, 300), (0.95, 0, 5, 500), (1, 0.2, 0.1, 500) |
| | | 8 | 60 | 2.2 | 0.6 | 1 | 0.08 | (1, 0, 0.35, 500), (1, 0, 5, 500), (1, 0.2, 1, 500) |
| | | 10 | 100 | 2.5 | 0.1 | -1 | -0.1 | (1, 0, 0.35, 500), (0.95, 0, 5, 500), (1, 0.2, 1, 500) |

Table 8: Parameters by model for the *direct algorithm*

| Examples | Basis functions | dim | r | Initial value | | | a | p | Γ |
|----------------------------|-----------------|-----|-----|---------------|--------------------------|----------------------|------|-------------------|---|
| | | | | η | $\mathfrak{z}^{0,\cdot}$ | $\mathfrak{z}^{n,k}$ | | | |
| Quadratic model | Pre-wavelets | 5 | 2 | 0.5 | -0.2 | 0 | 1 | 1 | (1, 0, 0.8, 100), (0.9, 0, 1, 100), (0.84, 0.02, 0.05, 100) |
| | | | | | | | | 2 | (1, 0, 0.3, 100), (0.9, 0, 0.4, 100), (0.84, 0.01, 0.02, 100) |
| | | | | | | | | $p \geq 3$ | (1, 0, 0.2, 100), (0.9, 0, 0.2, 100), (0.84, 0.005, 0.01, 100) |
| | Hat | 25 | 2.8 | 2 | 0.1 | 0 | 1 | $1 \leq p \leq 3$ | (0.9, 0, 0.5, 100), (0.8, 0, 0.8, 100), (1, 0.003, 0.01, 1000) |
| Financial example | Pre-wavelets | 4 | 2 | 5 | 0.1 | -0.01 | N.A. | 1 | (1, 0, 1, 1000), (1, 0, 20, 1000), (1, 0.001, 0.01, 1000) |
| | | | | | | | | 2 | (1, 0, 0.3, 1000), (1, 0, 5, 1000), (1, 0.0005, 0.005, 1000) |
| | | | | | | | | 3 | (1, 0, 0.2, 1000), (1, 0, 5, 1000), (1, 0.0003, 0.003, 1000) |
| | | | | | | | | 4, 5 | (1, 0, 0.15, 1000), (1, 0, 3, 1000), (1, 0.0002, 0.002, 1000) |
| | | | | | | | | $p \geq 6$ | (1, 0, 0.1, 1000), (1, 0, 2, 1000), (1, 0.0001, 0.001, 1000) |
| | Hat | 20 | 2.5 | 8 | 0 | 0 | N.A. | 1 | (0.9, 0, 0.6, 1000), (1, 0, 5, 1000), (1, 0.001, 0.01, 1000) |
| | | | | | | | | 2 | (0.9, 0, 0.2, 1000), (1, 0, 4, 1000), (1, 0.001, 0.01, 1000) |
| | | | | | | | | 3 | (0.9, 0, 0.15, 1000), (1, 0, 3, 1000), (1, 0.0005, 0.005, 1000) |
| | | | | | | | | $p \geq 4$ | (0.9, 0, 0.1, 1000), (1, 0, 2, 1000), (1, 0.0005, 0.005, 1000) |
| Limits to Picard algorithm | Pre-wavelets | 2 | 2 | 0.3 | 0 | 0 | -0.4 | $1 \leq p \leq 9$ | (1, 0, 1, 300), (1, 0, 1, 300), (1, 0.6, 0.1, 300) |
| | | | | 0 | 0 | 0 | -1.5 | $1 \leq p \leq 9$ | (1, 0, 2, 300), (1, 0, 1, 300), (1, 0.6, 0.1, 300) |

Table 9: Parameters by model for the *Picard algorithm*

| Examples | Basis functions | dim | r | Initial value | | | N | p | Γ |
|-------------------------------|-----------------|-----|-----|---------------|--------------------------|----------------------|-----|-------------------|---|
| | | | | η | $\mathfrak{z}^{0,\cdot}$ | $\mathfrak{z}^{n,k}$ | | | |
| The challenging example | Hat | 1 | 2 | 0.5 | 0 | 0 | 10 | $1 \leq p \leq 5$ | $(1, 0, 0.5 * (0.8)^{p-1}, 100),$ $(1, 0, 3 * (0.8)^{p-1}, 100),$ $(1, 0.1 * (0.8)^{p-1}, 0.1 * (0.8)^{p-1}, 100)$ |
| | | 2 | 2 | 0.1 | 0 | 0 | 20 | $1 \leq p \leq 5$ | $(1, 0, 0.5 * (0.8)^{p-1}, 100),$ $(1, 0, 5 * (0.8)^{p-1}, 100),$ $(1, 0.2 * (0.8)^{p-1}, 0.5 * (0.8)^{p-1}, 100)$ |
| | | 5 | 2 | 0.4 | -2 | 0 | 40 | $1 \leq p \leq 5$ | $(1, 0, 0.5 * (0.8)^{p-1}, 300),$ $(0.95, 0, 5 * (0.8)^{p-1}, 500),$ $(1, 0.2 * (0.8)^{p-1}, 0.1 * (0.8)^{p-1}, 500)$ |
| | | 8 | 2.2 | 0.6 | 1 | 0.08 | 60 | $1 \leq p \leq 5$ | $(1, 0, 0.35 * (0.8)^{p-1}, 500),$ $(1, 0, 5 * (0.8)^{p-1}, 500),$ $(1, 0.2 * (0.8)^{p-1}, (0.8)^{p-1}, 500)$ |
| | | 10 | 2.5 | 0.1 | -1 | -0.1 | 100 | 1 | $(1, 0, 0.25, 500),$ $(0.95, 0, 4, 500),$ $(1, 0.15, 0.5, 500)$ |
| | | | | | | | | 2 | $(1, 0, 0.2, 500),$ $(0.95, 0, 3, 500),$ $(1, 0.12, 0.4, 500)$ |
| | | | | | | | | 3 | $(1, 0, 0.15, 500),$ $(0.95, 0, 2, 500),$ $(1, 0.1, 0.3, 500)$ |
| | | | | | | | | $p \geq 4$ | $(1, 0, 0.1, 500),$ $(0.95, 0, 1, 500),$ $(1, 0.08, 0.25, 500)$ |
| | | | | | | | | $p \geq 6$ | $(1, 0, 0.05, 500),$ $(0.95, 0, 0.5, 500),$ $(1, 0.05, 0.2, 500)$ |

Table 10: Parameters by model for the *Picard algorithm*

- [5] BENDER, C., AND DENK, R. A forward scheme for backward sdes. *Stochastic Processes and their Applications* 117, 12 (2007), 1793–1812.
- [6] BENVENISTE, A., MÉTIVIER, M., AND PRIOURET, P. *Adaptive algorithms and stochastic approximations*, vol. 22. Springer Science & Business Media, 2012.
- [7] BERGMAN, Y. Z. Option pricing with differential interest rates. *The Review of Financial Studies* 8, 2 (1995), 475–500.
- [8] BOHN, B. *Error analysis of regularized and unregularized least-squares regression on discretized function spaces*. PhD thesis, Institute for Numerical Simulation, University of Bonn, (2017).
- [9] BOHN, B. On the convergence rate of sparse grid least squares regression. In *Sparse Grids and Applications-Miami 2016*. Springer, (2018), pp. 19–41.
- [10] BOUCHARD, B., AND TOUZI, T. Discrete-time approximation and monte-carlo simulation of backward stochastic differential equations. *Stochastic Processes and their Applications* 111, 2 (2004), 175 – 206.
- [11] BRIAND, P., AND LABART, C. Simulation of bsdes by wiener chaos expansion. *The Annals of Applied Probability* 24, 3 (2014), 1129–1171.
- [12] BUNGARTZ, H.-J., AND GRIEBEL, M. Sparse grids. *Acta numerica* 13 (2004), 147–269.
- [13] CHASSAGNEUX, J.-F. Linear multistep schemes for bsdes. *SIAM Journal on Numerical Analysis* 52, 6 (2014), 2815–2836.
- [14] CHASSAGNEUX, J.-F., AND GARCIA TRILLOS, C. Cubature method to solve bsdes: Error expansion and complexity control. *Mathematics of Computation* 89, 324 (2020), 1895–1932.
- [15] CHASSAGNEUX, J.-F., AND RICHOU, A. Numerical simulation of quadratic bsdes. *The Annals of Applied Probability* 26, 1 (2016), 262–304.
- [16] CRISAN, D., AND MANOLARAKIS, K. Solving backward stochastic differential equations using the cubature method: application to nonlinear pricing. *SIAM Journal on Financial Mathematics* 3, 1 (2012), 534–571.
- [17] CRISAN, D., AND MANOLARAKIS, K. Second order discretization of backward sdes and simulation with the cubature method. *The Annals of Applied Probability* 24, 2 (2014), 652–678.
- [18] CRISAN, D., MANOLARAKIS, K., AND NIZAR, T. On the monte carlo simulation of bsdes: An improvement on the malliavin weights. *Stochastic Processes and their Applications* 120, 7 (2010), 1133 – 1158.
- [19] DUFLO, M. *Algorithmes stochastiques*, vol. 23 of *Mathématiques & Applications (Berlin) [Mathematics & Applications]*. Springer-Verlag, Berlin, (1996).
- [20] E, W., HAN, J., AND JENTZEN, A. Deep learning-based numerical methods for high-dimensional parabolic partial differential equations and backward stochastic differential equations. *Communications in Mathematics and Statistics* 5, 4 (2017), 349–380.

- [21] EL KAROUI, N., PENG, S., AND QUENEZ, M. C. Backward stochastic differential equations in finance. *Mathematical finance* 7, 1 (1997), 1–71.
- [22] FEUERSÄNGER, C. *Sparse grid methods for higher dimensional approximation*. PhD thesis, University of Bonn, (2010).
- [23] FRIEDMAN, A. *Partial differential equations of parabolic type*. Prentice-Hall, Inc., Englewood Cliffs, N.J., (1964).
- [24] FROMMERT, M., PFLÜGER, D., RILLER, T., REINECKE, M., BUNGARTZ, H.-J., AND ENSSLIN, T. Efficient cosmological parameter sampling using sparse grids. *Monthly Notices of the Royal Astronomical Society* 406, 2 (2010), 1177–1189.
- [25] GEISS, C., AND LABART, C. Simulation of bsdes with jumps by wiener chaos expansion. *Stochastic Processes and their Applications* 126, 7 (2016), 2123–2162.
- [26] GOBET, E., LEMOR, J.-P., AND WARIN, X. A regression-based monte carlo method to solve backward stochastic differential equations. *The Annals of Applied Probability* 15, 3 (2005), 2172–2202.
- [27] GOBET, E., LÓPEZ-SALAS, J. G., TURKEDJIEV, P., AND VÁZQUEZ, C. Stratified regression monte-carlo scheme for semilinear pdes and bsdes with large scale parallelization on gpus. *SIAM Journal on Scientific Computing* 38, 6 (2016), C652–C677.
- [28] GOBET, E., TURKEDJIEV, P., ET AL. Approximation of backward stochastic differential equations using malliavin weights and least-squares regression. *Bernoulli* 22, 1 (2016), 530–562.
- [29] GRIEBEL, M., AND OSWALD, P. Tensor product type subspace splittings and multilevel iterative methods for anisotropic problems. *Advances in Computational Mathematics* 4, 1 (1995), 171.
- [30] GU, Y., YANG, H., AND ZHOU, C. Selectnet: Self-paced learning for high-dimensional partial differential equations. *arXiv preprint arXiv:2001.04860* (2020).
- [31] HAN, J., JENTZEN, A., AND E, W. Overcoming the curse of dimensionality: Solving high-dimensional partial differential equations using deep learning. *arXiv preprint arXiv:1707.02568* (2017).
- [32] HAN, J., JENTZEN, A., AND E, W. Solving high-dimensional partial differential equations using deep learning. *Proceedings of the National Academy of Sciences* 115, 34 (2018), 8505–8510.
- [33] HAN, J., JENTZEN, A., AND E, W. Algorithms for solving high dimensional pdes: From nonlinear monte carlo to machine learning. *arXiv preprint arXiv:2008.13333* (2020).
- [34] HAN, J., AND LONG, J. Convergence of the deep bsde method for coupled fbsdes. *Probability, Uncertainty and Quantitative Risk* 5, 1 (2020), 1–33.
- [35] HENRY-LABORDÈRE, P., OUDJANE, N., TAN, X., TOUZI, N., AND WARIN, X. Branching diffusion representation of semilinear pdes and monte carlo approximation. *Ann. Inst. H. Poincaré Probab. Statist.* 55, 1 (02 2019), 184–210.

- [36] HU, Y., NUALART, D., AND SONG, X. Malliavin calculus for backward stochastic differential equations and application to numerical solutions. *The Annals of Applied Probability* 21, 6 (2011), 2379–2423.
- [37] HURÉ, C., PHAM, H., AND WARIN, X. Deep backward schemes for high-dimensional nonlinear pdes. *Mathematics of Computation* 89, 324 (2020), 1547–1579.
- [38] HUTZENTHALER, M., JENTZEN, A., KRUSE, T., AND E, W. Multilevel picard iterations for solving smooth semilinear parabolic heat equations. *arXiv preprint arXiv:1607.03295* (2016).
- [39] KUSHNER, H. J., AND YIN, G. G. *Stochastic approximation and recursive algorithms and applications*, second ed., vol. 35 of *Applications of Mathematics (New York)*. Springer-Verlag, New York, (2003). Stochastic Modelling and Applied Probability.
- [40] LADYŽENSKAJA, O. A., SOLONNIKOV, V. A., AND URAL’CEVA, N. N. *Linear and quasilinear equations of parabolic type*. Translated from the Russian by S. Smith. Translations of Mathematical Monographs, Vol. 23. American Mathematical Society, Providence, R.I., (1968).
- [41] MA, J., AND ZHANG, J. Path regularity for solutions of backward stochastic differential equations. *Probability Theory and Related Fields* 122, 2 (2002), 163–190.
- [42] MENOZZI, S., AND LEMAIRE, V. On some non asymptotic bounds for the euler scheme. *Electron. J. Probab.* 15 (2010), 1645–1681.
- [43] PAGÈS, G. *Numerical Probability: An Introduction with Applications to Finance*. Universi-text. Springer International Publishing, (2018).
- [44] PAGÈS, G., AND SAGNA, A. Improved error bounds for quantization based numerical schemes for bsde and nonlinear filtering. *Stochastic Processes and their Applications* 128, 3 (2018), 847 – 883.
- [45] PARDOUX, E., AND PENG, S. Adapted solution of a backward stochastic differential equation. *Systems Control Lett.* 14, 1 (1990), 55–61.
- [46] PARDOUX, E., AND PENG, S. Backward stochastic differential equations and quasilinear parabolic partial differential equations. In *Stochastic partial differential equations and their applications (Charlotte, NC, 1991)*, vol. 176 of *Lect. Notes Control Inf. Sci.* Springer, Berlin, (1992), pp. 200–217.
- [47] PARDOUX, E., AND TANG, S. Forward-backward stochastic differential equations and quasilinear parabolic PDEs. *Probab. Theory Related Fields* 114, 2 (1999), 123–150.
- [48] PENG, S. Probabilistic interpretation for systems of quasilinear parabolic partial differential equations. *Stochastics and Stochastics Reports (Print)* (1991).
- [49] ZHANG, J. A numerical scheme for bsdes. *The Annals of Applied Probability* 14, 1 (2004), 459–488.